Tarduno, J.A., Duncan, R.A., Scholl, D.W., et al., 2002
Proceedings of the Ocean Drilling Program, Initial Reports Volume 197

1. Leg 197 Summary[1]

Shipboard Scientific Party[2]

ABSTRACT

The bend in the Hawaiian-Emperor volcanic lineament is the most cited example of a change in plate motion recorded in a fixed hotspot frame of reference. Alternatively, the bend might primarily record variable motion of the Hawaiian hotspot relative to the Pacific lithosphere with time. Four lines of inquiry support the latter view: (1) global plate motions predicted from relative plate motion data, (2) spreading rate data from the North Pacific Basin, (3) mantle flow modeling utilizing geoid and seismic tomography constraints, and (4) paleomagnetic data from the Emperor chain. Although the rate of motion has been difficult to constrain because previous drilling was limited, the best available paleomagnetic data suggest Pacific hotspots may have moved rapidly, at rates comparable to those of lithospheric plates, in Late Cretaceous to early Tertiary times (81–43 Ma).

We drilled basement sites in the Emperor Seamount chain during Leg 197 to test the hypothesis of southward motion of the Hawaiian hotspot. The principal drilling objective was to achieve moderate basement penetration at these sites to obtain cores from lava flows suitable for paleomagnetic paleolatitude and radiometric age determinations. Because of the record-setting basement penetration (1220 m) during Leg 197 at Detroit (Sites 1203 and 1204; ~71–76 Ma), Nintoku (Site 1205; ~56 Ma), and Koko (Site 1206; ~48 Ma) Seamounts, we were able to meet our objectives. Paleolatitudes for these sites suggested by our preliminary shipboard paleomagnetic analyses clearly differ from the latitude of Hawaii. The values are consistent with and confirm prior results from Suiko (Deep Sea Drilling Project Site 433) and Detroit (Ocean Drilling Program Site 884) Seamounts. Our shipboard analysis of paleolatitude vs. age for the Emperor Seamounts must be supported by shore-based paleomagnetic studies and radiometric age determinations. However, the available data suggest that the Emperor Seamounts record the

[1]Examples of how to reference the whole or part of this volume.
[2]Shipboard Scientific Party addresses.

Ms 197IR-101

rapid southward motion of the Hawaiian hotspot in the mantle, requiring a major change in how we view this classic age-progressive volcanic lineament as a record of mantle convection and plate motions.

Another important science objective of the leg was to determine the geochemical variation of the volcanic products of the Hawaiian hotspot through time. Observations of lava flow thickness, vesicularity, crystallinity, and morphology, together with analysis of volcaniclastic sediment, have provided a picture of eruptions in subaerial to shallow-water conditions at Detroit and Koko Seamounts (Sites 1203, 1204, and 1206) and waning subaerial activity at Nintoku Seamount (Site 1205). Shipboard geochemical measurements suggest that we have captured the transition from Hawaiian tholeiitic shield stage to alkalic postshield stage at each of the volcanic complexes. Between Sites 1203 and 1204 and previously studied Sites 883 and 884, we have a range of compositions at Detroit Seamount that covers most of the variability seen in volcanoes of the island of Hawaii. The variability of incompatible element ratios (e.g., Ti/Zr) provide evidence that we have sampled different source compositions. It will remain for shore-based researchers to evaluate and define these suspected source heterogeneities through the examination of additional trace elements and isotopic compositions.

INTRODUCTION

Many of our ideas of where mantle plumes originate, how they interact with the convecting mantle, and how plates have moved in the past rest on interpretations of the Hawaiian-Emperor hotspot track. One reason this volcanic lineament has attained this conceptual stature lies in its prominent bend at 43 Ma. The bend, which separates the westward-trending Hawaiian Islands and seamounts from the northward-trending Emperor Seamounts (Fig. **F1**) has no equal among the Earth's hotspot tracks; it is the most cited physical manifestation of a change in plate motion in a fixed hotspot reference frame. Because the bend is so distinct, it can be used to estimate plume diameters and to place bounds on the convecting mantle wind that may deflect plumes (Duncan and Richards, 1991). However, shortly after hotspots were used as a frame of reference (Morgan, 1971), apparent discrepancies involving the Hawaiian-Emperor track arose (Molnar and Atwater, 1973). Attempts to model past plate motions failed to predict the bend; instead, a more westerly track was derived (Solomon et al., 1977). Tests of the fixed hotspot hypothesis based on global plate circuits suggested large relative motions between Hawaii and hotspots in the Atlantic and Indian Ocean Basins (Molnar and Atwater, 1973; Molnar and Stock, 1987), but uncertainties in the relative plate motions employed in these tests limited their resolving power (Acton and Gordon, 1994).

Several works have readdressed these questions. Norton (1995) suggests that the Hawaiian-Emperor bend records the time when the moving hotspot became fixed in the mantle. Prior to 43 Ma, Norton argues that the hotspot moved southward, creating the Emperor Seamount chain. The accuracy of this work is difficult to assess because of the lack of formal error analyses, but the interpretation reiterates findings of updated plate circuit studies that consider rotation pole errors (Cande et al., 1995). In addition, no obvious change occurs in the spreading rate at 43 Ma for the well-studied marine magnetic anomaly record of the North Pacific Ocean (Atwater, 1989). Many feel the lack of such a response by overlying plates to a change of absolute plate motion as large

F1. Locations of Emperor Seamount sites, p. 26.

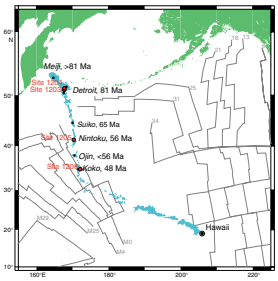

as that indicated by the Hawaiian-Emperor bend is reason enough to question hotspot fixity. New modeling efforts utilizing a viscosity structure based on geoid constraints, mantle flow fields consistent with tomographic data, and plate motion estimates also predict motion of hotspot groups (Steinberger and O'Connell, 1997). For the Emperor trend, the predicted motion is 10–15 mm/yr (Steinberger, 1996) (Fig. F2).

Whereas these recent studies have revitalized discussions regarding hotspot fixity (see also Christensen, 1998; Wessel and Kroenke, 1998), they face some fundamental data limitations. However, the hypothesis of hotspot motion can be tested independently using paleomagnetism (e.g., Duncan et al., 1972; McElhinny, 1973; Hargraves and Duncan, 1973). The most direct approach is to sample volcanoes that construct a given hotspot track. In the example of the Hawaiian hotspot, the paleolatitudes of extinct volcanic edifices of the Emperor chain should match the present-day latitude of Hawaii if the hotspot has remained fixed with respect to the Earth's spin axis. But this type of test is difficult, in practice, to apply. Paleolatitude values derived from the paleomagnetic analysis of deep-sea sediment overlying seamounts must be interpreted carefully because compaction can induce a flattening of inclinations (Celaya and Clement, 1988; Arason and Levi, 1990; Tarduno, 1990). Such problems can be avoided through the study of drill cores from well-dated lava flows. But until recently, only a few sites had sufficient depth penetration to conduct direct paleomagnetic tests of hotspot fixity. This situation improved after Pacific Ocean drilling during Ocean Drilling Program (ODP) Legs 143–145. Data from Legs 143 and 144 indicate significant motions between hotspot groups in the Atlantic and Pacific Ocean Basins during the mid-Cretaceous (128–95 Ma) (Tarduno and Gee, 1995). The motion is rapid, at speeds within the range of lithospheric plate velocities (30 mm/yr).

These findings indicate an older episode of hotspot motion and, coupled with the inferences based on relative plate motions, suggest that Hawaiian hotspot motion is a viable hypothesis that should be tested further; this test became the primary objective of ODP Leg 197. Data obtained from the analysis of cores obtained during ODP Leg 145 (Tarduno and Cottrell, 1997) and Deep Sea Drilling Project (DSDP) Leg 55 (Kono, 1980) from the Emperor Seamount chain (Fig. F1), summarized below, allowed a preliminary test (Cottrell and Tarduno, in press) that guided the drilling plan of Leg 197. The sites chosen to address the question of hotspot fixity were also designed to obtain geochemical data needed for understanding the compositional variability of volcanic products from the Hawaiian hotspot, another important goal of Leg 197.

F2. Hotspot motion and predicted motion of the Hawaiian plume, p. 27.

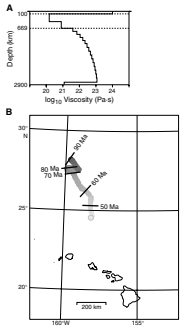

BACKGROUND AND PREVIOUS RESULTS

During Leg 145, 87 m of lava flows was penetrated at Detroit Seamount Site 884 (Fig. F1) (Rea et al., 1995). ^{40}Ar-^{39}Ar radiometric analyses yield an age (81.2 ± 1.3 Ma) (Keller et al., 1995) older than that predicted (~75 Ma) from hotspot-based best-fit linear plate motion models (Duncan and Clague, 1985). Characteristic magnetizations derived from basalt samples have mainly negative inclinations, indicating reversed polarity. This polarity assignment is consistent with the radiometric age data, suggesting eruption of these lava flows during Chron 33r (Tarduno and Cottrell, 1997).

A potential problem in obtaining reliable paleomagnetic data from any basement drill hole is the uncertain timescale between lava flow eruptions. If most flows reflect rapid eruptions, one could easily obtain a biased paleolatitude estimate by giving equal weight to each flow unit. To address this concern, the inclination-only averages derived from each flow unit (McFadden and Reid, 1982) must be checked for serial correlation (Cox, 1970; Kono, 1980; Tarduno and Sager, 1995). These analyses lead to inclination group models (Fig. **F3**). The directional angular dispersion, estimated from the inclination model data and transformed into pole space (Cox, 1970; Tarduno and Sager, 1995), is indistinguishable from the predicted virtual geomagnetic pole scatter from global data sets (McFadden et al., 1991) (Fig. **F3**). As discussed below, only one other paleomagnetic data set exists for the Emperor Seamount trend that satisfies these geomagnetic sampling requirements.

The preferred inclination group model, where groups are distinct at >95% confidence (N = 10) (Tarduno and Cottrell, 1997), produces a paleolatitude of 36.2° (+6.9°/–7.2°), clearly discordant from the present-day latitude of Hawaii (~19°) (Fig. **F3**). This discrepancy is too large to be explained by tectonic tilt. Tilts of 1°–3° have been previously reported for some of the northern Emperor Seamounts (Lonsdale et al., 1993). Because these tilts are small and the angle between the remanent magnetization vector and downdip azimuth of tilt is large (>60°), the effect on the paleolatitude is negligible. Measurements made at unit contacts also fail to indicate significant dips.

The new paleomagnetic result directly questions the validity of the Late Cretaceous Pacific apparent polar wander path (APWP) (Fig. **F3**). But how could these prior results be so errant? Previous Late Cretaceous poles are dominantly or solely based on the inversion of magnetic surveys over seamounts (Gordon, 1983; Sager and Pringle, 1988). Reviews of the methods used to fit these poles suggest they are far more uncertain than commonly supposed (Parker, 1991). Viscous and induced magnetizations can also bias the resulting pole positions (Gee et al., 1989; Cottrell and Tarduno, 2000b). Interestingly, high-latitude poles similar to the new colatitude result (Fig. **F3**) have been reported from preliminary analyses of the skewness of marine magnetic anomaly data of comparable age (Vasas et al., 1994).

The other paleolatitude value from the Emperor trend that adequately averages secular variation was derived from Suiko Seamount (65 Ma) (Kono, 1980) (Fig. **F1**). The 8° discrepancy between the Suiko Seamount paleolatitude and the present-day latitude of Hawaii has been previously attributed to early Cenozoic true polar wander (Gordon and Cape, 1981; Sager and Bleil, 1987), which is defined as a rotation of the entire solid Earth in response to mass redistribution (e.g., convection of density heterogeneities in the mantle and growth and disappearance of glacial ice) (Goldreich and Toomre, 1969). True polar wander predictions based on global paleomagnetic data from the continents (Besse and Courtillot, 1991), however, do not agree with the new Detroit Seamount data (Tarduno and Gee, 1995; Tarduno and Cottrell, 1997). Furthermore, renewed tests of Cretaceous true polar wander models show that the solid Earth rotations proposed are not seen in paleomagnetic data from regions where large changes in latitude should be observed (Cottrell and Tarduno, 2000b; Tarduno and Smirnov, 2001). Therefore, the proposed true polar wander rotations appear to be artifacts related to the fixed hotspot reference frame employed.

Because Late Cretaceous true polar wander predictions are inconsistent with Pacific observations, we must now consider hotspot motion

F3. Inclination group models for Detroit Seamount, p. 28.

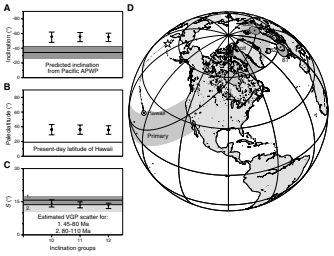

as an explanation for the new paleomagnetic data. Although limited in number, paleomagnetic data from the Hawaiian chain younger than the age of the Hawaiian-Emperor bend do not suggest large southward latitudinal displacement relative to the fixed hotspot model (Gromme and Vine, 1972) nor do results from relative plate motion models (e.g., Cande et al., 1995). Thus, the possibility of large latitudinal motion of the Hawaiian hotspot is best examined by focusing our attention on the time interval during which the Emperor Seamounts were formed. We can isolate the latitudinal history of the Emperor Seamounts from that of the Hawaiian chain by subtracting the difference between the present-day latitudes of the 43-Ma bend and Hawaii from the present-day latitudes of each of the Emperor Seamounts. In effect, we slide the Emperor trend down the Hawaiian chain to the present-day latitude of Hawaii (Fig. F4). In so doing, we produce a plot predicting the paleolatitude of the Emperor Seamounts as if they were formed by a hotspot moving southward at constant velocity beneath a stationary plate. Site 884 Detroit Seamount results together with the Suiko Seamount data (Kono, 1980) parallel this predicted trend and provide support for the hotspot motion hypothesis. Differences between the data and predicted values also allow for some northward plate motion. It is difficult to place error bounds on the rate of motion because only two estimates of paleolatitude are available. Nevertheless, the data suggest that the Hawaiian hotspot could have moved southward from 81 to 43 Ma (Norton, 1995) at a constant rate of 30–50 mm/yr while the Pacific plate moved slowly northward, in a paleomagnetic (spin axis) frame of reference (Fig. F4).

F4. Distance from the 43-Ma bend in the hotspot track vs. age, p. 29.

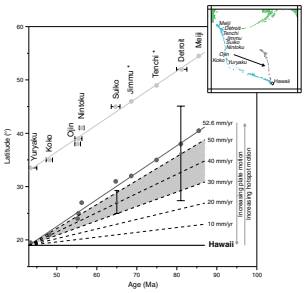

Interpretations of the Hawaiian-Emperor bend have had a tremendous impact on our ideas of the history and dynamics of plate motions. But the data sets described above suggest that these interpretations may be wrong or, at best, largely incomplete. Our primary motivation during Leg 197, as outlined in "Scientific Objectives" below, is to test the hypothesis of Hawaiian hotspot motion with further drilling in the Emperor Seamounts. This objective provided additional opportunities to learn more about the geometry and paleointensity of the Late Cretaceous to Tertiary geomagnetic field and to study the source and melting history of the Hawaiian hotspot.

SCIENTIFIC OBJECTIVES

Determining the Paleolatitude and Age of the Emperor Seamounts

The primary goal of Leg 197 was to obtain accurate and precise paleolatitude and age estimates for each of the sites drilled. These data, when compared with fixed and moving hotspot predictions, form the basis of our paleomagnetic test. To accomplish our goal, we targeted moderate penetration of lava flow sections with the aim of obtaining an average of secular variation at each site.

Our objectives differed slightly from site to site. At Detroit Seamount, we hoped to improve the precision of prior paleolatitude estimates and, possibly, obtain new time-averaged paleolatitude data with ages different from those determined at Detroit Seamount Site 884. At Nintoku Seamount and Koko Guyot, we hoped to investigate the mechanisms for discrepancies between paleomagnetic data and predictions based on fixed hotspot models. Combined with data from Suiko Seamount

(Kono, 1980), time-averaged paleomagnetic data of known age from these seamounts should allow us to test existing models and potentially develop new models for the generation of the Emperor Seamount trend and the Hawaiian-Emperor bend.

New paleomagnetic data from Detroit, Nintoku, and Koko Seamounts could also allow for the construction of an improved Pacific apparent polar wander path. In addition to its utility in the study of Pacific plate kinematics, a refined APWP could provide the basis for improved paleogeographic reconstructions important for paleoclimate studies. Such reconstructions are needed when proxy climate data are used to define past latitudinal gradients (e.g., Huber et al., 1995; Zachos et al., 1994). APWP data may serve as a more stable reference frame for Pacific plate reconstructions than one based on fixed hotspots (Cottrell and Tarduno, 1997b.)

Through our drilling approach (obtaining time-averaged paleomagnetic data at each site), we also hoped to address other aspects of the geomagnetic field through Late Cretaceous to early Teriary time (Fig. F5). For the present field and models of the Late Cretaceous to early Tertiary field, the axial dipole term is overwhelmingly dominant. Therefore, other terms will not greatly affect the accuracy of data used to test the hotspot motion hypothesis. However, the data obtained can be used to better constrain the Gauss coefficients of the past field. Data from the Pacific Basin are essential because of its sheer size; no global description of the field can be considered complete without data from the region.

Although the general importance and need for Pacific data are generally appreciated, the methods used to summarize past data prior to modeling have been given less consideration. For the early Tertiary and Late Cretaceous plate motion can not be neglected, as it can for analyses of data over the past 5 m.y. (Constable, 1992), but instead the data must be first rotated into a common reference frame. The few analyses that have tried to incorporate data from the Pacific Basin (principally older seamount results) have relied on a fixed hotspot frame of reference; hence, previous estimates of Gauss coefficients may contain considerable errors if the hotspot motion hypothesis is correct. Interestingly, these analyses show a dramatic change in the Gauss coefficients (a change in sign) during the critical Late Cretaceous to early Tertiary interval we targeted for study (Livermore et al., 1984). Therefore, we hoped that the data collected from the Leg 197 sites could simultaneously address the hypothesis of hotspot motion and the reality of this change in sign of the spatially varying Late Cretaceous–early Tertiary geomagnetic field.

When compared to the considerable success of studies that utilize directional data derived from paleomagnetic measurements, work devoted to understanding the past intensity of the geomagnetic field has advanced more slowly. However, the long-term variations of paleointensity are essential for a complete description of the field, as well as for understanding the long-term magnetic signature of ocean crust. One reason progress has been slow is related to selection criteria needed to ensure reliable paleointensity determination. The preferred method of paleointensity measurement, Thellier-Thellier double heating experiments of basalt (Thellier and Thellier, 1959; modified by Coe, 1967), often encounters problems resulting from chemical alteration during heating. Significant recent progress has been made in studying basaltic glass (Pick and Tauxe, 1993) that appears to show ideal magnetic properties. The available DSDP and ODP sites where basaltic glass was sam-

F5. Gauss coefficients and paleointensity determinations, p. 30.

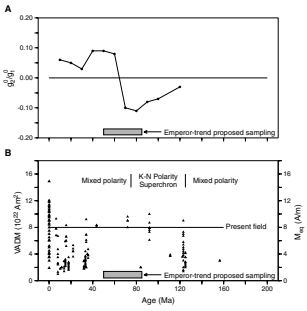

pled have now been analyzed (Juarez et al., 1998), so further progress requires additional drilling.

The Leg 197 drilling plan included the potential recovery of reference sites for Late Cretaceous–early Tertiary paleointensity. We planned whole-rock, basaltic glass, and single plagioclase crystal (Cottrell and Tarduno, 1997a, 2000a; Tarduno et al., 2001) approaches to analyze the recovered cores and to derive Late Cretaceous to early Tertiary interval paleointensity data through shore-based study.

Source and Melting History of the Hawaiian Hotspot

Hotspots are of continuing interest to mantle geochemists because they provide "windows" into parts of the mantle that lie beneath the upper mantle source region for mid-ocean ridges. An observed range of distinct mantle compositions offers the means to investigate such important issues as the geochemical evolution of the mantle, temporal and spatial scales of mantle convection, and lithosphere-mantle interactions. No hotspot has been more intensely examined from a geochemical perspective than Hawaii, through compositional studies of lava sequences from the islands at the southeast end (e.g., Chen and Frey, 1985; Garcia et al., 1998) to dredged and drilled rocks from ~30 sites along this prominent and long-lived lineament (e.g., Lanphere et al., 1980; Clague and Dalrymple, 1987; Lonsdale et al., 1993; Keller et al., 2000).

As an example, the Sr isotope ratios of tholeiitic basalt from the Hawaiian hotspot track show a systematic trend through time (Fig. **F6**). These ratios are approximately constant along the Hawaiian Ridge (out to the 43-Ma bend) then decrease steadily northward along the Emperor Seamounts to Suiko Seamount. This decrease has been attributed to a decrease in distance between the hotspot and the nearest spreading ridge (Lanphere et al., 1980). Only the tholeiitic lava flows from the shield phases of volcano construction show this trend because only these magmas appear to have escaped contamination by the oceanic lithosphere (Chen and Frey, 1985). Keller et al. (2000) have extended this analysis to Detroit and Meiji Seamounts, and they find that Sr isotope ratios continue to decrease northward, with a minimum value at Detroit Seamount well within the range of compositions for Pacific mid-ocean-ridge basalt (MORB). This composition (confirmed with other isotopic and elemental ratios) is unprecedented in the Hawaiian hotspot–produced volcanism to the south but is consistent with the interpretation from plate reconstructions that the hotspot was located close to a spreading ridge at ~80 Ma. The seamount magmas, then, appear to be derived from a mixture of plume ("enriched") and predominantly asthenosphere ("depleted") mantle sources. The plume endmember is more like the "Kilauea" than the "Koolau" component of the modern hotspot.

Plate reconstructions (e.g., Mammerickx and Sharman, 1988; Atwater, 1989) include a spreading ridge close to the Hawaiian hotspot at ~80 Ma. In other locations where a plume is close to a ridge (Galapagos Islands, Easter Island, and Iceland), the isotopic compositions of hotspot products extend toward MORB values. Several processes may lead to this effect. The nearby spreading ridge could have provided a higher temperature and lower viscosity and density regime, leading to significant entrainment of asthenosphere within the rising plume. Thinner lithosphere near the ridge would promote a longer melting column in the plume, leading to greater degrees of partial melting and ho-

F6. Changes in Hawaiian hotspot magmas through time, p. 31.

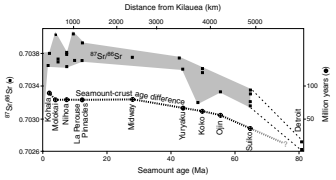

mogenization of geochemical heterogeneities (M. Regelous et al., unpubl. data). Also, younger, hotter lithosphere may be more readily assimilated by the ascending plume melts. Thus, the thickness of the lithosphere could determine how much aesthenosphere contributes to hotspot volcanism or how possible isotopic heterogeneities within the plume itself are expressed through partial melting. The (deep mantle?) region where the Hawaiian plume acquires its geochemical characteristics has probably not been homogeneous and static. But the degree of geochemical variability at given sites within the Emperor Seamounts has not been established on the basis of the few analyses reported so far.

The Leg 197 study plan called for the generation of geochemical data from lava flows recovered from the Emperor Seamount sites to document the compositional and thermal characteristics of mantle sources and melting conditions of the early history of the Hawaiian hotspot. We planned to measure major and trace element abundances to place limits on the depth and extent of melting and track magma evolution (fractionation and contamination) to the surface. We also planned to use such data to categorize rocks as tholeiitic shield, alkalic postshield, or posterosional lavas for comparison with models of Hawaiian Islands construction. Shore-based isotopic work (Sr, Nd, Pb, and Hf isotope ratios and parent-daughter measurements of whole rocks and He for glasses and fresh olivine) and trace element analyses were planned to help identify mantle source components. Studies of volatiles in recovered glasses and melt inclusions in phenocryst phases were also planned, as well as microanalyses of opaque minerals (Fe-Ti oxides) that will reveal alteration and cooling conditions and aid in the rock magnetic and paleomagnetic investigations of the leg.

Knowledge of the physical volcanology of the lava flows at Emperor Seamount sites is important for understanding the mechanisms and timescales of eruptions. Studies of the physical characteristics of historic lava flows on Hawaii have led to the means of linking outcrop-scale observations to important eruption parameters, such as flow volume, velocity, viscosity, relative eruption rate, and distance from source. We planned to measure flow thickness, direction, structure, vesicularity, and crystallinity in the recovered cores and to integrate this information with evidence for eruptive environment (submarine vs. subaerial and volcano flank vs. summit) and secular variation measurements from the paleomagnetic studies to estimate timescales for the recovered sections.

DRILLING STRATEGY AND OPERATIONS

Secular Variation in Previous Deep-Sea Drilling Studies

A key question concerning paleomagnetic tests such as those conducted during Leg 197 is the penetration needed to adequately average secular variation. Analysis of cores from Site 884 on the eastern flank of Detroit Seamount indicates that at some sites as little as 85 m of basement penetration is sufficient to obtain an average of secular variation. Where basement penetration was >120 m at Cretaceous plateaus, seamounts, and guyots in the Pacific Basin, enough independent time units were recovered to average secular variation (Tarduno and Sager, 1995; Tarduno and Gee, 1995). This depth does not differ greatly from that over which secular variation is averaged (100–200 m) in analyses

(Holt et al., 1996) of cores from lava flows obtained by drilling on Hawaii.

However, it is not possible to determine the time sequence represented by the volcanic section at a given site prior to drilling. It is necessary to evaluate the angular dispersion of independent lava flows (inclination units) and compare this with global paleomagnetic data to confirm whether secular variation has been adequately sampled at a given site. We planned to collect on-site paleomagnetic data and to make angular dispersion calculations to evaluate whether the resulting record provides an adequate average.

Paleolatitude Experiment

We planned basement penetration to moderate depth (150–250 m) at the Emperor Seamount sites (Fig. F1; Table T1). Our preferred strategy was to employ minicones for reentry. The nominal depths for basement penetration were based on drilling of other Pacific Basin seamounts and plateaus (Tarduno and Gee, 1995). Whereas these estimates were needed for the planning process, we envisioned an interactive process based on recovery. Ideally, we hoped to recover at least 15 flow units (distinct eruption units rather than lobes of compound flows) from each hole for detailed paleomagnetic and radiometric age (^{40}Ar-^{39}Ar incremental heating) analysis. Below, we include a brief description and rationale for each of the drilling sites. This approach, with age information provided by micropaleontology and relative time information provided by physical volcanology, guided our decisions at sea.

T1. Coring summary, Leg 197, p. 91.

Originally, the northernmost site to be drilled during Leg 197 was on Meiji Guyot. Unfortunately, clearance for drilling was denied by the Russian government in May 2001. Consequently, drilling on Detroit Seamount (~81 Ma) became the highest priority for Leg 197. We planned single holes at two summit sites, proposed Sites HE-3A and HE-3B, which were included in a seismic survey by the *JOIDES Resolution* en route. Proposed Site HE-3A became our first site drilled (Site 1203) (Table T2).

T2. Operations summary, Leg 197, p. 92.

The relatively thick sequences of volcaniclastic rocks recovered at Site 1203 indicated proximity of a Campanian volcanic source; we felt that nearby proposed Site HE-3B might largely repeat the section already cored. Therefore, we elected to return to Site 883 (proposed Site HE-3) to drill deeper and obtain more flow units than previously acquired (during Leg 145) to increase the precision of the oldest paleomagnetic data to be used in our paleolatitude test. The final selected location near Site 883 became Site 1204, where two holes were drilled.

In addition to confirming the already recognized discrepancy between the paleolatitudes of Suiko and Detroit Seamounts and the present latitude of Hawaii, we saw an opportunity to investigate how this difference accumulated with time. We planned sites on Nintoku, Ojin, and Koko Seamounts (Fig. F1) to obtain this record. Because of time devoted to deepening Site 1203 below volcaniclastic intervals (to obtain additional time-independent lava flows) and operational delays related to a clogged drill bit at Site 1204 (forcing the drilling of a second hole), drilling at Ojin Seamount was canceled. We allotted the time saved in roughly equal proportions to deeper drilling at Nintoku Seamount and Koko Guyot (which became Sites 1205 and 1206, respectively).

If the Emperor trend represents southward motion of the Hawaiian hotspot, we expected to obtain a paleolatitude of 25°–27° for Nintoku

Seamount. Our proposed Site HE-4A was positioned at DSDP Hole 432A, near the northwest edge of the seamount on flat-lying, stratified sediment that could be used to stabilize the bottom-hole assembly. Previous drilling indicated that the sediment was 42 m thick above basement and that the uppermost lava flows were separated by a soil horizon. Soils indicate significant time intervals between lava flows and ideal conditions for deeper drilling.

Our planned site on Koko Guyot (proposed Site HE-6A) was positioned at DSDP Site 308. Previous drilling penetrated ~70 m of clay and volcaniclastic sandstone. Biostratigraphic data indicated an Eocene age for the base of the section, suggesting the hole was terminated (because of sea conditions) near basement.

SITE 1203

Principal Results

Site 1203 (50°57.00′N, 167°44.40′E) is located toward the central region of the summit area of Detroit Seamount (Fig. F7). This position was initially selected along an available, high-exaggeration (12–15:1) single-channel (analog) seismic reflection profile collected in 1988 (Londsdale et al., 1993). An underway geophysical survey was conducted to gather digital seismic reflection data to more adequately characterize the stratigraphic and structural setting of the site; high-resolution profiles were collected using a single 80-in³ water gun firing every 6 s. Basement was clearly imaged, and Site 1203 was positioned along the crossing points of three survey lines.

Hole 1203A was spudded at a water depth of 2593 m. In the vicinity of the selected site, an acoustically prominent basement reflection is overlain by a 400- to 500-m-thick carapace of sedimentary deposits. The greater part of this sequence consists of late Oligocene and younger sediment of the Meiji drift (Rea et al., 1995). Coring began at a depth of 300 meters below seafloor (mbsf) in diatom and nannofossil ooze beds of late, middle, and early Miocene age. At ~390 mbsf, diatomaceous material gave way to chalk with abundant but poorly preserved nannofossils of late Oligocene age. Lower Eocene (upper part of Zone NP12; ~51 Ma) (Berggren et al., 1995) chalky and sandy-silty sediment immediately overlies basaltic lava flows of the basement rock sequence. Beds of volcaniclastic sediment and chalk in the upper part of the cored basement complex contain Campanian nannofossils assigned to Zones CC22–CC23, the estimated age of which is 71.3–76.0 Ma. Toward the base of the basement section (~400 m into basement, or ~865 mbsf), nannofossils characteristic of Zone CC22 were identified, indicating an age of 75–76 Ma (Berggren et al., 1995).

We reached basement at 462 mbsf. The underlying ~453 m of cored basement consists of 18 lava units and 14 volcaniclastic interbeds (Fig. F8). The average recovery in basement was 56.5%. The upper part of the basement sequence defines deposition or emplacement in a distal environment relative to eruptive centers and at relatively shallow water depths. It is characterized by nonvesicular pillow lavas and thick, sparsely vesicular pahoehoe lava flow units interbedded with volcaniclastic sedimentary sequences of primary and resedimented basaltic tuff (ash fall deposits) and vitric siltstone and sandstone.

The lower part of the basement succession is dominated by highly vesicular compound pahoehoe lavas (up to 65 m thick) and includes

F7. Site 1203 survey 1, Line 6, migrated time section, p. 32.

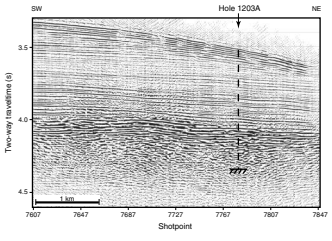

F8. Site 1203 basement rocks and biostratigraphic ages compared to logging data, p. 33.

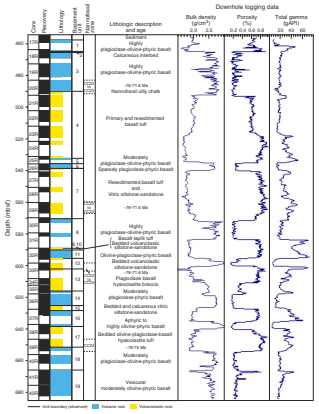

subordinate lapillistone (i.e., scoria fall deposits), pillow lava, hyaloclastite tuff, and breccia, along with thin vitric siltstone to sandstone sequences. The highly vesicular pahoehoe flows and the lapilli scoria deposits are characteristic of eruption and emplacement in a subaerial setting close to a source vent. The presence of pillow lavas, hyaloclastite tuff, and marine vitric sandstone and siltstone in the sequence indicates emplacement (or deposition) in water (Fig. **F9**). These contrasting indicators imply that the depositional environment extended from shallow marine to land, an interpretation consistent with an early subaqueous emplacement and then subsequent emergence of the lava section as it thickened.

Similarities are noted between the Site 1203 basalt units and those recovered during Leg 145 at Sites 883 and 884, positioned, respectively, on the summit and at the base of the eastern flank of Detroit Seamount (Rea et al., 1995). Notwithstanding probable age differences, we note that a plagioclase-phyric basalt containing centimeter-sized glomerocrystic plagioclase phenocrysts (Fig. **F10**) is similar to seven of the ten igneous units described from Site 884. Differences include the presence of olivine-rich zones (that also contain Cr spinel) in Hole 1203A (Fig. **F11**).

Tholeiitic to transitional basalt is present at the top of the sequence, and alkali basalt occurs intercalated lower downsection (Fig. **F12**). Some alkali basalt lavas are geochemically distinct in that they have a substantially lower Ti/Zr ratio (Fig. **F13**). Whereas Na and K are subject to mobility during alteration, at Site 1203 the designation of basalt units as alkalic is supported by elevated abundances of Ti, Zr, and Y relative to the tholeiitic basalt. The Site 1203 alkalic basalt, which erupted as subaerial pahoehoe lavas, may be analogous to the dominantly alkalic postshield-stage lavas that erupt as Hawaiian volcanoes migrate away from the hotspot. However, the shift upsection to tholeiitic pillow lavas is not easily understood with reference to the evolution of single Hawaiian volcanoes. This sequence could have developed from interfingering of lava flows from two distinct volcanic centers that were in different stages of growth. This possibility is supported by the observation that at least one flow unit in the lower alkalic section is compositionally related to lavas in the upper tholeiitic section.

The igneous rocks recovered at Site 1203 have undergone secondary alteration and weathering. Evidence for pervasive low-temperature alteration is exhibited by vesicle- and vein-filling secondary minerals. The degree of alteration increases downsection (Fig. **F14**). Alteration mineral assemblages in the upper part of the hole are dominated by calcite, Fe oxyhydroxide, and brown and green (saponite) clay. Associated secondary minerals are sulfide (pyrite), blue-green clay (celadonite), and zeolite. Most vesicles are filled with calcite or saponite. Near the bottom of the hole (~415 m into basement) vesicles are mostly filled with zeolite and Fe oxyhydroxide.

Bulk density measurements for that part of the sedimentary section cored (300–462 mbsf) show an increase with depth from ~1.5 to 2.3 g/cm^3. This gradient correlates with an overall decrease in porosity downhole, from ~65% to ~40%, which probably largely reflects increasing compaction, although the proportion of calcareous material with respect to diatomaceous debris also increases below ~390 mbsf.

In the basement section, variations in index properties, gamma ray counts, and thermal conductivity correspond to the alternation of volcaniclastic sediment and basaltic lava flows. In the volcaniclastic sediment, bulk density and thermal conductivity are generally low, whereas

F9. Partially altered glassy lobe margins with calcareous interlobe sediment, p. 35.

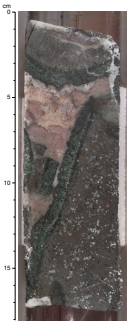

F10. Zonation in plagioclase, p. 36.

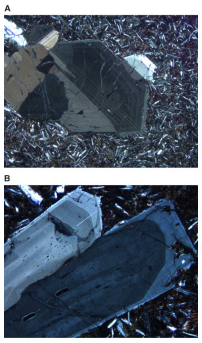

F11. Olivine-rich zone, p. 37.

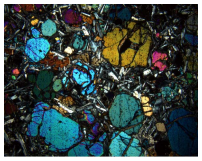

F12. Total alkali content vs. SiO_2 plots, p. 38.

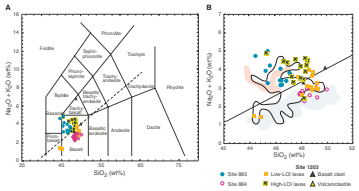

F13. Ti/Zr abundance ratio vs. depth, Hole 1203A, p. 39.

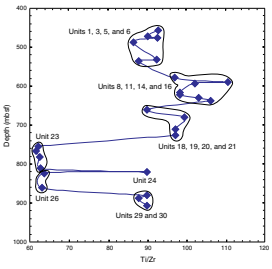

porosity is high (>40%). Conversely, in the basalt units, bulk density and thermal conductivity are high and porosity is correspondingly low (<20%). For the basalt, natural gamma ray measurements uncorrected for background radiation generally range between ~15 and 30 counts per second. To orient core segments to their in situ position, digital photos of 200 m of whole-round cores were taken to compare with Formation MicroScanner (FMS) logging images.

Logging operations in Hole 1203A were extensive, including the collection of downhole natural gamma ray, density, porosity, electrical resistivity, and temperature data with the triple combination tool and FMS and velocity measurements in a second tool string. Downhole magnetometer data were also collected with the Goettingen Borehole Magnetometer (GBM) in a third run (Figs. **F15, F16**). Excellent data quality and repeatability were observed along the entire section during the three runs. Basaltic sections are characterized by high electrical resistivity (up to 10 Ωm), low porosity (<0.5%), high density (up to 2.5 g/cm^3), and low natural gamma ray (<20 gAPI). In contrast, sediment and volcaniclastic units exhibit low resistivity, high porosity, and high natural gamma ray counts. FMS electrical images are of high quality and can be used to distinguish pillow basalt and more massive units (Fig. **F17**). The borehole magnetometer, which employed three fluxgate sensors and an innovative fiber-optic sensor to record tool rotation, yielded data that can be used to identify sequences of basalt and volcaniclastic sediment (Fig. **F18**). The strength of the recorded vertical to the horizontal component of the anomalous field suggests that in the basalt section the combined remanent and induced magnetic field has an inclination >45°.

A total of 258 discrete samples were taken from cores of volcanic basement rock. These samples were measured for natural remanent magnetization and then were demagnetized in an alternating field to 80 mT in 5- and 10-mT steps. Inclination, declination, and intensity were measured and orthogonal vector plots employed to determine the stability of remanence and the number of magnetic components present (Figs. **F19, F20**). Principal component analysis was used to determine the characteristic remanent magnetization direction. All samples exhibit normal polarity.

The average inclination of volcaniclastic units is 54.7° (+3.1°/–6.4°; 95% confidence level), which is a minimum value because compaction processes in sediment can rotate the remanent magnetic vector toward a reading shallower than originally set (Fig. **F21**). The minimum paleolatitude is thus 35.2° (+3.2°/–5.9°). Paleomagnetic inclination data for the lava flows were grouped according to flow unit and averaged. The means of the individual flow units were averaged to determine an overall mean inclination for the thickness of the basement section penetrated. Based on 16 units, the average inclination is 48.0° (+6.8°/–10.1°), a value that corresponds to a paleolatitude of 29.0° (+6.3°/–7.7°) (Fig. **F22**). This reading will change with improved age control (several flows may together represent a short period of time) and shore-based thermal demagnetization studies to address evidence that a high-coercivity component of magnetization present in some units was not adequately demagnetized with the alternating-field treatments applied.

The significant result of shipboard measurement is that the range of preliminary mean paleolatitude determinations extracted from volcaniclastic sediment and lava flow units (29°–35°) and the distributions of the data are distinct from the value predicted by the fixed hotspot model (i.e., ~19°N).

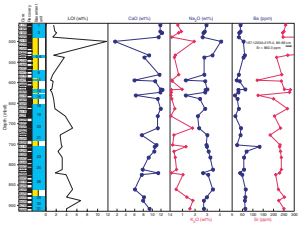

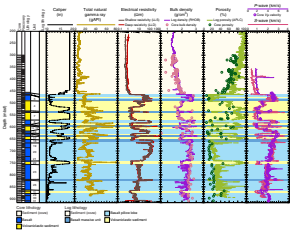

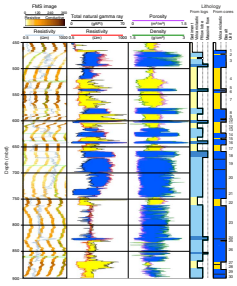

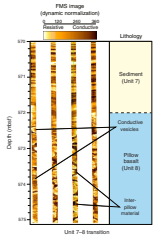

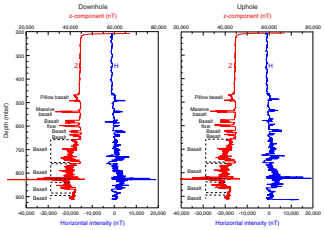

SITE 1204

Principal Results

The two holes drilled at Site 1204 (1204A: 51°11.68′N, 167°46.36′E, and 1204B: 51°11.64′N, 167°46.42′E) are located toward the northern end of the summit platform of Detroit Seamount in international waters ~18 km southeast of the Russian Exclusive Economic Zone. Prior to spudding in Hole 1204A, an underway geophysical survey was run to more fully characterize the stratigraphic and structural setting of the site. Crossing high-resolution seismic reflection profiles were collected using a single 80-in³ water gun firing every 6 s. Basement was cleanly imaged at the site as an upward-terminated sequence of discontinuous reflection events beneath a prominently layered set of reflectors representing sedimentary beds ~850 m thick. The bulk of these sedimentary beds are part of the areally extensive Meiji drift sequence of Oligocene and younger age (Rea et al., 1995).

The location for Site 1204 was selected on the basis of two seismic lines digitally recorded during the underway survey and information from previously drilled Leg 145, Site 883, at virtually the same location (Fig. **F23**). Because lengths of drilling pipe were left behind at Site 883, Hole 1204A was moved ~460 m southeast along one of the new seismic lines, where a flat basement reflector could be distinguished. After a clogged bit forced us to abandon the first hole, Hole 1204B was spudded ~100 m southeast of Hole 1204A.

Coring in Hole 1204A began beneath the Meiji sediment drift sequence at a depth of ~762 mbsf, where a relatively condensed sequence of chalk with volcanic ash containing middle Eocene to upper Paleocene nannofossils was recovered. Parts of this section could be correlated to the geomagnetic polarity timescale through shipboard paleomagnetic measurements. The lower Eocene carbonate units contain an interesting zone of sedimentary beds deformed and disrupted by sliding. Similar units are also preserved at Site 883 and at Site 884, which is at the base of the eastern flank of Detroit Seamount (Fig. **F24**). Ash in the sequence produces elevated magnetic susceptibility values that helped distinguish sedimentary subunits. The chalk beds overlie low-carbonate clay, diamictite, and ash-rich strata containing ~71- to 76-Ma Campanian nannofossils (CC22–CC23). Coring began in Hole 1204B at a depth of 810 mbsf in sediment immediately overlying basement containing the same nannofossil assemblage as that found in Hole 1204A. This age suggests that the Site 1204 basement may be roughly coeval with that at Sites 1203 and 883.

The Site 1204 basement consists of basalt that occurs as pahoehoe lava flows constructed of multiple lobes (Fig. **F25**). The association of pahoehoe lava, carbonate sand, and low-density lapilli and vesicular basalt breccia (Fig. **F26**) suggests that these flows originated from subaerial vents and that the lava was emplaced in a nearshore environment. The sequence was altered at low temperature in the seafloor weathering and alkali mobility zone. Prominent reduced zones with saponite clay and secondary pyrite are intermixed with more common oxidized zones characterized by Fe oxyhydroxide. Particularly noteworthy are unaltered glassy margins of flow lobes (Figs. **F27, F28**). The lava flows recovered at Site 1204 have alkali basalt compositions, but with significantly lower abundances of incompatible elements than postshield-stage alkalic basalt lava flows erupted at Hawaiian volcanoes such as Mauna Kea

F19. Stable magnetic behavior in Site 1203 volcaniclastic sediment, p. 45.

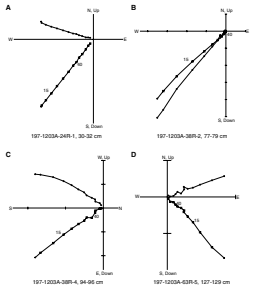

F20. Stable magnetic behavior in Site 1203 basalt, p. 46.

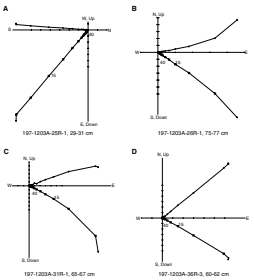

F21. Inclination values derived from Hole 1203A volcaniclastic sediment, p. 48.

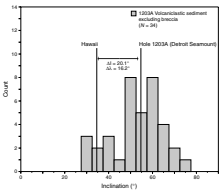

F22. Inclination values derived from Hole 1203A basement basalt, p. 49.

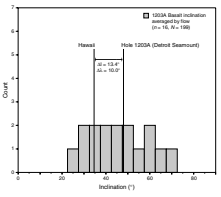

F23. Site 1204 survey 2, Line 3, migrated time section, p. 50.

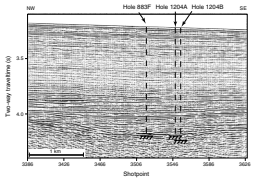

Volcano. The abundance and ratios of certain trace elements (e.g., Ti and Zr) in the Site 1204 lavas fall along the trend for Suiko Seamount and most other Detroit Seamount compositions (Fig. F29).

Detailed shipboard paleomagnetic analyses of basalt at Site 1204 (Figs. F30, F31) yielded an average inclination of 58.9° (+5.8°/–6.4°; 95% confidence level) and a preliminary paleolatitude estimate of 39.7° (+4.4°/–3.7°). The estimated angular dispersion of the data, however, indicates that the full range of geomagnetic secular variation important for obtaining a high-resolution paleolatitude value has not been sampled. Nevertheless, the Site 1204 values are in agreement with our preliminary data collected at Site 1203 and data from Site 884 (a data set known to average secular variation) (Tarduno and Cottrell, 1997). Together, these data suggest that Detroit Seamount formed some 1500 km north of the present latitude of Hawaii.

SITE 1205

Principal Results

Site 1205, the third site we occupied during Leg 197, was targeted at DSDP Site 432 (Leg 55) at the northwestern edge of Nintoku Seamount, a guyot or flat-topped volcanic complex in the central sector of the Emperor chain. Nintoku Seamount, at ~41°N, is positioned approximately two-thirds the distance southward along the line of north-northeast–south-southeast–trending Emperor volcanoes extending from Meiji Seamount (~53°N) in the north to Kammu Seamount (~32°N) at the chain's southern terminus near the Hawaiian-Emperor bend. Nintoku Seamount was named after the 16th emperor of Japan by Robert Dietz (Dietz, 1954)

To provide acoustic images of the stratigraphic and structural setting of the proposed site, a short underway geophysical survey was conducted. Hole 1205A was spudded ~100 m southwest of Site 432 over what appeared to be a broad sediment-filled (~70 m) swale in the surface of the main volcanic shield of Nintoku Seamount (Fig. F32). Coring sampled the entire sedimentary section before encountering basement at 42 mbsf, a depth similar to that reported at Site 432. Further penetration showed that the "sediment fill" was largely a stack of lava flows (~95%) with interbedded soil horizons. Coring continued to a final depth of 326 mbsf.

Five sediment cores (only 2%–16% recovery) established that Nintoku Seamount's sediment carapace consists of sandstone and siltstone containing well-rounded to subrounded basalt clasts (Fig. F33), volcanic ash, and fossil fragments of mollusks, benthic foraminifers, bryozoans, and coralline red algae. These observations document a relatively shallow-water, high-energy depositional environment. Further drilling in Hole 1205A penetrated 283 m into the volcanic basement of Nintoku Seamount and recovered parts of at least 25 different lava flow units (Fig. F34). Little systematic variation with depth was observed in average *P*-wave velocity, bulk density, grain density, and porosity, except for interbedded low-density, high-porosity soil horizons. It is presumed that these low-velocity interbeds are the underlying cause for the acoustically recorded layering in the upper 200–230 m of basement rock, below which the occurrence of soil horizons diminishes.

The age of the youngest volcanic rocks in Hole 1205A is constrained by nannofossils (Zone NP10) in the sediment immediately overlying

F24. Rotated, broken sediment block overlying thin, faulted, very finely laminated bed, p. 51.

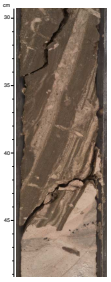

F25. Recovery, age, and lithology of basement units, Holes 1204A and 1204B, p. 52.

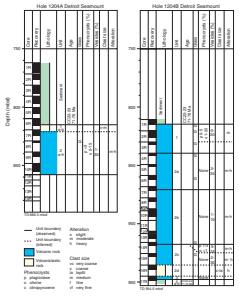

F26. Breccia with altered glass and vesicular basalt in carbonate cement, p. 53.

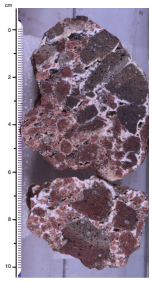

F27. Unaltered olivine and plagioclase laths in glassy lobe margin, p. 54.

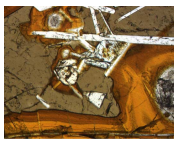

F28. Unaltered olivine and plagioclase laths in glassy lobe margin, p. 55.

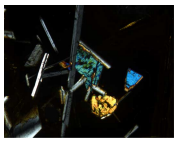

basement to be older than 53.6–54.7 Ma, an age range that is just younger than a radiometric age of 56.2 ± 0.6 Ma (Dalrymple et al., 1980) obtained for alkali basalt from nearby Hole 432A. The thickness and vesicularity of the flows from Site 1205 and the presence of oxidized flow tops and soil horizons, together with the lack of pillow structure indicate that the flows erupted subaerially. They range from aphyric to highly plagioclase and olivine-phyric basalt. At 230–255 mbsf, two flows of tholeiitic basalt are intercalated within alkalic basalt flows. Above these flows the degree of alkalinity tends to increase upsection. Interflow soil horizons are also most common in this interval, suggesting that eruption rates may have been lower during this period. Internal flow gradients in very thick lava flows have produced aligned groundmass crystals (Fig. F35) that help delineate flow structure. Clasts of hawaiite recovered in the basal conglomerate of the sedimentary section were not found as flow units in the underlying basement sequence.

Lavas from Nintoku Seamount have similar major element compositions to lavas erupted during the postshield stage of Hawaiian volcanoes such as Mauna Kea Volcano (Fig. F36). Slight differences in trace element composition between lavas from Nintoku Seamount and active Hawaiian volcanoes probably result from differences in source composition or variations in the degree of mantle melting (Fig. F37).

All the lava flows recovered at Site 1205 are only slightly altered except thin, highly weathered flow tops. The low-temperature (30°–60°C) alteration assemblage is homogeneous downhole and is composed of Fe oxyhydroxide, saponite and/or nontronite, celadonite, and zeolite. Veining is sparse, indicating only small-scale fluid circulation. In contrast to the first two sites (1203 and 1204) drilled during Leg 197 at Detroit Seamount, K_2O was not mobilized during alteration event(s) at Nintoku Seamount Site 1205.

Rock magnetic data (low-field magnetic susceptibilities, Koenigsberger ratios, and median destructive field values) obtained from oriented minicores suggest that the lava flows from Site 1205 carry a remanent magnetization suitable for paleolatitude analysis (Figs. F38, F39). Although the demagnetization characteristics of some samples indicate the need for thermal demagnetization studies, most samples yielded data suitable to make a preliminary determination of magnetic inclinations (Fig. F40).

Twenty-two independent paleomagnetic inclination groups were identified, yielding a mean (reversed polarity) inclination of –45.7° (+10.5°/–6.3°; 95% confidence interval) (Fig. F41). The preliminary mean inclination suggests a latitude of formation of an early Eocene Nintoku Seamount at 27.1° (+5.5°/–7.7°). This value, together with paleolatitudes from paleomagnetic analyses of basement rocks at DSDP Site 433 (Kono, 1980), Site 884 (Tarduno and Cottrell, 1997), and Sites 1203 and 1204 (Leg 197), form a consistent data set indicating southward motion of the Hawaiian hotspot from Late Cretaceous to early Tertiary time.

SITE 1206

Principal Results

The last and southernmost drilling site occupied during Leg 197, Site 1206, was located on the southeastern side of the lower summit terrace of Koko Seamount. Koko Seamount is a flat-topped seamount or guyot

F29. Ti vs. Zr for Detroit Seamount lavas, p. 56.

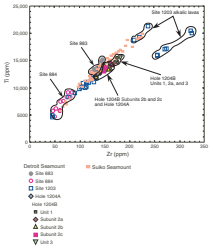

F30. Stable magnetic behavior in Hole 1204B basalt, p. 57.

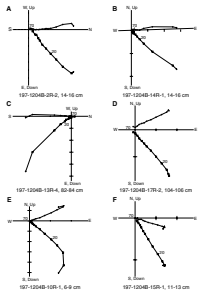

F31. Stable magnetic behavior in Hole 1204B diabase, p. 58.

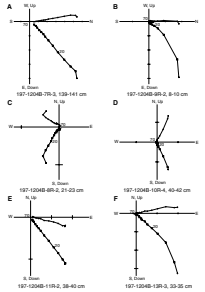

F32. Site 1205 survey 3, Line 4, migrated time section, p. 59.

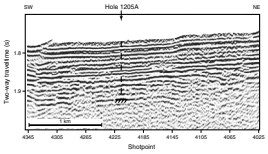

F33. Conglomerate with hawaiite clasts in fossiliferous sandy matrix, p. 60.

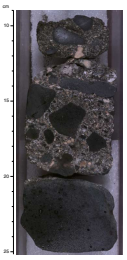

with a crowning ornamentation of small reefal bodies. It rises from the abyssal floor (~5000 m) of the western subtropical Pacific Basin at 35.3°N, thus just north of the "bend" (~32°N) in the ~5000-km-long Hawaiian-Emperor Seamount chain. The seamount was named by Thomas Davies and colleagues in 1972 for the 58th emperor of Japan (Davies et al., 1972).

A short seismic survey was conducted to locate a suitable structural and stratigraphic setting for Site 1206, which was initially targeted for the vicinity of DSDP Site 308, drilled in 1973 during Leg 32 (Larson, Moberly, et al., 1975). Weather conditions prevented Leg 32 from reaching basement during drilling at this site, which penetrated to a depth of 68.5 m in Koko Seamount's sediment cover. In consideration of the short time remaining in Leg 197 to conduct basement coring at Koko Seamount, a location was sought where a thin sedimentary section covered its main shield-building volcanic mass. Site 1206, at a water depth of ~1545 m, was located ~6.2 km south of Site 308 in an area where the surficial section of acoustically layered material, presumably all or mostly sedimentary beds, was less than one-half that recorded at Site 308 (Fig. **F42**). At Site 1206 (34°55.55′N, 172°8.75′E), basement was reached at a subsurface depth of 57 m. Coring continued to a depth of 335 mbsf, or 278 m into basement.

The top 57 m of sediment was washed through with the core barrel in place. Recovered debris in the wash core included fragments of fossiliferous calcarenite and calcareous mudstone and siltstone indicative of shallow-water depositional settings. The lower part of the wash core recovered a 15- to 20-cm-long section of laminated, shell debris–bearing mudstone containing a nannofossil assemblage typical of Zones NP14 and NP15, of the early to middle Eocene (43.5–49.7 Ma). This age range brackets a radiometric analysis (48.1 Ma) reported for a dredged rock (Clague and Dalrymple, 1973) from Koko Seamount. Although volcaniclastic beds commonly rich in shell fragments were recovered from Hole 1206A in the underlying sequence of volcanic basement rock, none of these deposits contained identifiable nannofossils.

Lava flows dominated the lithology in Hole 1206A, with smaller proportions of volcaniclastic beds and thin lenses of calcarenite (Fig. **F43**). Many lavas are pahoehoe flows interbedded with subordinate a'a units that show evidence of subaerial extrusion. A large degree of variability in bulk density, grain density, and porosity of these basement rocks was observed downcore. Although *P*-wave velocity varies widely (2215–4820 m/s) with depth, velocity correlates strongly with bulk density, and thus inversely with the degree of vesicularity. The bulk of the basalt flows are aphyric to olivine-phyric lava (Fig. **F44**) and tholeiitic or transitional to alkalic in composition. With respect to major and trace element geochemistry, the basaltic lavas from Koko Seamount resemble those drilled during DSDP Leg 55 at Suiko Seamount (Figs. **F45, F46**).

All the basalt flows recovered at Site 1206 are slightly altered, in the form of a patchy homogeneous assemblage of Fe oxyhydroxide, clay (brown clay, saponite, aliettite, and celadonite), carbonate, and zeolite. Unaltered olivine is characteristic of many of tholeiitic lava flows. The occurrence of aliettite (alternating talc and saponite-layered smectite), which expands in contact with water, caused the mechanical disintegration of some massive basalt intervals. Possibly, this phenomenon led to the onset of unstable hole conditions that, with respect to probable tool loss, made logging too risky to conduct.

Low-field magnetic susceptibilities, Koenigsberger ratios, and high median destructive field values (Figs. **F47, F48, F49**) suggested that the

F34. Recovery, thickness, composition, and lithology of Hole 1205A basement, p. 61.

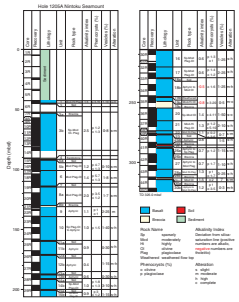

F35. Strain bands in trachytic texture, p. 62.

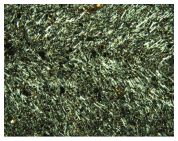

F36. Total alkali content vs. SiO_2 plot for Nintoku Seamount, p. 63.

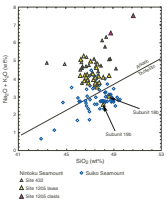

F37. Abundance of Y and Zr/Y vs. Zr, p. 64.

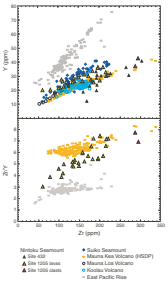

F38. Lowrie-Fuller tests on Site 1205 basalt samples, p. 65.

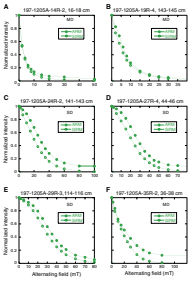

lava flow units from Hole 1206A carry a stable remanent magnetization and are suitable for the determination of preliminary paleomagnetic inclinations. Three early Tertiary polarity chrons were recognized in the lava flow units. Geomagnetic polarity reversals were not found at other Leg 197 sites. At Koko Seamount, 14 independent paleomagnetic inclination groups were identified, yielding a mean inclination of 38.5° (+8.4°/–10.9°; 95% confidence interval) (Fig. F50). The preliminary mean inclination of the lava flow units suggests a paleolatitude of 21.7° (+6.4°/–7.0°) for Koko Seamount.

The paleolatitude result gained at Koko Seamount strengthens confidence in the correctness of the implications of the paleomagnetically determined latitude of formation for Nintoku, Suiko, and Detroit Seamounts. These volcanic edifices, each located progressively north of Koko Seamount, also formed paleomagnetically progressively farther north of the present location of the Hawaii hotspot (~19°). Thus, singularly and as a linear group, the latitudes of formation of these four Emperor Seamounts establish that to reach its present position, the Hawaii hotspot moved rapidly southward during the Late Cretaceous and early Tertiary (i.e., from ~81 to 43 Ma).

SUMMARY

Paleomagnetism and the Hotspot Test

The main goal of Leg 197 was to obtain sufficient basement penetration at several Emperor Seamount sites to test the hypothesis that the Hawaiian hotspot migrated southward during Late Cretaceous to early Tertiary time. This hypothesis further challenges long-standing notions about the tectonic implications of the bend in the Hawaiian-Emperor Seamount chain. The bend is usually considered to represent a large change in Pacific plate motion at 43 Ma; this interpretation can be found in nearly all textbook descriptions of hotspots and plate motions.

Because of the record-setting basement penetration achieved during the leg, we were able to meet all of our goals. A key part of our study plan involved assessing whether secular variation had been averaged by lava flows recovered at a given site through a large number of shipboard paleomagnetic and rock magnetic measurements. These data have provided a firm basis both for an initial assessment of the results of the Leg 197 paleolatitude experiment and for guiding the shore-based work that must be completed to finalize the hotspot motion test.

Prior to the leg, only two time-averaged paleomagnetic data sets were available to address fixity of the Hawaiian hotspot during formation of the Emperor Seamounts. Paleolatitudes derived from analyses of basement cores recovered from Site 433 on Suiko Seamount (Kono, 1980) and Site 844 on Detroit Seamount (Tarduno and Cottrell, 1997) clearly differ from the latitude of Hawaii (~19°) (Fig. F4). Although each paleolatitude represents the summary of a large data set composed of many paleomagnetic measurements, rates of motion ultimately depend on paleolatitudes for many separate times; therefore, additional data were needed both to confirm the motion suggested and to better constrain potential hotspot drift rates. Our shipboard data allow us to draw preliminary conclusions on both of these aspects.

The paleolatitudes suggested from our preliminary paleomagnetic analysis of the basement cores recovered at Sites 1203, 1204, 1205, and

F39. Calculation of coercivity of remanence from Hole 1205A basalt, p. 66.

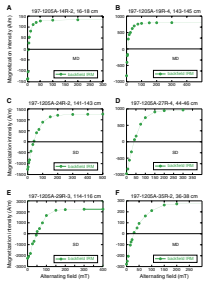

F40. Stable magnetic behavior in Site 1205 basalt, p. 67.

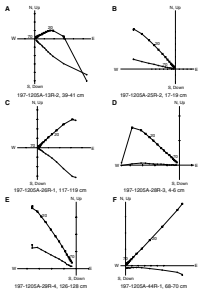

F41. Inclination values derived from Site 1205 lava flows, p. 68.

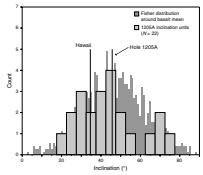

F42. Site 1206 survey 4, Line 6, finite-difference migrated time section, p. 69.

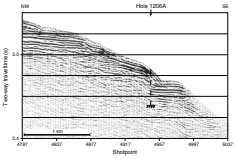

F43. Recovery, thickness, composition, and lithology of Hole 1206A basement, p. 70.

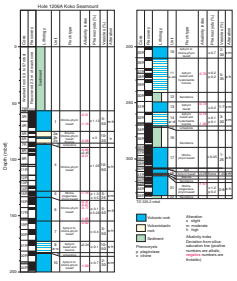

1206 also clearly differ from the latitude of Hawaii. The values are consistent with prior data from Suiko and Detroit Seamounts and the hypothesis that the Hawaiian hotspot moved southward from 81 to 43 Ma at rates of 30–50 mm/yr. These values, which are within the range of velocities typical of some lithospheric plates, force us to reconsider the cause of the Hawaiian-Emperor bend, rates of mantle convection, and Pacific plate reconstructions based on the fixed hotspot assumption. The latter issue is of particular interest for ODP studies, as Leg 198 and Leg 199 scientists will require accurate paleolatitude control in their studies of Paleogene paleoceanography in the Pacific Basin.

Whereas the implications of the Leg 197 shipboard paleomagnetic data are exciting and multifaceted, the results are nevertheless preliminary and must be supported by shore-based paleomagnetic, rock magnetic, and radiometric measurements. In particular, analyses employing detailed stepwise thermal demagnetization are needed to better resolve our estimates, which are currently based solely on alternating-field demagnetization data. Thermal demagnetization is necessary because secondary magnetic minerals with intermediate to high coercivities could carry important magnetizations that might contaminate the characteristic directions we have isolated in our shipboard analyses.

Evidence for such magnetic mineral carriers has indeed been found in cores from some sites (especially Site 1204), as recorded in observations under reflected-light microscopy and in the results of rock magnetic measurements. Additional shore-based rock magnetic analyses including magnetic hysteresis, Curie temperature, and low-temperature measurements are needed to further characterize the magnetic carriers in the basement rocks recovered at each site.

The shore-based thermal demagnetization and rock magnetic data hold the promise of achieving much more than confirming our preliminary paleolatitude values. Because thermal demagnetization is a more efficient means of magnetic cleaning than the application of alternating magnetic fields (given the presence of high-coercivity magnetic minerals), the data may allow us to better constrain the uncertainty limits of each paleolatitude data set. Several units with limited recovery were reserved for shore-based thermal demagnetization study; inclusion of data from these units will increase the precision of the mean paleolatitudes. In addition, for Sites 1205 and 1206 thermal demagnetization analysis of recovered soils and deeply weathered lava flow tops (Fig. **F51**) will provide paleolatitude constraints based on a natural recording medium that averages significantly more time than a given lava flow. Finally, the application of thermal demagnetization analyses together with a host of rock magnetic measurements will allow us to isolate and identify magnetic overprints. If properly understood, such overprints can be used to reorient cores and obtain paleodeclination information (Cottrell and Tarduno, in press). Complementary studies of zeolite assemblages in the recovered cores (Fig. **F52**) may allow us to constrain the temperatures responsible for magnetic overprints and use them with greater confidence for tectonic studies.

The principal motivation for obtaining paleodeclination data is to address predictions of relative plate motion studies (e.g., Cande et al., 1995) that call for a rotational component of Hawaiian hotspot motion during Late Cretaceous to early Tertiary time. In addition to the use of magnetic overprints, we will use FMS, general purpose inclinometer tool (GPIT), and Deutsche Montan Technologie (DMT) color scanner data to reorient basement cores. Veins and fractures have been imaged in the recovered cores with the DMT system (Fig. **F53**). Similar features

F44. Euhedral olivine with unaltered interior and altered rims, p. 71.

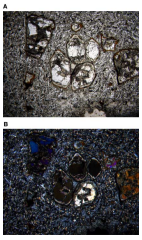

F45. Total alkali vs. SiO_2 for Koko Seamount basaltic lava flows, p. 72.

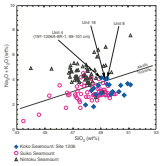

F46. Na_2O, K_2O, TiO_2, CaO, Al_2O_3, and Zr vs. MgO, p. 73.

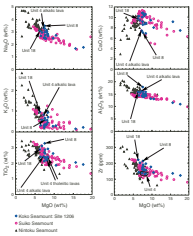

F47. Lowrie-Fuller tests on Site 1206 lava flow samples, p. 74.

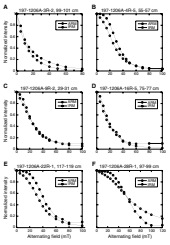

F48. Calculation of coercivity of remanence on Hole 1206A lava flows, p. 75.

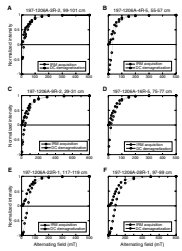

can be seen in the high-quality FMS images (which are automatically oriented with respect to north with the GPIT data) obtained from logging at Detroit Seamount Site 1203 (Fig. F54). We plan to use these data to orient declinations derived from core pieces having veins and fractures and to use the information to constrain a Late Cretaceous paleomagnetic pole for the Pacific plate.

Additional constraints on paleodeclination may become available through shore-based analyses of downhole data collected with the GBM. This was the first deployment of a magnetometer at an ODP site with a sensor to record tool rotation. Preliminary analyses of the data indicate the rotation history of the tool was successfully recorded (Fig. F55).

In addition to obtaining cores and data needed for the test of the hotspot hypothesis, during Leg 197 we recovered an outstanding collection of basement rocks that will be used to investigate inclination anomalies of geomagnetic origin. These anomalies, although much smaller than those associated with the debate over hotspot drift rates, are nevertheless important for our understanding of the geodynamo. In fact, because few data are available of Late Cretaceous to early Tertiary age from the Pacific region, the paleomagnetic data resulting from thermal demagnetization studies of the Leg 197 sites will carry considerable weight in efforts to study the geometry of the past geomagnetic field. Similarly, the recovery of basaltic glass and whole rocks with favorable rock magnetic characteristics bodes well for paleointensity investigations that will be part of postcruise science studies.

Source and Melting History of the Hawaiian Hotspot

One of the significant initial achievements of Leg 197 has been the setting of a new record for total basement penetration (1220 m; 52% recovery). This augurs well for a variety of planned postcruise investigations, including the long-term petrochemical variability of source and melting, volcano-stratigraphic and environmental setting of eruptions, the timing and duration of volcanism, and the cooling and alteration conditions of lava flows produced by the Hawaiian hotspot.

Observations of lava flow thickness, vesicularity, crystallinity, and morphology, together with analysis of volcaniclastic sediment, have provided a picture of eruptions in subaerial to shallow-water conditions at Detroit and Koko Seamounts and waning subaerial activity at Nintoku Seamount (Fig. F56). Further study of core material from all sites and integration with the downhole logging data, particularly FMS images from Site 1203 (Fig. F17), promises to reveal additional details about eruption rate, volume of flows, and distance from source.

From a limited number of shipboard geochemical measurements, we believe we have captured the transition from Hawaiian tholeiitic shield stage to alkalic postshield stage at each of the volcanic complexes. Between Sites 1203 and 1204 and previously studied Sites 883 and 884, we have a range of compositions at Detroit Seamount that covers most of the variability seen in the volcanoes of the island of Hawaii (Fig. F57). Site 1205 (Nintoku Seamount) basalt is dominantly alkalic but includes tholeiitic compositions, whereas Site 1206 (Koko Seamount) basalt is dominantly tholeiitic but includes alkalic basalt compositions. We did not sample any of the posterosional stage of evolved compositions that occur at the end of Hawaiian island volcanic activity, except as cobbles in a conglomerate above basement at Site 1205.

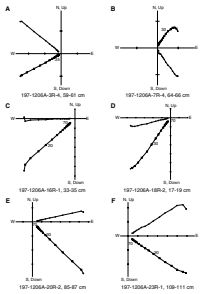

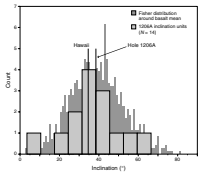

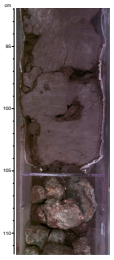

We have hints that we have sampled different source compositions through the variability of trace element ratios, such as Ti/Zr (Fig. **F58**). It will remain for shore-based studies of additional trace elements and isotopic compositions (Sr, Nd, Pb, Hf, and He) to evaluate and define these suspected source heterogeneities. We are assured, however, that appropriate material has been recovered in the cores for such a comprehensive geochemical program. Unaltered olivine (Fig. **F59**), which will be separated for He isotopic studies, was observed at all sites. We will probe melt inclusions in olivine and feldspar (Fig. **F60**) to discover parental melt compositions. Fresh glass is common and will be the source of information about melt volatile content and magma evolution. The latter subject will also be addressed through studies of zoned feldspar phenocrysts (Fig. **F10**). Opaque minerals provide a rich source of information about cooling rates of lava flows and subsequent alteration history (Fig. **F61**). Low-temperature alteration will be studied through the composition of secondary minerals in multiple generations of vesicle and vein fillings (Fig. **F62**).

Time is an important aspect of the volcanic history recorded at each site. Excellent material was recovered for both mineral (feldspar) and whole-rock age determinations to estimate the timing and duration of volcanism through ^{40}Ar-^{39}Ar incremental heating radiometric dating. In particular, the evidence for prolonged volcanic activity (soil horizons at Site 1205 and alternating shallow-water volcaniclastic sediment with subaerial lava flows at Site 1206) will be investigated, as will the apparent underestimate of current ages from Nintoku and Koko Seamounts relative to the long-term age progression within the Emperor Seamounts (Clague and Dalrymple, 1987).

F54. Fractures and veins seen in FMS images, p. 81.

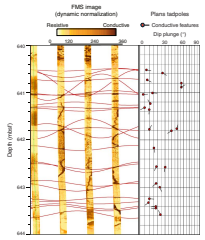

F55. Rotation about the vertical axis for the magnetometer tool, Site 1203, p. 82.

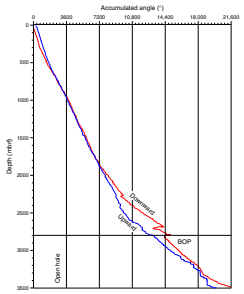

F56. Inferred volcanic environments at Detroit, Nintoku, and Koko Seamounts, p. 83.

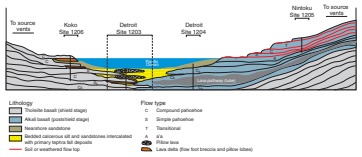

F57. Total alkalis vs. SiO_2 for Detroit, Nintoku, and Koko Seamounts, p. 84.

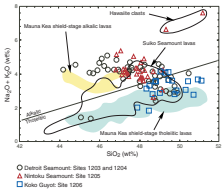

F58. Ti/Zr and alkalinity vs. depth in basalt from Detroit, Nintoku, and Koko Seamounts, p. 85.

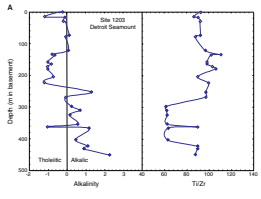

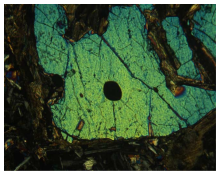

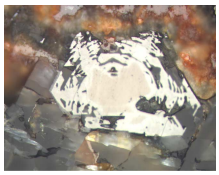

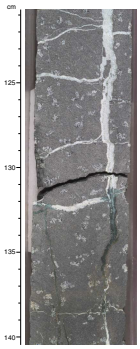

REFERENCES

Acton, G.D., and Gordon, R.G., 1994. Paleomagnetic tests of Pacific plate reconstructions and implications for motions between hotspots. *Science,* 263:1246–1254.

Arason, P., and Levi, S., 1990. Compaction and inclination shallowing in deep-sea sediments from the Pacific Ocean. *J. Geophys. Res.,* 95:4501–4510.

Atwater, T., 1989. Plate tectonic history of the northeast Pacific and western North America. *In* Winterer, E.L., Hussong, D.M., and Decker, R.W. (Eds.), *The Eastern Pacific Ocean and Hawaii,* Geol. Soc. Am., Geol. of North America Ser., N:21–72.

Berggren, W.A., Kent, D.V., Swisher, C.C., III, and Aubry, M.-P., 1995. A revised Cenozoic geochronology and chronostratigraphy. *In* Berggren, W.A., Kent, D.V., Aubry, M.-P., and Hardenbol, J. (Eds.), *Geochronology, Time Scales and Global Stratigraphic Correlation.* Spec. Publ.—Soc. Econ. Paleontol. Mineral. (Soc. Sediment. Geol.), 54:129–212.

Besse, J., and Courtillot, V., 1991. Revised and synthetic apparent polar wander paths of African, Eurasian, North American and Indian plates, and true polar wander since 200 Ma. *J. Geophys. Res.,* 96:4029–4051.

Cande, S.C., Raymond, C.A., Stock, J., and Haxby, W.F., 1995. Geophysics of the Pitman Fracture Zone and Pacific-Antarctic plate motions during the Cenozoic. *Science,* 270:947–953.

Celaya, M.A., and Clement, B.M., 1988. Inclination shallowing in deep sea sediments from the North Atlantic. *Geophys. Res. Lett.,* 15:52–55.

Chen, C.-Y., and Frey, F.A., 1985. Trace element and isotopic geochemistry of lavas from Haleakala Volcano, East Maui, Hawaii: implications for the origin of Hawaiian basalts. *J. Geophys. Res.,* 90:8743–8768.

Christensen, U., 1998. Fixed hotspots gone with the wind. *Nature,* 391:739–740.

Clague, D.A., and Dalrymple, G.B., 1973. Age of Koko Seamount, Emperor Seamount chain. *Earth. Planet. Sci. Lett.,* 17:411–415.

————, 1987. The Hawaiian-Emperor volcanic chain, Part I. Geologic evolution. *In* Decker, R.W., Wright, T.L., and Stauffer, P.H. (Eds.), *Volcanism in Hawaii.* Geol. Surv. Prof. Pap. U.S., 1350:5–54.

Coe, R.S., 1967. Paleo-intensities of the Earth's magnetic field determined from Tertiary and Quaternary rocks. *J. Geophys. Res.,* 72:3247–3262.

Constable, C., 1992. Link between geomagnetic reversal paths and secular variation of the field over the past 5 Myr. *Nature,* 358:230–233.

Cottrell, R.D., and Tarduno, J.A., 1997a. Magnetic hysteresis properties of single crystals: prelude to paleointensity studies, Suppl. *Eos,* Am. Geophys. Union, 78:F185.

————, 1997b. Tectonic and paleoclimatic implications of a high latitude Late Cretaceous pole position for the Pacific plate. Suppl. *Eos,* Am. Geophys. Union, 78:S117.

————, 2000a. In search of high fidelity geomagnetic paleointensities: a comparison of single plagioclase crystal and whole rock Thellier-Thellier analyses. *J. Geophys. Res.,* 105:23579–23594.

————, 2000b. Late Cretaceous true polar wander: not so fast. *Science,* 288:2283a.

————, in press. A Late Cretaceous pole for the Pacific plate: implications for apparent and true polar wander and the drift of hotspots. *Tectonophysics.*

Cox, A.V., 1970. Latitude dependence of the angular dispersion of the geomagnetic field. *Geophys. J. R. Astron. Soc.,* 20:253–269.

Dalrymple, G.B., Lanphere, M.A., and Clague, D.A., 1980. Conventional and $^{40}Ar/^{39}Ar$ K-Ar ages of volcanic rocks from Ojin (Site 430), Nintoku (Site 432) and Suiko (Site 433) Seamounts and the chronology of volcanic propagation along the Hawaiian-Emperor chain. *In* Jackson, E.D., Koizumi, I., et al., *Init. Repts. DSDP,* 55: Washington (U.S. Govt. Printing Office), 659–676.

Davies, T.A., Wilde, P., and Clague, D.A., 1972. Koko Seamount: a major guyot at the southern end of the Emperor Seamounts. *Mar. Geol.,* 13:311–321.

Dietz, R.S., 1954. Marine geology of northwestern Pacific: description of Japanese bathymetric chart 6901. *Geol. Soc. Am. Bull.,* 65:1199–1224.

Duncan, R.A., and Clague, D.A., 1985. Pacific plate motion recorded by linear volcanic chains. *In* Nairn, A.E.M., Stehli, F.G., and Uyeda, S. (Eds.), *The Ocean Basins and Margins* (Vol. 7A): *The Pacific Ocean:* New York (Plenum), 89–121.

Duncan, R.A., Petersen, N., and Hargraves, R.B., 1972. Mantle plumes, movement of the European plate, and polar wandering. *Nature,* 239:82–86.

Duncan, R.A., and Richards, M.A., 1991. Hotspots, mantle plumes, flood basalts, and true polar wander. *Rev. Geophys.,* 29:31–50.

Fisher, F.A., 1953. Dispersion on a sphere. *Proc. R. Soc. London A,* 217:295–305.

Frey, F.A., Garcia, M.O., Wise, W.S., Kennedy, A., Gurriet, P., Albarede, F., 1991. The evolution of Mauna Kea Volcano, Hawaii; petrogenesis of tholeiitic and alkalic basalts. *J. Geophys. Res.,* 96:14347–14375.

Frey, F.A., Wise, W.S., Garcia, M.O., West, H., Kwon, S.T., Kennedy, A., 1990. Evolution of Mauna Kea Volcano, Hawaii; petrologic and geochemical constraints on postshield volcanism. *J. Geophys. Res.,* 95:1271–1300.

Garcia, M.O., Ito, E., Eiler, J.M., and Pietruszka, A.J., 1998. Crustal contamination of Kilauea Volcano magmas revealed by oxygen isotope analyses of glass and olivine from puu oo eruption lavas. *J. Petrol.,* 39:803–817.

Gee, J., Staudigel, H., and Tauxe, L., 1989. Contribution of induced magnetization to magnetization of seamounts. *Nature,* 342:170–173.

Goldreich, P., and Toomre, A., 1969. Some remarks on polar wandering. *J. Geophys. Res.,* 74:2555–2567.

Gordon, R.G., 1983. Late Cretaceous apparent polar wander of the Pacific plate: evidence for a rapid shift of the Pacific hotspots with respect to the spin axis. *Geophys. Res. Lett.,* 10:709–712.

Gordon, R.G., and Cape, C., 1981. Cenozoic latitudinal shift of the Hawaiian hotspot and its implications for true polar wander. *Earth Planet. Sci. Lett.,* 55:37–47.

Gromme, S., and Vine, F.J., 1972. Paleomagnetism of Midway atoll lavas and northward movement of the Pacific plate. *Earth Planet. Sci. Lett.,* 17:159–168.

Hargraves, R.B., and Duncan, R.A., 1973. Does the mantle roll? *Nature,* 245:361–363.

Holt, J.W., Kirschvink, J.L., and Garnier, F., 1996. Geomagnetic field inclinations for the past 400 kyr from the 1-km core of the Hawaii Scientific Drilling Project. *J. Geophys. Res.,* 101:11655–11663.

Huber, B.T., Hodell, D.A., and Hamilton, C.P., 1995. Mid- to Late Cretaceous climate of the southern high latitudes: stable isotopic evidence for minimal equator-to-pole thermal gradients. *Geol. Soc. Am. Bull.,* 107:1164–1191.

Juarez, M.T., Tauxe, L., Gee, J.S., and Pick, T., 1998. The intensity of the Earth's magnetic field over the past 160 million years. *Nature,* 394:878–881.

Keller, R.A., Duncan, R.A., and Fisk, M.R., 1995. Geochemistry and $^{40}Ar/^{39}Ar$ geochronology of basalts from ODP Leg 145 (North Pacific Transect). *In* Rea, D.K., Basov, I.A., Scholl, D.W., and Allan, J.F. (Eds.), *Proc. ODP, Sci. Results,* 145: College Station, TX (Ocean Drilling Program), 333–344.

Keller, R.A., Fisk, M.R., and White, W.M., 2000. Isotopic evidence for Late Cretaceous plume-ridge interaction at the Hawaiian hotspot. *Nature,* 405:673–676.

Kono, M., 1980. Paleomagnetism of DSDP Leg 55 basalts and implications for the tectonics of the Pacific plate. *In* Jackson, E.D., Koizumi, I., et al., *Init. Repts. DSDP,* 55: Washington (U.S. Govt. Printing Office), 737–752.

Lanphere, M.A., Dalrymple, G.B., and Clague, D.A., 1980. Rb-Sr systematics of basalts from the Hawaiian-Emperor volcanic chain. *In* Jackson, E.D., Koizumi, I., et al., *Init. Repts. DSDP,* 55: Washington (U.S. Govt. Printing Office), 695–705.

Larson, R.L., Moberly, R., et al., 1975. *Init. Repts. DSDP,* 32: Washington (U.S. Govt. Printing Office).

Le Bas, M.J., Le Maitre, R.W., Streckeisen, A., and Zanettin, B., 1986. A chemical classification of volcanic rocks based on the total alkali-silica diagram. *J. Petrol.* 27:745–750.

Livermore, R.A, Vine, F.J., and Smith, A.G., 1984. Plate motions and the geomagnetic field. II. Jurassic to Tertiary. *Geophys. J. R. Astron. Soc.,* 79:939–961.

Lonsdale, P., Dieu, J., and Natland, J., 1993. Posterosional volcanism in the Cretaceous part of the Hawaiian hotspot trail. *J. Geophys. Res.,* 98:4081–4098.

Lowrie, W., and Fuller, M., 1971. On the alternating field demagnetization characteristics of multidomain thermoremanent magnetization in magnetite. *J. Geophys. Res.,* 76:6339–6349.

Macdonald, G.A., and Katsura, T., 1964. Chemical composition of Hawaiian lavas. *J. Petrol.,* 5:82–133.

Mammerickx, J., and Sharman, G.F., 1988. Tectonic evolution of the North Pacific during the Cretaceous Quiet Period. *J. Geophys. Res.,* 93:3009–3024.

McElhinny, M.W., 1973. Mantle plumes, palaeomagnetism, and polar wandering. *Nature,* 241:523–524.

McFadden, P.L., Merrill, R.T., McElhinny, M.W., and Lee, S., 1991. Reversals of the Earth's magnetic field and temporal variations of the dynamo families. *J. Geophys. Res.,* 96:3923–3933.

McFadden, P.L., and Reid, A.B., 1982. Analysis of paleomagnetic inclination data. *Geophys. J. R. Astron. Soc.,* 69:307–319.

Molnar, P., and Atwater, T., 1973. Relative motion of hotspots in the mantle. *Nature,* 246:288–291.

Molnar, P., and Stock, J., 1987. Relative motions of hotspots in the Pacific, Atlantic, and Indian Oceans since Late Cretaceous time. *Nature,* 327:587–591.

Morgan, W.J., 1971. Convection plumes in the lower mantle. *Nature,* 230:42–43.

Norton, I.O., 1995. Plate motions in the North Pacific: the 43 Ma nonevent. *Tectonics,* 14:1080–1094.

Parker, R.L., 1991. A theory of ideal bodies for seamount magnetization. *J. Geophys. Res.,* 96:16101–16112.

Pick, T., and Tauxe, L., 1993. Geomagnetic paleointensities during the Cretaceous Normal Superchron measured using submarine basaltic glass. *Nature,* 366:238–242.

Rea, D.K., Basov, I.A., Krissek, L.A., and the Leg 145 Scientific Party, 1995. Scientific results of drilling the North Pacific transect. *In* Rea, D.K., Basov, I.A., Scholl, D.W., and Allan, J.F. (Eds.), *Proc. ODP, Sci. Results,* 145: College Station, TX (Ocean Drilling Program), 577–596.

Rhodes, J.M., 1996. Geochemical stratigraphy of lava flows sampled by the Hawaii Scientific Drilling Project. *J. Geophys. Res.,* 101:11729–11746.

Sager, W., and Bleil, U., 1987. Latitudinal shift of Pacific hotspots during the Late Cretaceous and early Tertiary. *Nature,* 326:488–490.

Sager, W.W., and Pringle, M.S., 1988. Mid-Cretaceous to early Tertiary apparent polar wander path of the Pacific plate. *J. Geophys. Res.,* 93:11753–11771.

Solomon, S.C., Sleep, N.H., and Jurdy, D.M., 1977. Mechanical models for absolute plate motions in the early Tertiary. *J. Geophys. Res.,* 82:203–213.

Steinberger, B., 1996. Motion of hotspots and changes of the Earth's rotation axis caused by a convecting mantle. [Ph.D. Thesis]. Harvard Univ., Cambridge, MA.

————, 2000. Plumes in a convecting mantle: models and observations for individual hotspots. *J. Geophys. Res.,* 105:11127–11152.

Steinberger, B., and O'Connell, R.J., 1997. Changes of the Earth's rotation axis owing to advection of mantle density heterogeneities. *Nature,* 387:169–173.

————, 1998. Advection of plumes in mantle flow: implications for hotspot motion, mantle viscosity and plume distribution. *Geophys. J. Int.,* 132:412–434.

Tarduno, J.A., 1990. Absolute inclination values from deep sea sediments: a reexamination of the Cretaceous Pacific record. *Geophys. Res. Lett.,* 17:101–104.

Tarduno, J.A., and Cottrell, R.D., 1997. Paleomagnetic evidence for motion of the Hawaiian hotspot during formation of the Emperor Seamounts. *Earth Planet. Sci. Lett.,* 153:171–180.

Tarduno, J.A., Cottrell, R.D., and Smirnov, A.V., 2001. High geomagnetic field intensity during the mid-Cretaceous from Thellier analyses of single plagioclase crystals. *Science,* 291:1179–1183.

Tarduno, J.A., and Gee, J., 1995. Large scale motion between Pacific and Atlantic hotspots. *Nature,* 378:477–480.

Tarduno, J.A., and Sager, W.W., 1995. Polar standstill of the mid-Cretaceous Pacific plate and its geodynamic implications. *Science,* 269:956–959.

Tarduno, J.A., and Smirnov, A.V., 2001. Stability of the Earth with respect to the spin axis for the last 130 million years. *Earth Planet. Sci. Lett.,* 184:549–553.

Thellier, E., and Thellier, O., 1959. Sur l'intensité du champ magnétique terreste dans le passé historique et geologique. *Ann. Geophys.,* 15:285–375.

Vasas, S.M., Gordon, R.G., and Petronotis, K.E., 1994. New paleomagnetic poles for the Pacific plate from analysis of the shapes of anomalies 33N and 33R. *Eos,* Trans. Am. Geophys. Union, 75:203.

Wessel, P., and Kroenke, L.W., 1998. Factors influencing the locations of hotspots determined by the hot-spotting technique. *Geophys. Res. Lett.,* 25:555–558.

Yang, H.-J., Frey, F.A., Rhodes, J.M., Garcia, M.O., 1996. Evolution of Mauna Kea Volcano: inferences from lava compositions recovered in the Hawaii Scientific Drilling Project. *J. Geophys. Res.,* 101:11747–11767.

Zachos, J.C., Stott, L.D., and Lohmann, K.C., 1994. Evolution of early Cenozoic marine temperatures. *Paleoceanography,* 9:353–387.

Figure F1. Location of Leg 197 sites and previous DSDP and ODP sites on the Emperor Seamounts (solid circles).

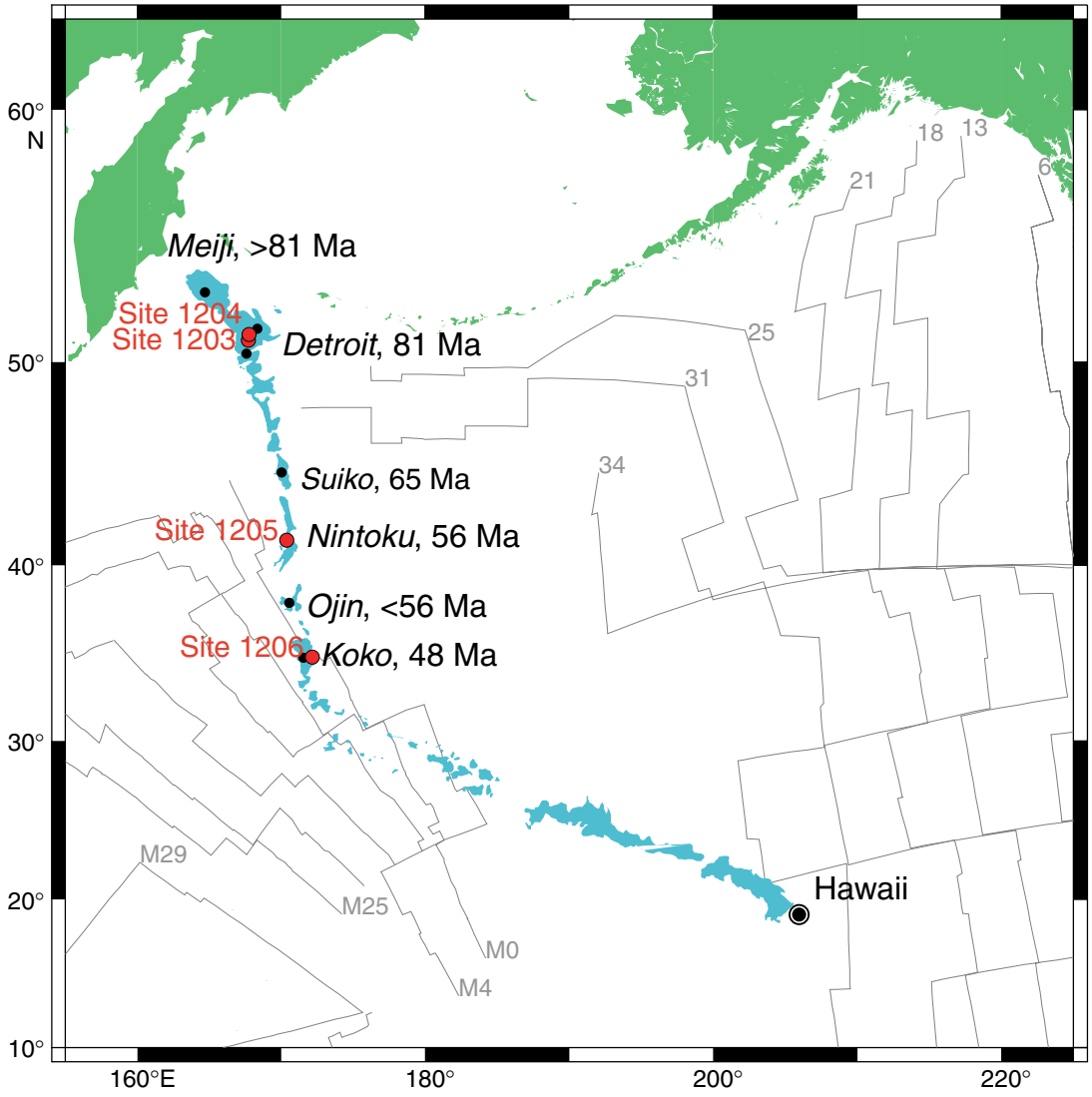

Figure F2. A. Preferred viscosity structure used to calculate hotspot motion from Steinberger and O'Connell (1998). A low-viscosity upper mantle is used to reproduce the Hawaiian-Emperor bend. A high-viscosity lower mantle is employed; otherwise, the relative motions between hotspots are greater than observations. Harvard tomographic model S12WM13 was used to infer mantle density heterogeneities. The gradual increase in viscosity was chosen to minimize disagreement with models based on postglacial rebound, which mainly constrain viscosity in the upper half of the mantle. **B.** The predicted motion of the Hawaiian plume between 90 and 43 Ma (after Steinberger, 2000). The model predicts a southward component of motion of ~10 mm/yr. This result is from the mantle flow at depth, which also tends to have a southward component of the same magnitude, partly due to a return flow opposite of Pacific plate motion in the model. The model predicts only a small relative motion between the Hawaiian and Louisville hotspots, in accordance with the age progressions observed along the two hotspot tracks. Other models with a lower viscosity in the lower mantle predict substantially higher flow speeds and substantially larger southward motion of the Hawaiian hotspot.

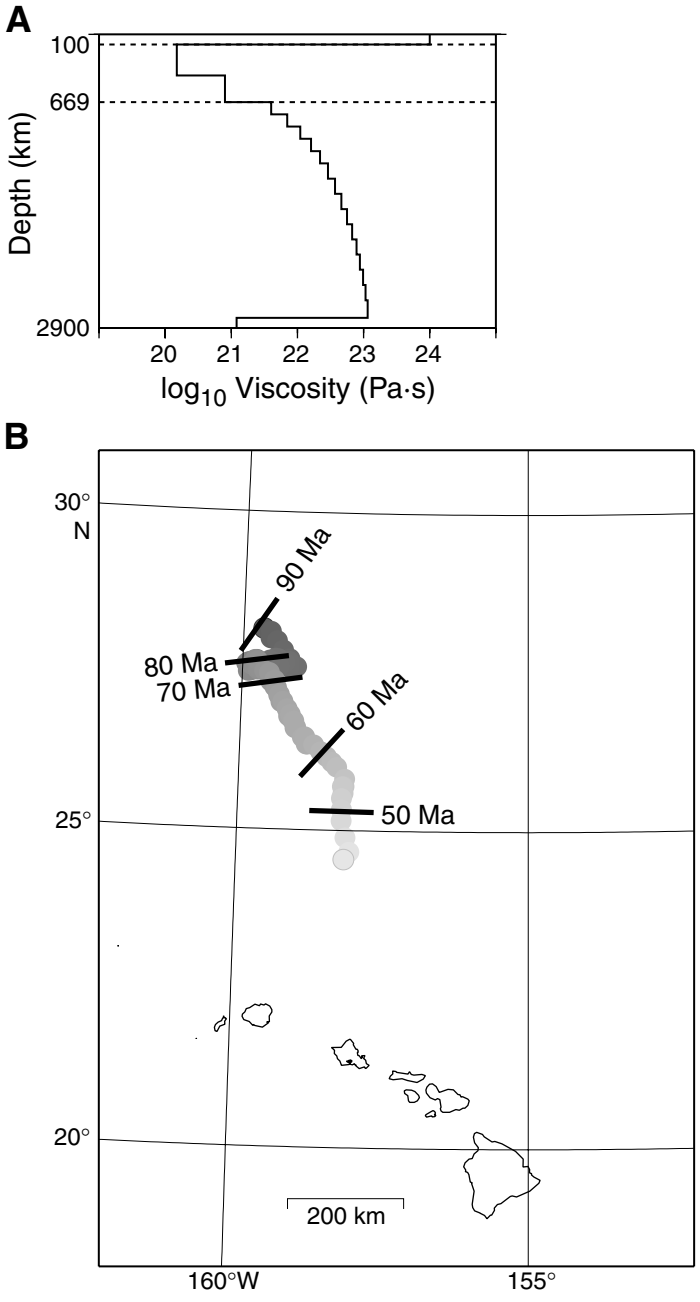

Figure F3. A. Average inclination values for three inclination group models from Detroit Seamount; error bars = 95% confidence intervals. The predicted inclination at 81 Ma based on prior Pacific apparent polar wander path (APWP) poles (Gordon, 1983) is also shown. **B.** Paleolatitude values with 95% confidence intervals for the inclination groups. The present-day latitude of the Hawaiian hotspot (solid line) is also shown. **C.** Estimated angular dispersion (*S*) of the inclination groups (solid line) vs. the predicted values for 45–80 Ma (dark field) and 80–110 Ma (light field) from McFadden et al. (1991). VGP = virtual geomagnetic pole. **D.** Orthographic projection of the colatitude (primary) for Detroit Seamount (star). The colatitude is distinct at the 99% confidence level (shaded) from previous 81–82 Ma poles (ellipses). Poles are derived from the following: 81 Ma (Gordon, 1983), 82 Ma (Sager and Pringle, 1988), and 33n (79.1–73.6 Ma) (Vasas et al., 1994). The sense of offset between the natural remanent magnetization data and the demagnetized (primary) data is the same as that between the new paleolatitude result and results based on prior Pacific pole positions. This is the expected effect if these previous pole positions are contaminated by secondary magnetizations. This figure is after Tarduno and Cottrell (1997).

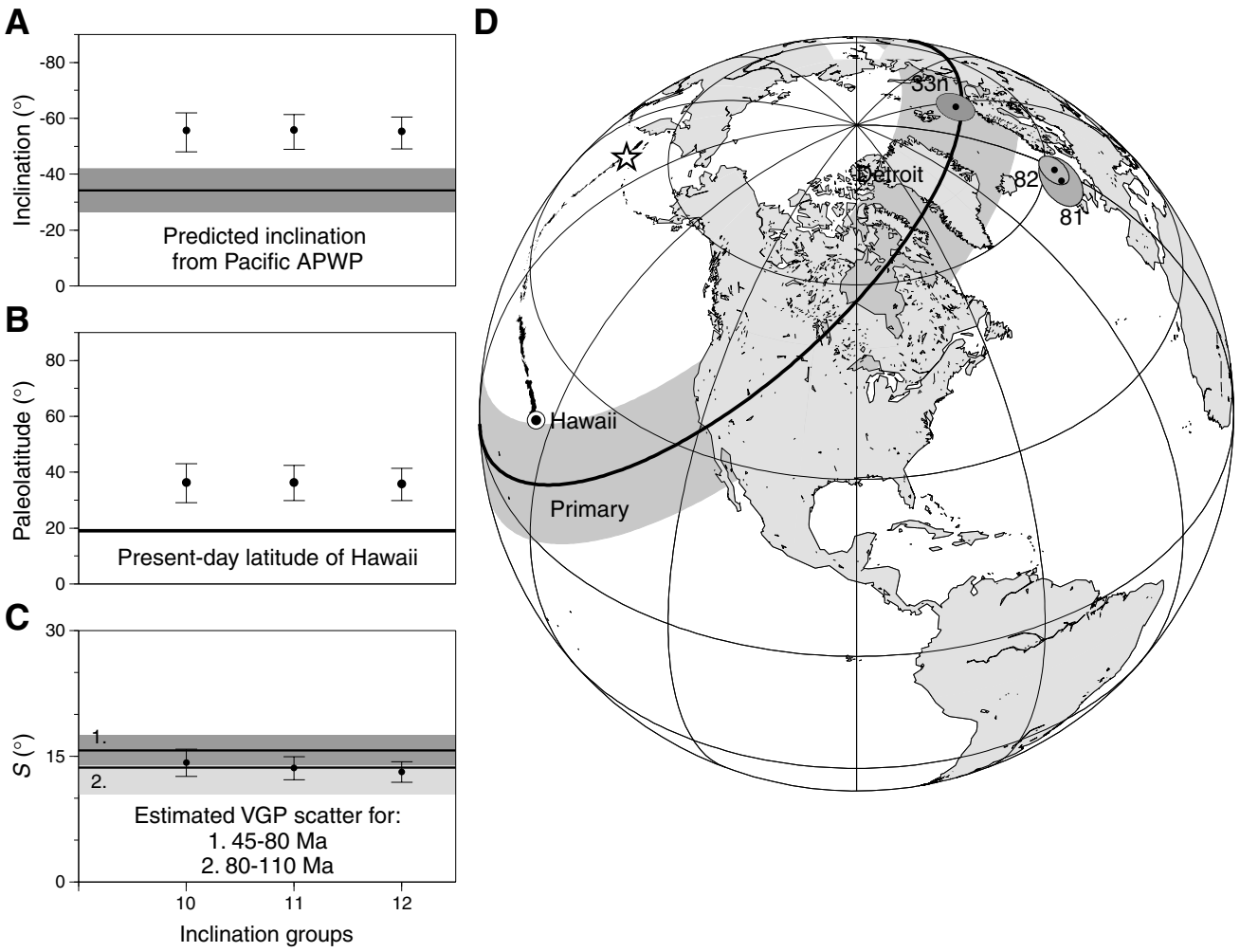

Figure F4. Plot of latitudinal distance from the 43-Ma bend in the Hawaiian-Emperor hotspot track vs. age (light circles). Age data are not available for Meiji, Tenchi, and Jimmu Seamounts; their positions, based on a constant latitudinal progression, are shown for reference. Dark circles indicate positions after the difference between the present-day latitude of the 43-Ma bend and Hawaii is subtracted from each of the present-day latitudes of the Emperor Seamounts. In effect, we slide the Emperor trend down the Hawaiian chain so that the bend coincides with the position of Hawaii (inset). This reconstruction allows the following test. If the Emperor Seamounts record mainly motion of the Hawaiian hotspot, paleolatitudes should fall close to this corrected latitudinal trend; if the hotspot has been stationary, the paleolatitudes should fall close to the present-day latitude of Hawaii. Triangles = paleolatitudes of Suiko and Detroit Seamounts, with 95% confidence intervals. The null hypothesis that the paleolatitude result from the Suiko Seamount is drawn from the same population as the Detroit Seamount data can be rejected at the 95% confidence level using nonparametric tests (Kolmogorov-Smirnov). In the absence of a rotation of the entire Earth with respect to the spin axis, known as true polar wander (Tarduno and Cottrell, 1997; Cottrell and Tarduno, 2000b; Tarduno and Smirnov, 2001), the hotspot may have moved continuously southward at a rate of 30–50 mm/yr while the plate also drifted slowly northward (shaded area). This figure is after Tarduno and Cottrell (1997).

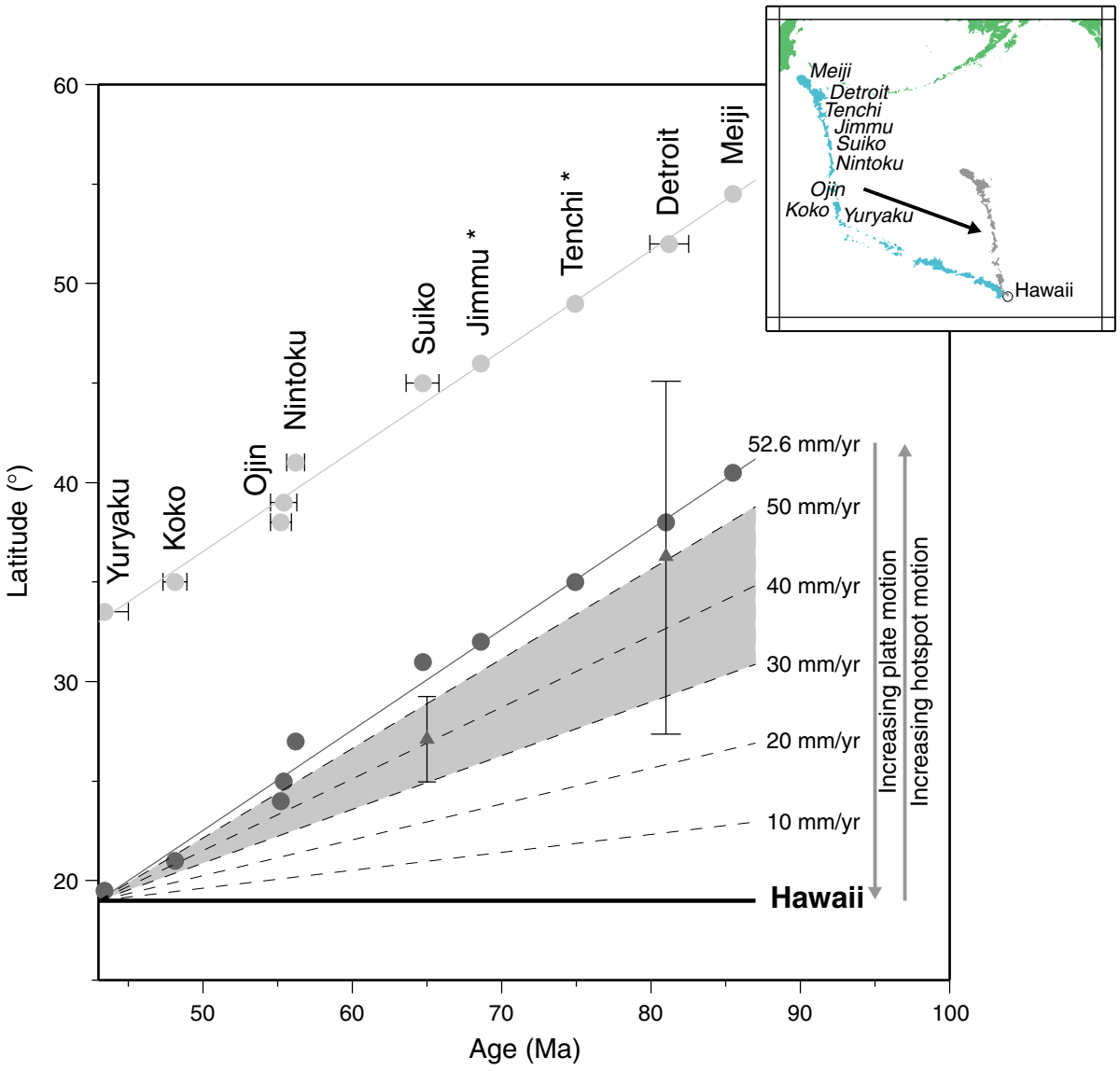

Figure F5. A. Estimates of zonal quadrupole Gauss coefficients (g_2^0) relative to the axial dipole (g_1^0), from Livermore et al. (1984). Pacific data are rotated using a fixed hotspot reference frame (see model "B" in Livermore et al., 1984). Our proposed sampling covers the range where Livermore et al. (1984) propose a change in sign of the quadrupole term. **B.** Paleointensity determined from studies of submarine basaltic glass complied by Juarez et al. (1998). The proposed sampling covers the transition from the Cretaceous Normal Polarity Superchron (K-N) to the Late Cretaceous–Cenozoic mixed polarity interval. VADM = virtual axial dipole moment.

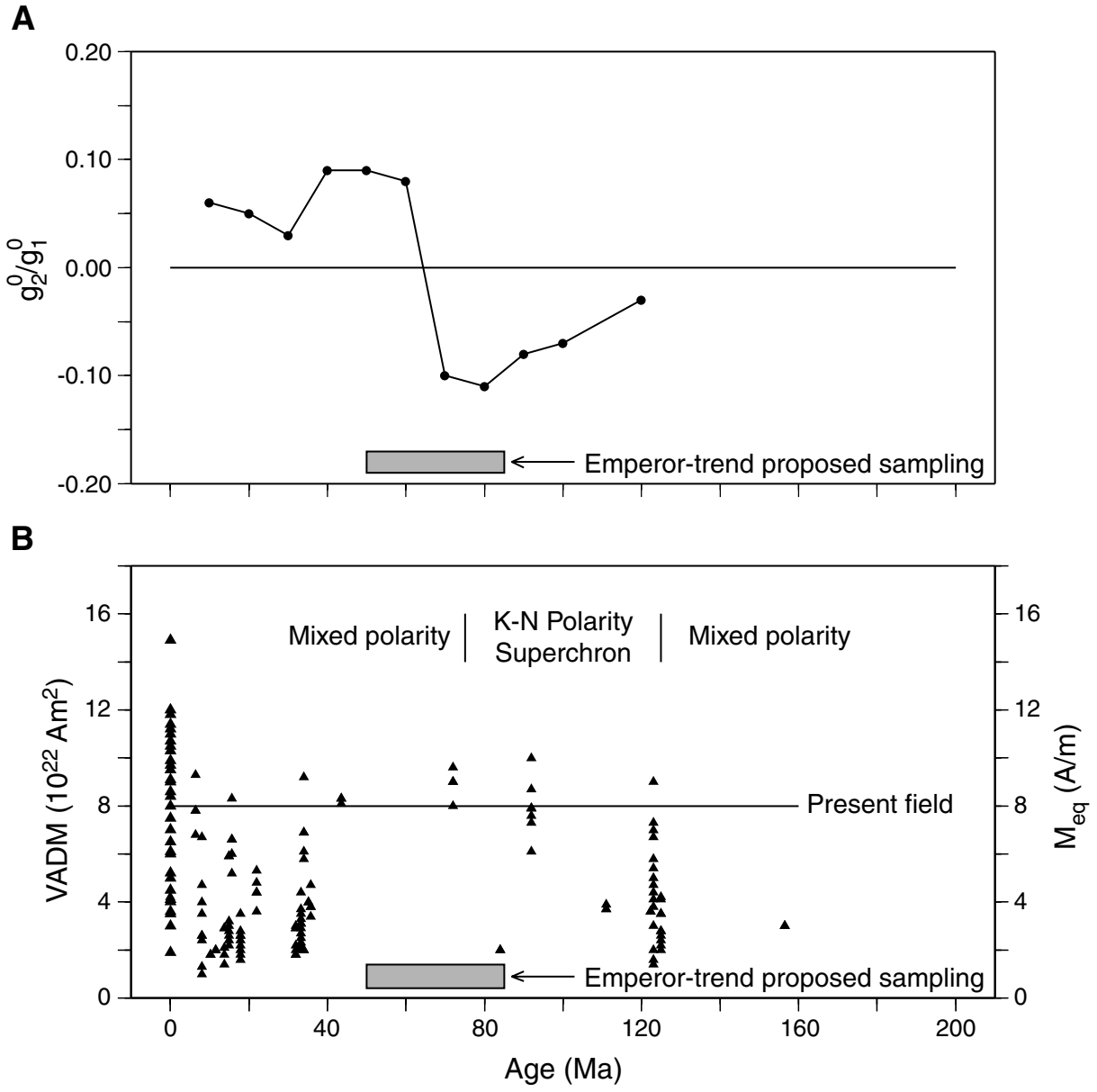

Figure F6. Compositional changes in magmas produced by the Hawaiian hotspot through time. The shaded field shows the range of published $^{87}Sr/^{86}Sr$ ratios of tholeiitic basalt vs. age and distance along the Hawaiian-Emperor chain. Note that data from Detroit Seamount are significantly less radiogenic than those from younger volcanoes. The circles with crosses connected by the thick dotted line show the trend in age difference between seamounts and the underlying ocean crust (from Keller et al., 2000).

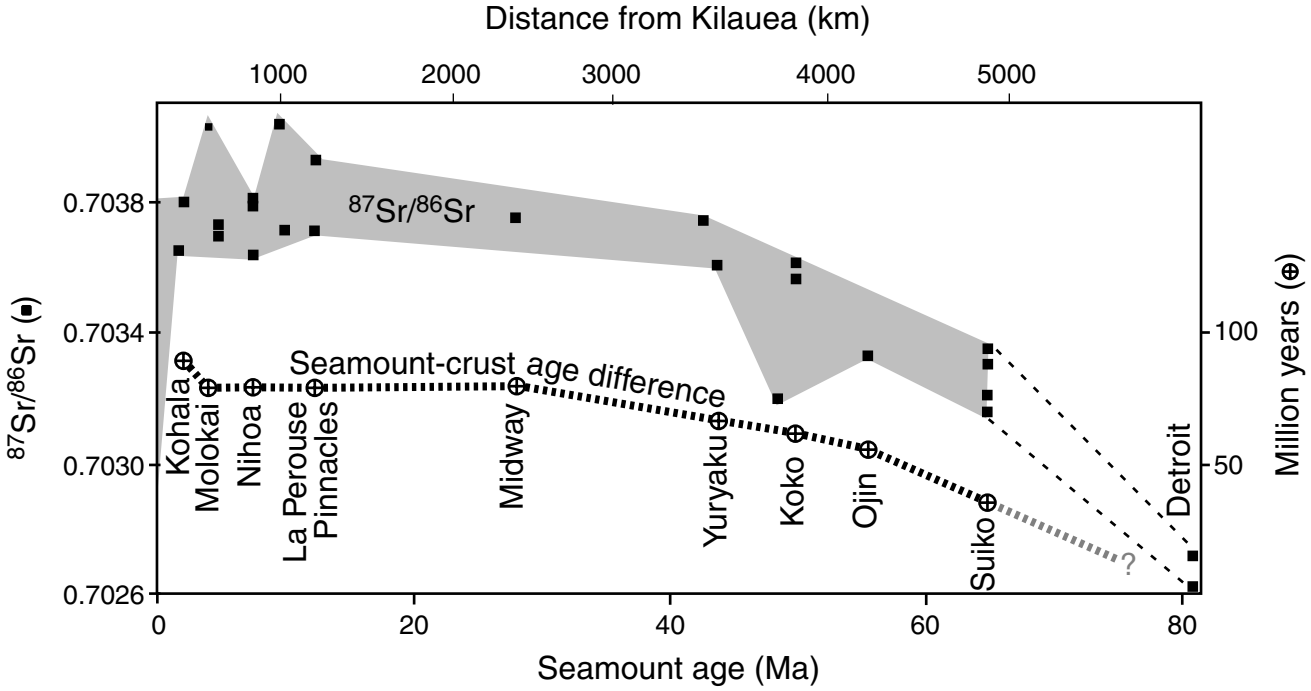

Figure F7. Site 1203 survey 1, Line 6, 5-km-long migrated time section. Data are bandpass filtered between 40 and 100 Hz. Hole 1203A is situated at about shotpoint 7780. Trace-to-trace distance = ~18.8 m; vertical exaggeration at the seafloor = ~3:1; bottom of hole = ~4.34 s two-way traveltime.

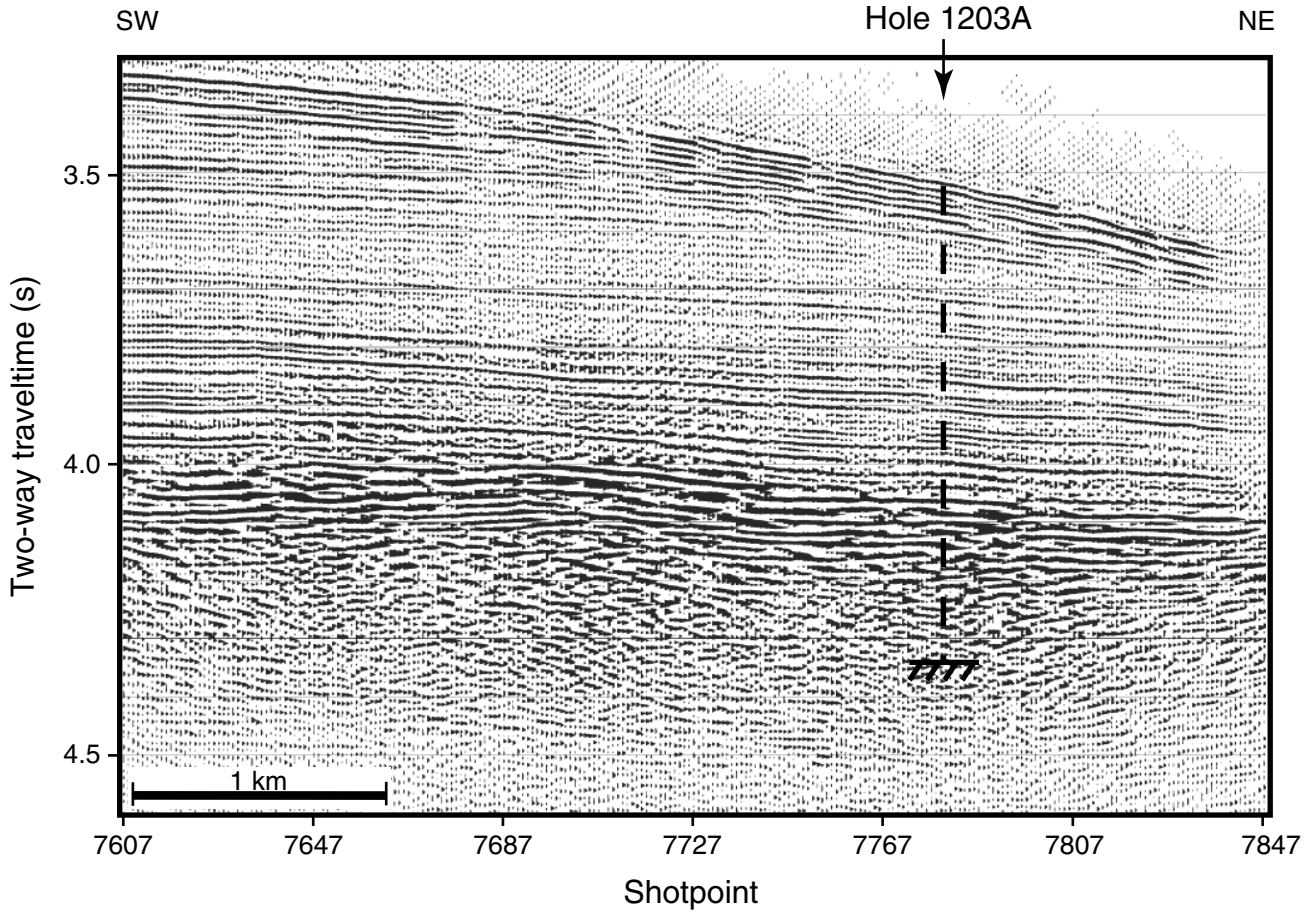

Figure F8. Summary of Site 1203 basement rocks and biostratigraphic ages with provisional downhole logging data for comparison. TD = total depth. (Continued on next page.)

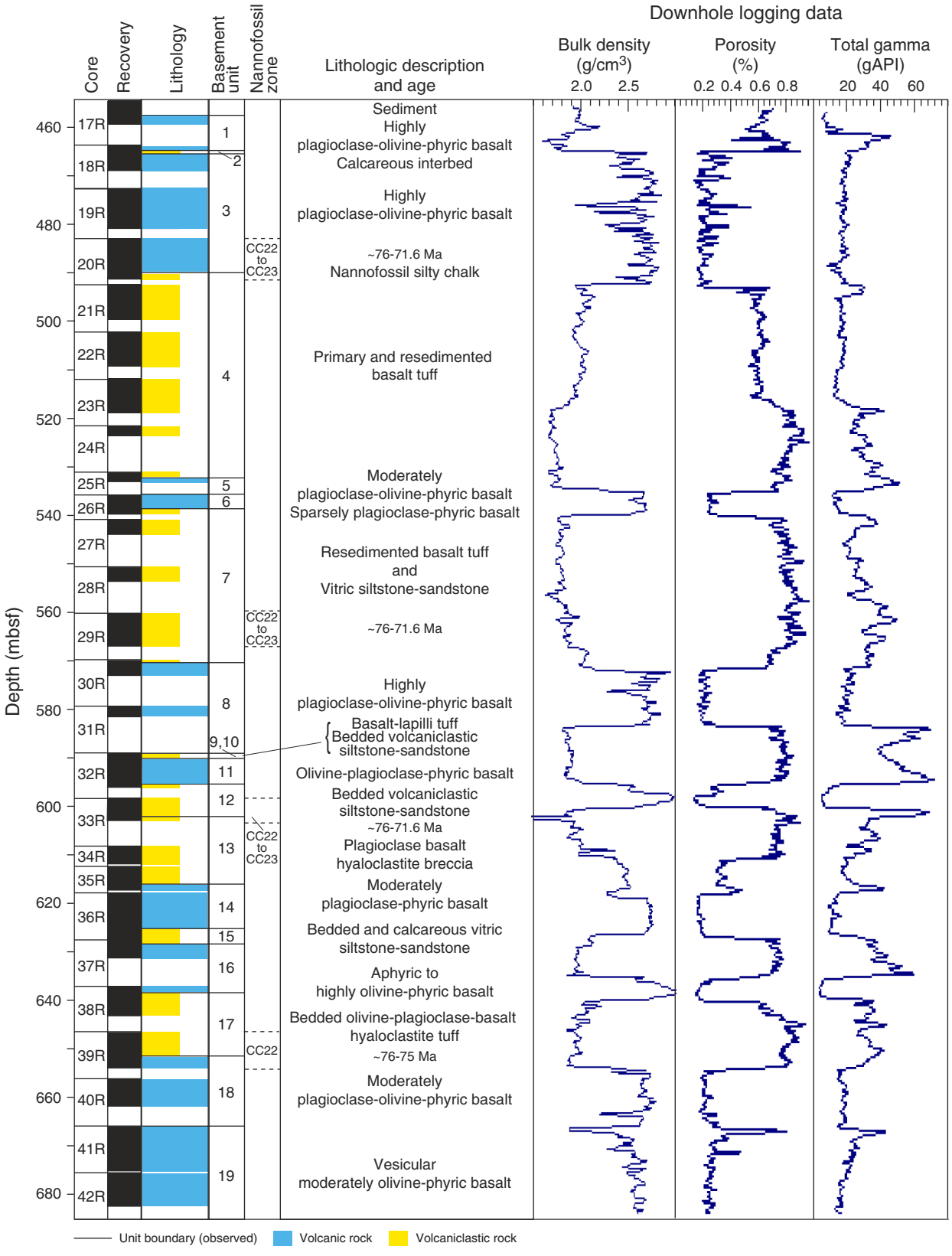

Figure F8 (continued).

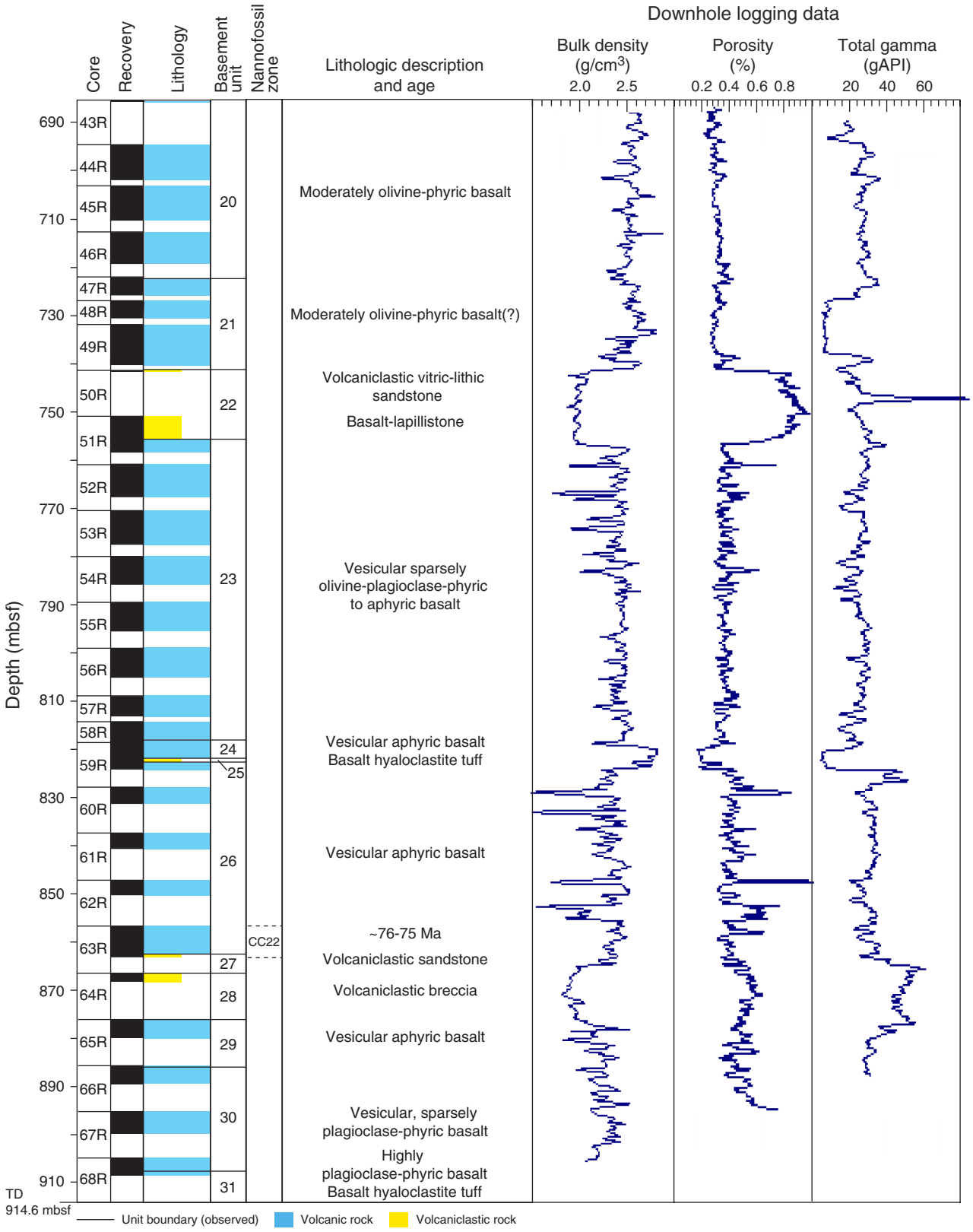

Figure F9. Close-up photograph showing partially altered glassy lobe margins with calcareous interlobe sediment (interval 197-1203A-41R-2, 0–18 cm).

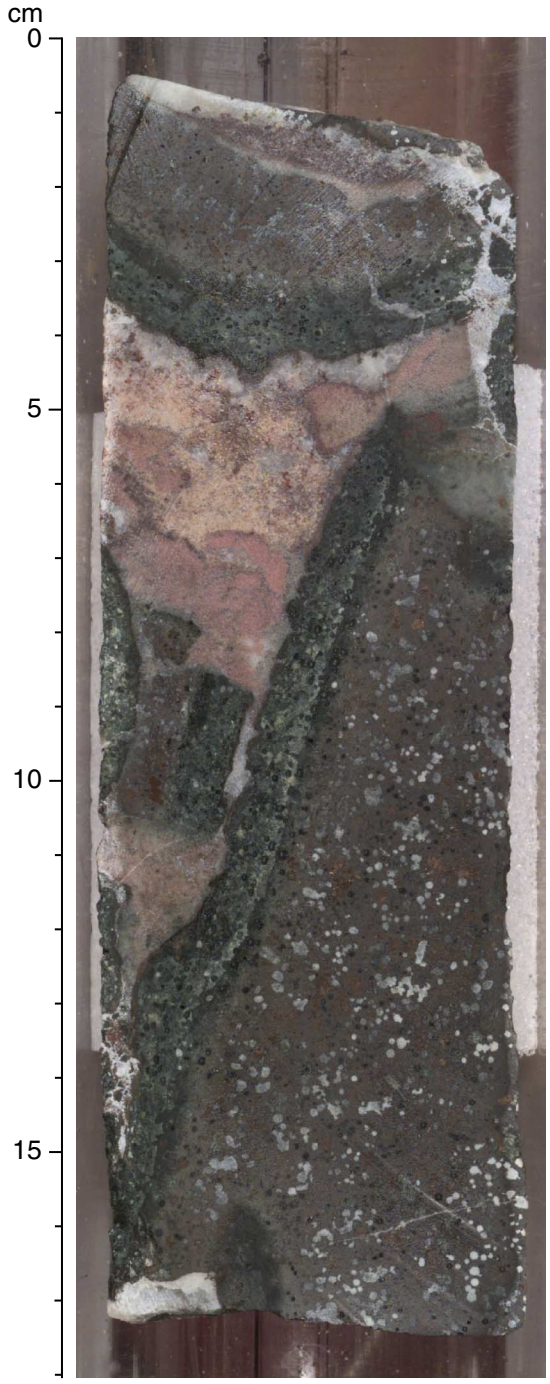

Figure F10. Photomicrographs of zonation in plagioclase (Sample 197-1203A-35R-4 [Piece 1F, 47–49 cm]) (cross-polarized light). **A.** Field of view = 10 mm; photomicrograph 1203A-59. **B.** Field of view = 2.5 mm; photomicrograph 1203A-60.

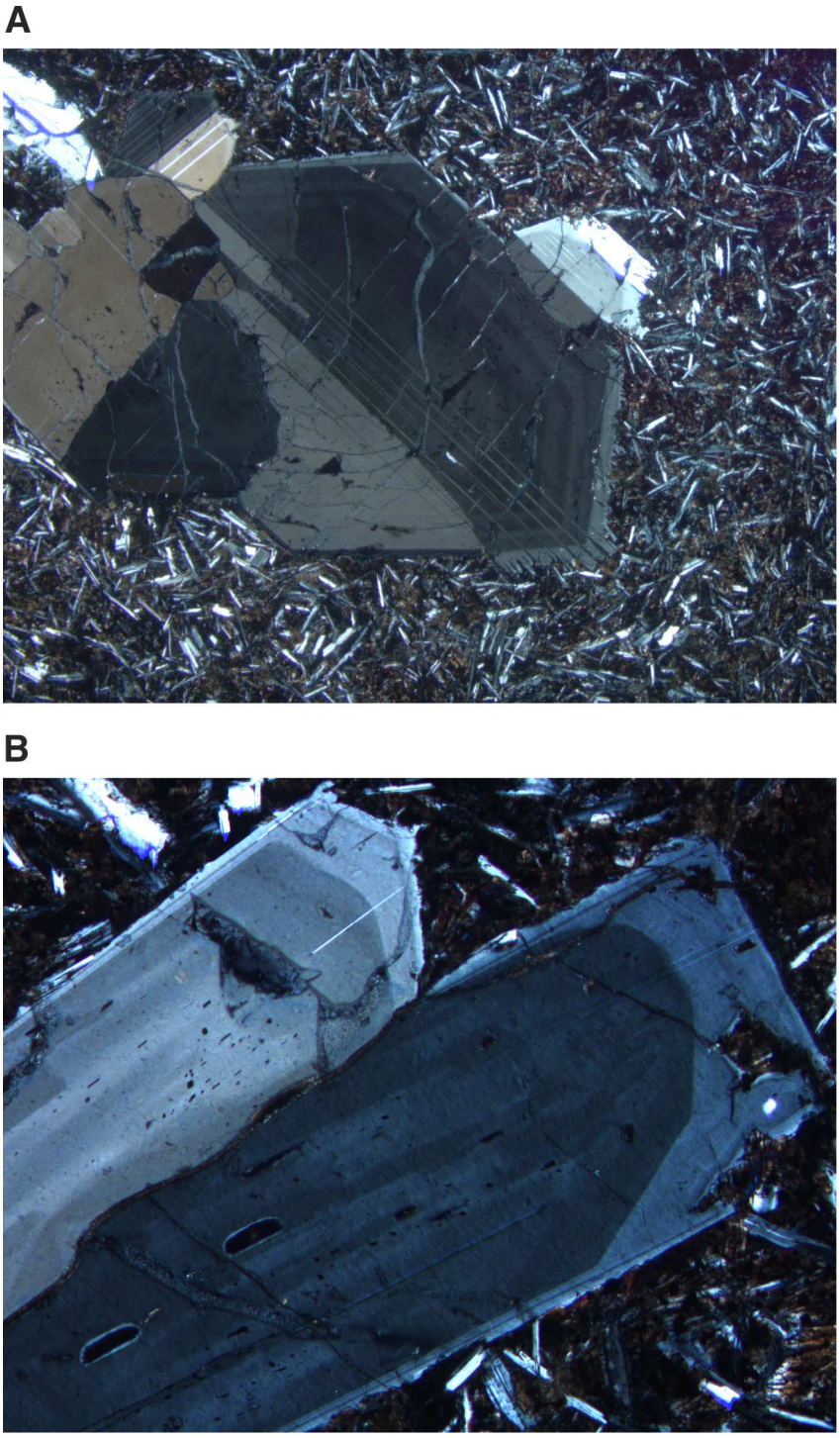

Figure F11. Photomicrograph of the olivine-rich zone in Unit 16 (Sample **197-1203A-37R-3 [Piece 1A, 10–13 cm]**) (cross-polarized light; field of view = 5.5 mm; photomicrograph 1203A-22).

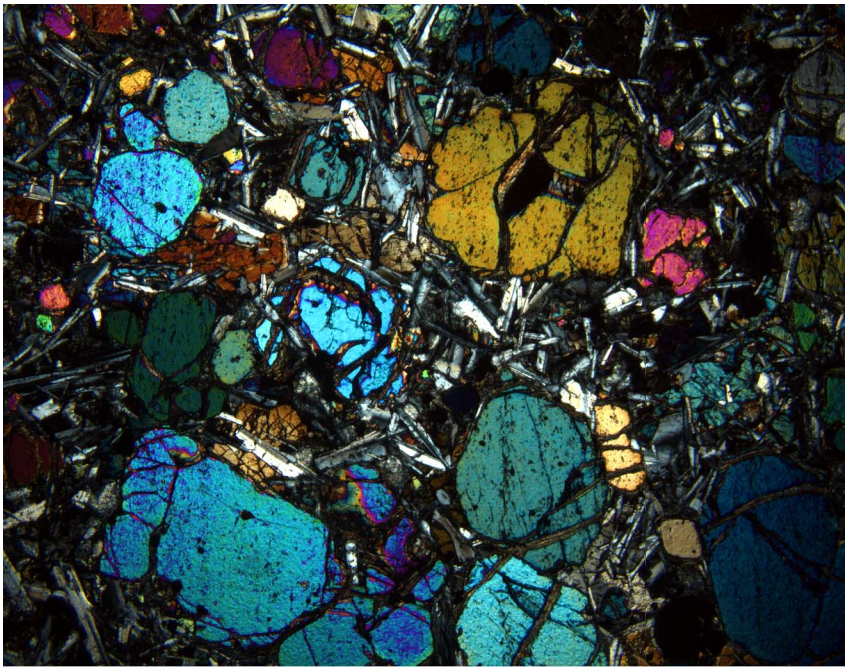

Figure F12. A. Total alkali content ($Na_2O + K_2O$) vs. SiO_2 classification plot (from Le Bas et al., 1986) for volcanic rocks showing lava compositions from Detroit Seamount. The dashed line is the alkalic-tholeiitic dividing line for Hawaiian basalt. Lavas from Site 884 are tholeiitic basalt, whereas lavas from Site 883 are alkalic basalt, although Keller et al. (1995) inferred that prior to alteration these lavas were transitional between alkalic and tholeiitic basalt. Data for these two Leg 145 sites in this and all subsequent figures are from Keller et al. (2000) and M. Regelous et al. (unpubl. data). Lavas from Site 1203 range from tholeiitic, overlapping with Site 884 lavas, to alkalic, overlapping with Site 883 lavas. Most of the alkalic Site 1203 lavas have loss on ignition (LOI) >2 wt%. The volcaniclastite sample has high total alkalis, which we interpret as a result of alkali gain during alteration. The two Site 1203 basalt samples in the tholeiitic field at <45 wt% SiO_2 are picritic as a result of olivine accumulation. **B.** Total alkali content ($Na_2O + K_2O$) vs. SiO_2 comparing Detroit Seamount lava compositions with those from Mauna Kea Volcano (shield- and postshield-stage lavas—lower and upper shaded areas, respectively) on the island of Hawaii. Site 884 and some Site 1203 lavas overlap with the shield-stage tholeiitic basalt, whereas Site 883 and some Site 1203 lavas overlap with Hawaiian postshield alkalic basalt. The irregular line encloses postshield-stage lava erupted at Mauna Kea Volcano, Hawaii.

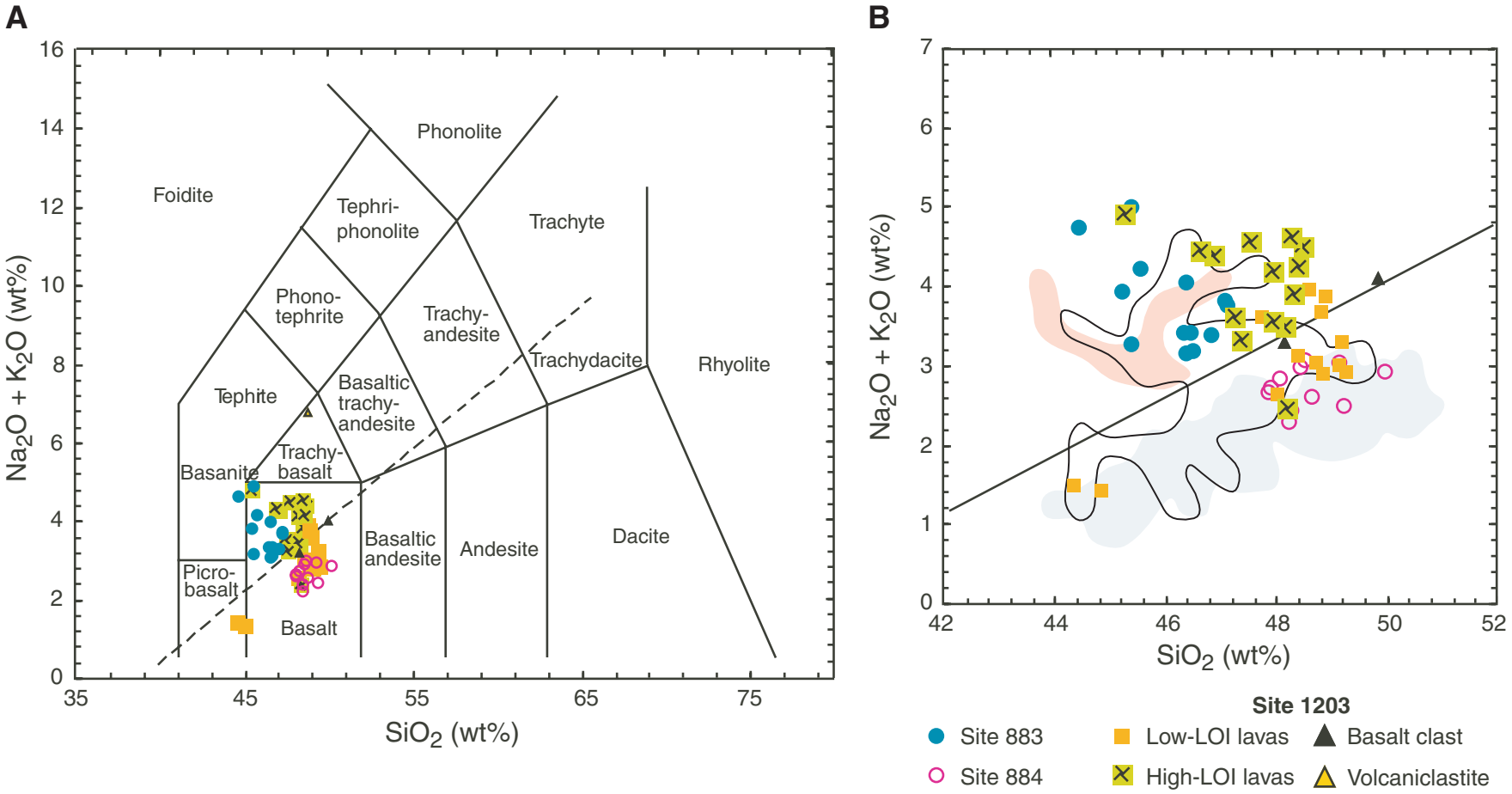

Figure F13. Ti/Zr abundance ratio vs. depth for Hole 1203A lavas. The alkalic basalt of Units 23 and 26 near the bottom of the hole have relatively low Ti/Zr ratios. This result contrasts with the classic Hawaiian trend of increasing alkalinity with decreasing eruption age during the transition from shield- to postshield-stage volcanism.

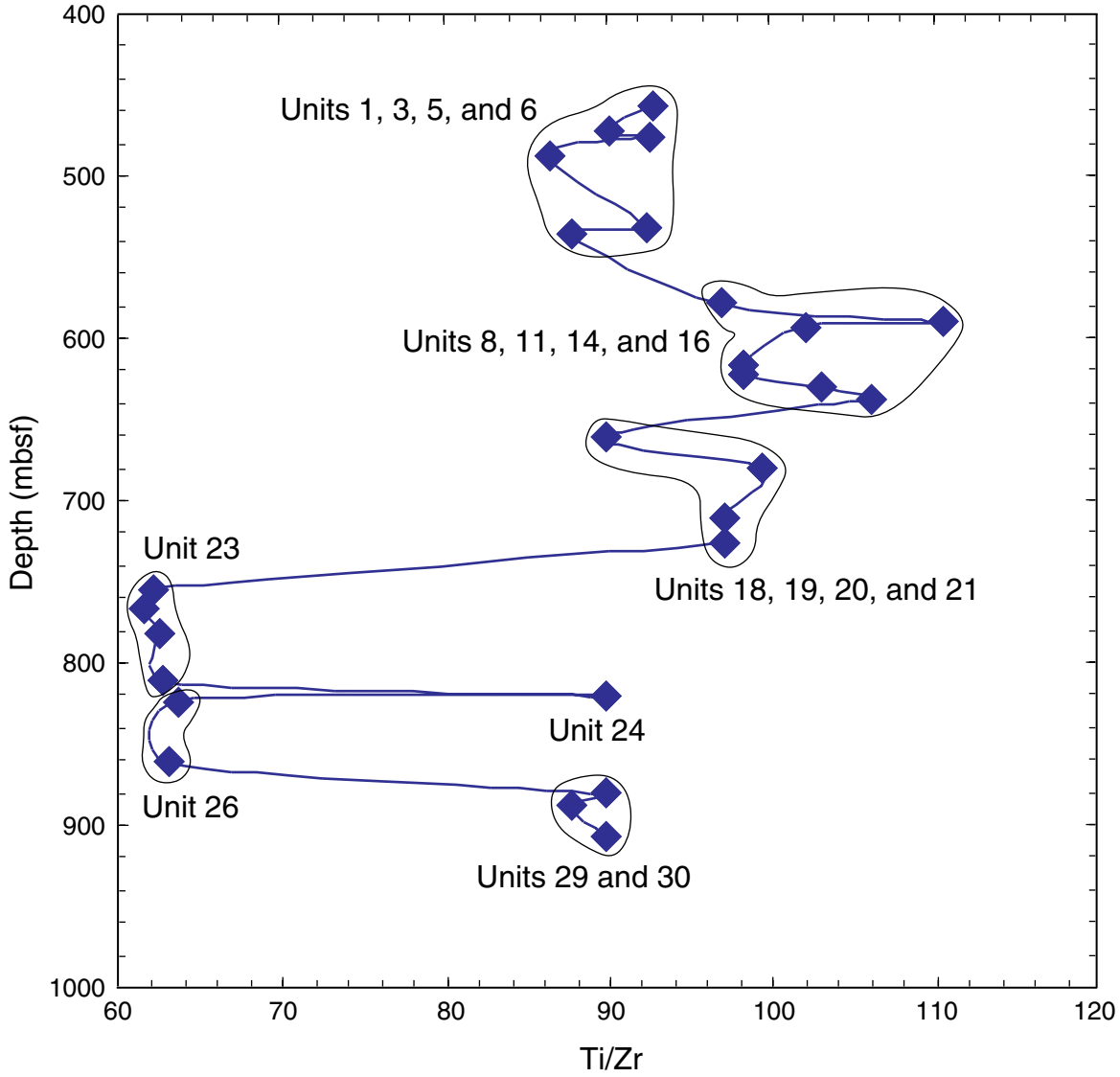

Figure F14. Variations of loss on ignition (LOI), CaO, K_2O, Na_2O, Ba, and Sr with depth. Basaltic units are represented in blue and are labeled. Volcaniclastic units are represented in yellow.

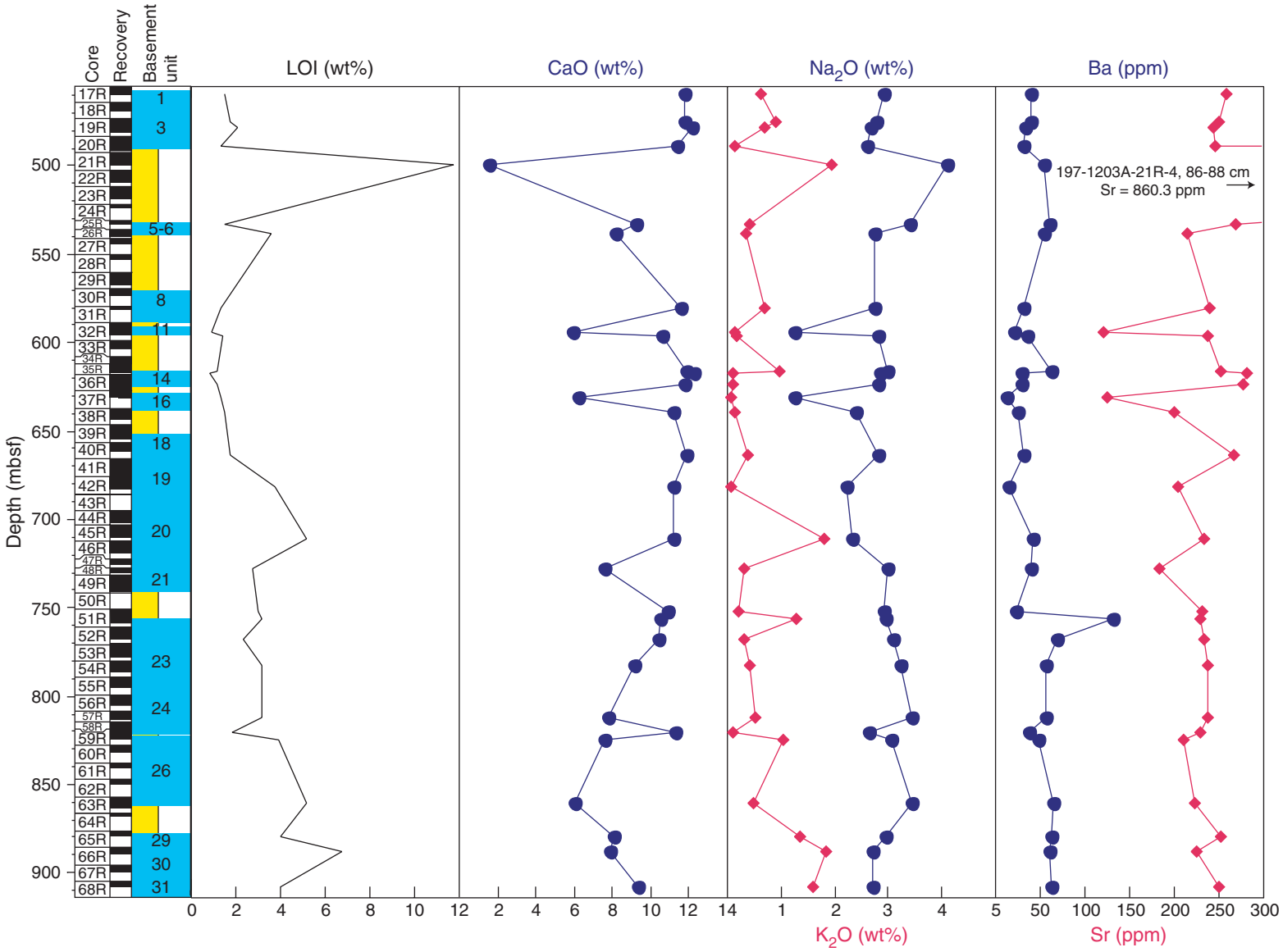

Figure F15. Logging data summary for Hole 1203A. Circles plotted under bulk density, porosity, and *P*-wave log columns are values from discrete measurements on recovered core samples.

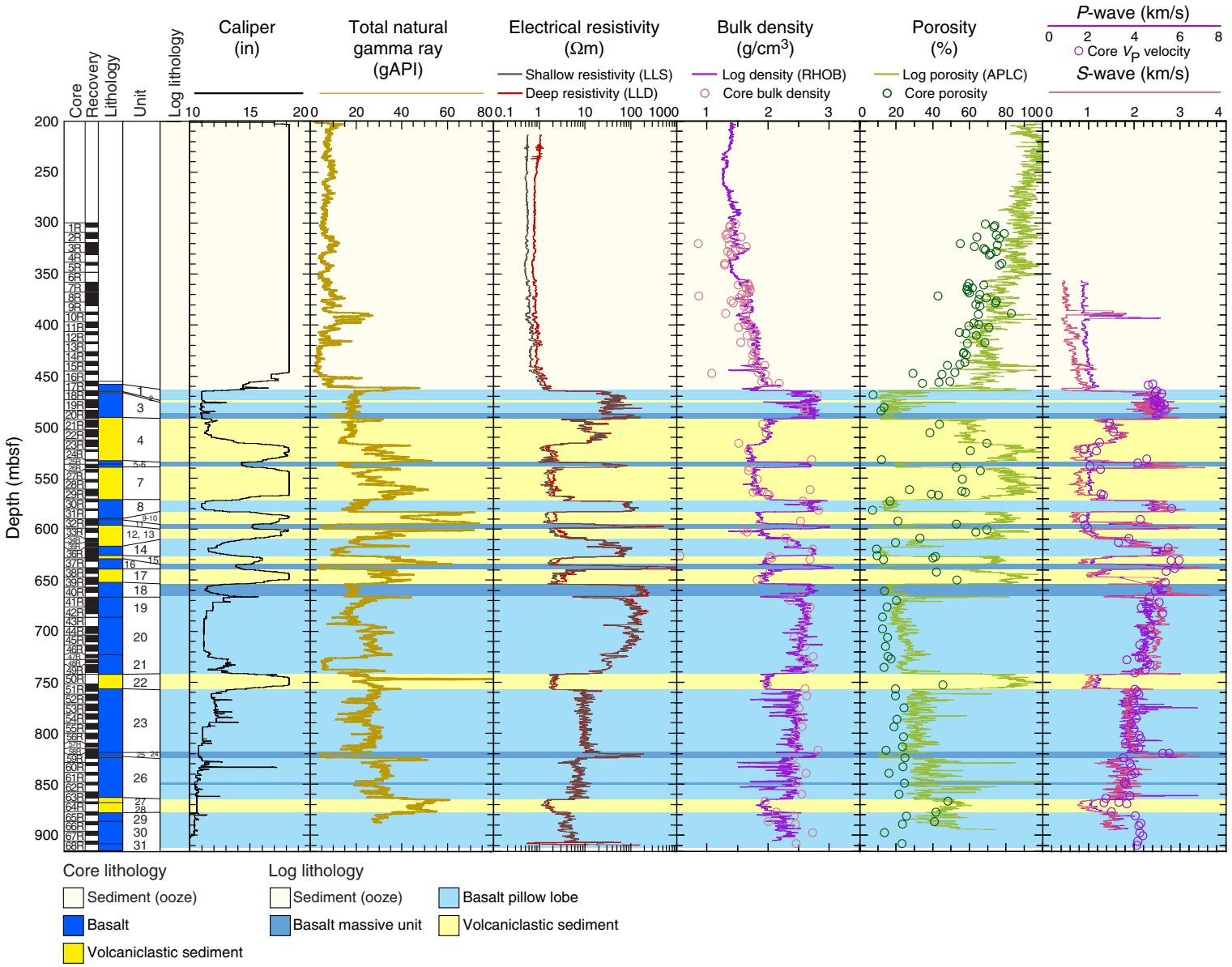

Figure F16. Comparison of FMS images and wireline measurements (electrical resistivity, natural gamma ray, porosity, and density) with the core-derived lithology and logging lithology in basement.

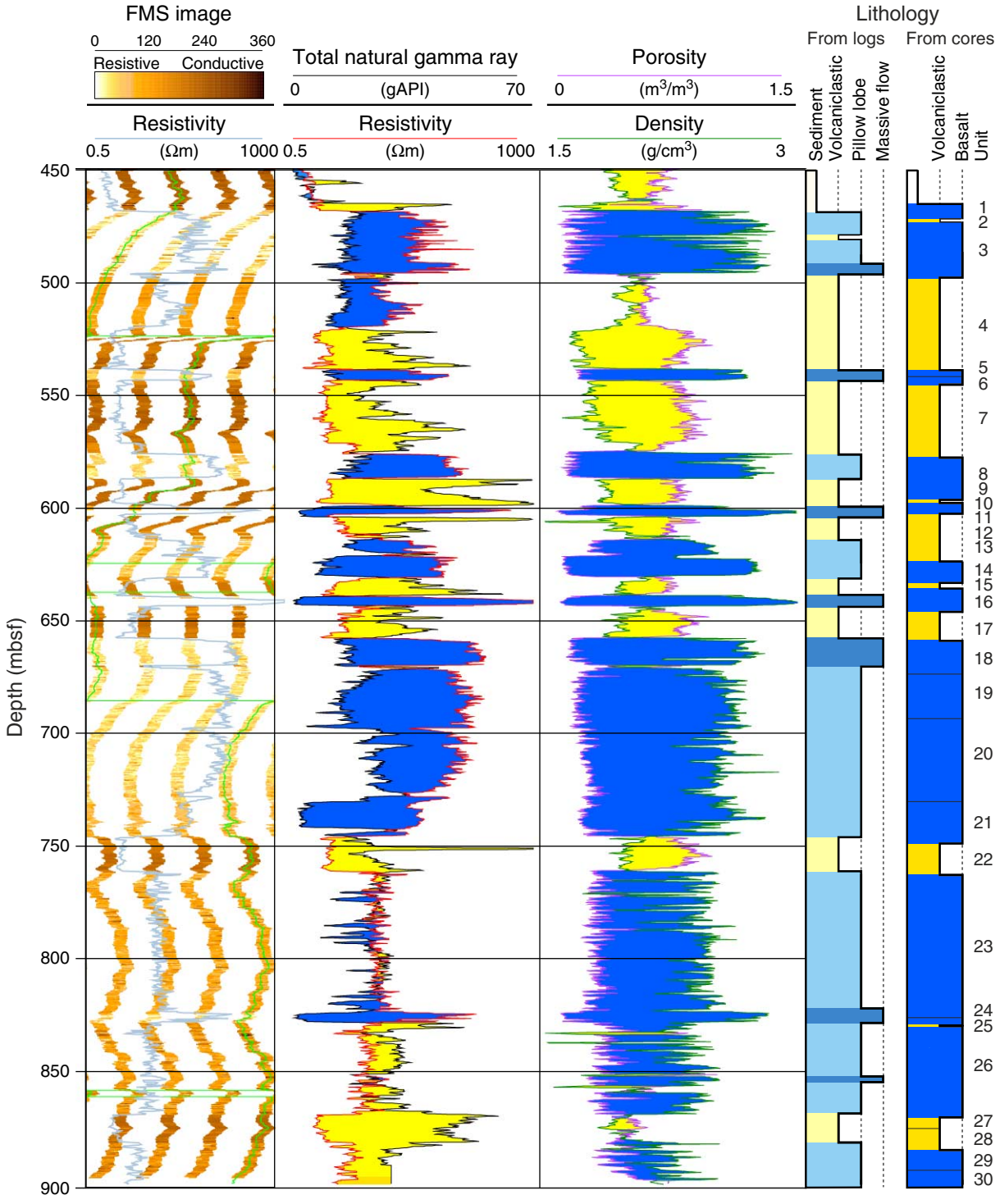

Figure F17. Example of detailed FMS image displaying the transition between basement Units 7 (layered volcaniclastic sediment) and 8 (pillow lava).

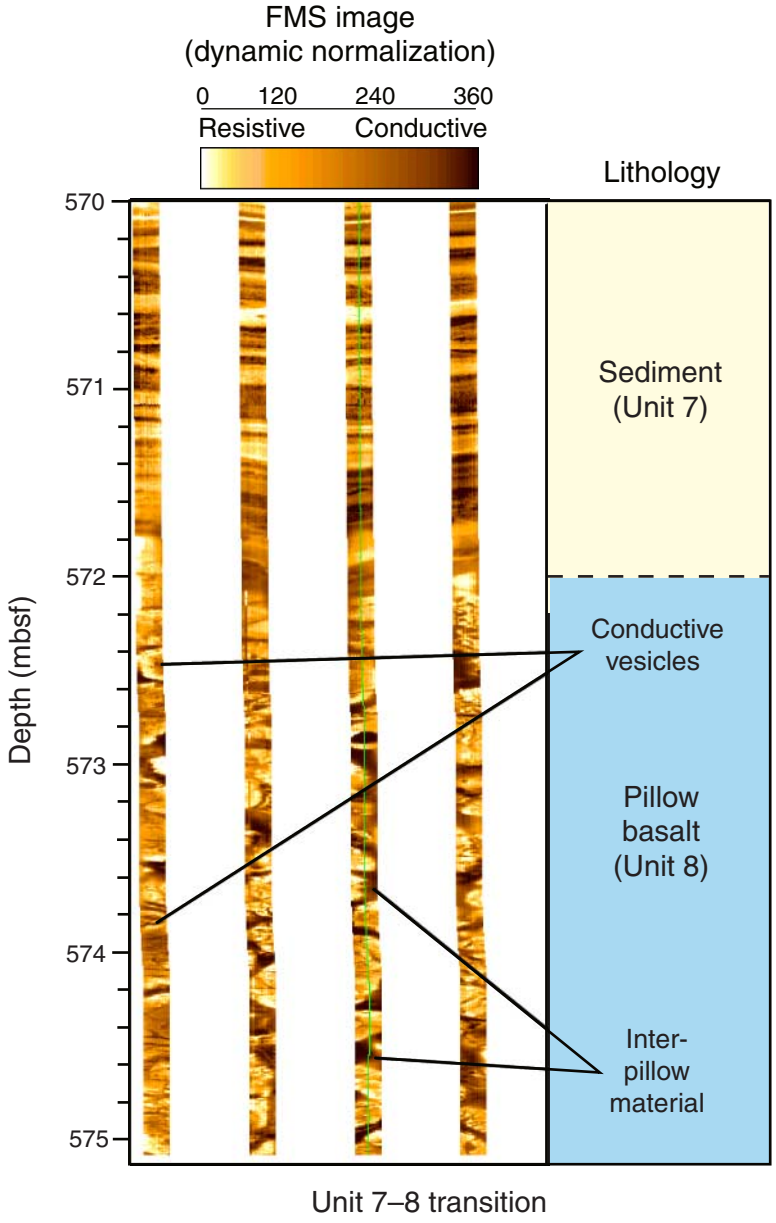

Figure F18. Downhole and uphole run of the Goettingen Borehole Magnetometer. Intensities of the horizontal and vertical field are compared to the sequences of volcaniclastic sediment and lava flows.

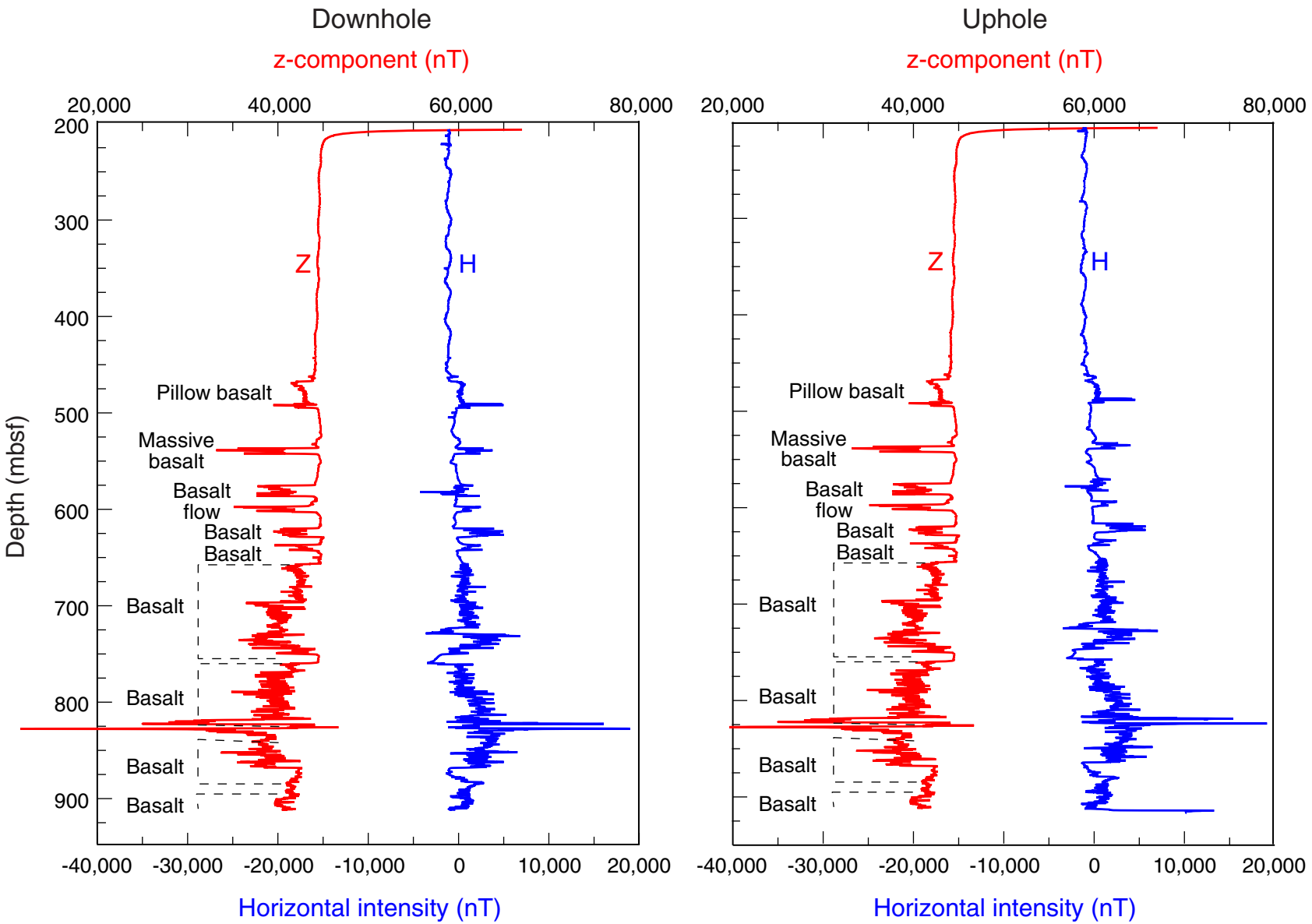

Figure F19. Example orthogonal vector plot showing well-defined, stable magnetic behavior recorded by Site 1203 volcaniclastic sediment samples. **A.** Sample 197-1203A-24R-1, 30–32 cm. **B.** Sample 197-1203A-38R-2, 77–79 cm. **C.** Sample 197-1203A-38R-4, 94–96 cm. **D.** Sample 197-1203A-63R-5, 127–129 cm. Open squares = vertical projection of magnetization, solid circles = horizontal projection of magnetization.

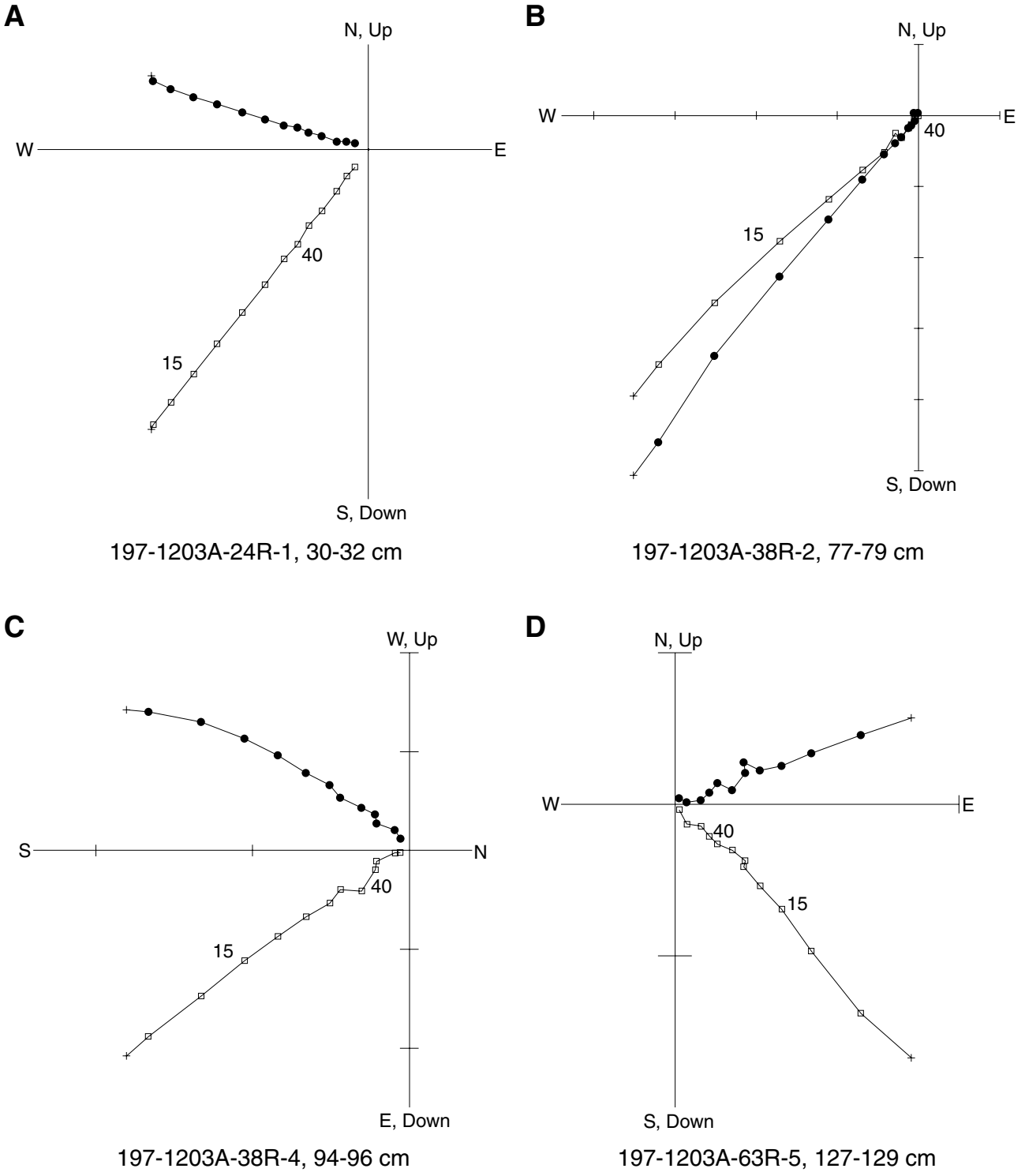

Figure F20. Example orthogonal vector plot showing well-defined, stable magnetic behavior recorded by Site 1203 basalt samples. Open squares = vertical projection of magnetization, solid circles = horizontal projection of magnetization. **A.** Sample 197-1203A-25R-1, 29–31 cm. **B.** Sample 197-1203A-26R-1, 75–77 cm. **C.** Sample 197-1203A-31R-1, 65–67 cm. **D.** Sample 197-1203A-36R-3, 60–62 cm. (Continued on next page.)

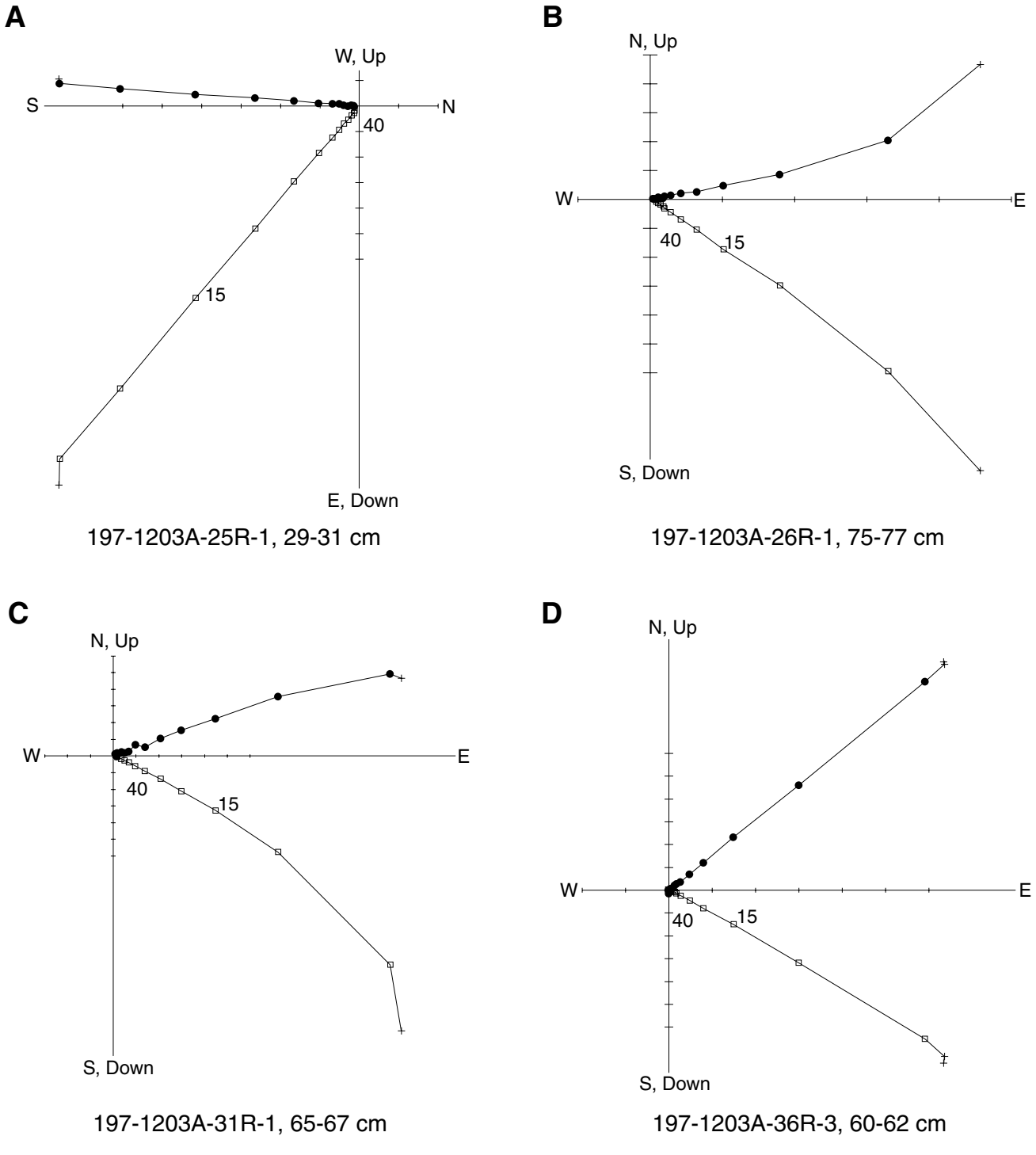

Figure F20 (continued). **E.** Sample 197-1203A-37R-3, 113–115 cm. **F.** Sample 197-1203A-47R-4, 18–20 cm. **G.** Sample 197-1203A-55R-5, 17–19 cm. **H.** Sample 197-1203A-59R-4, 124–126 cm.

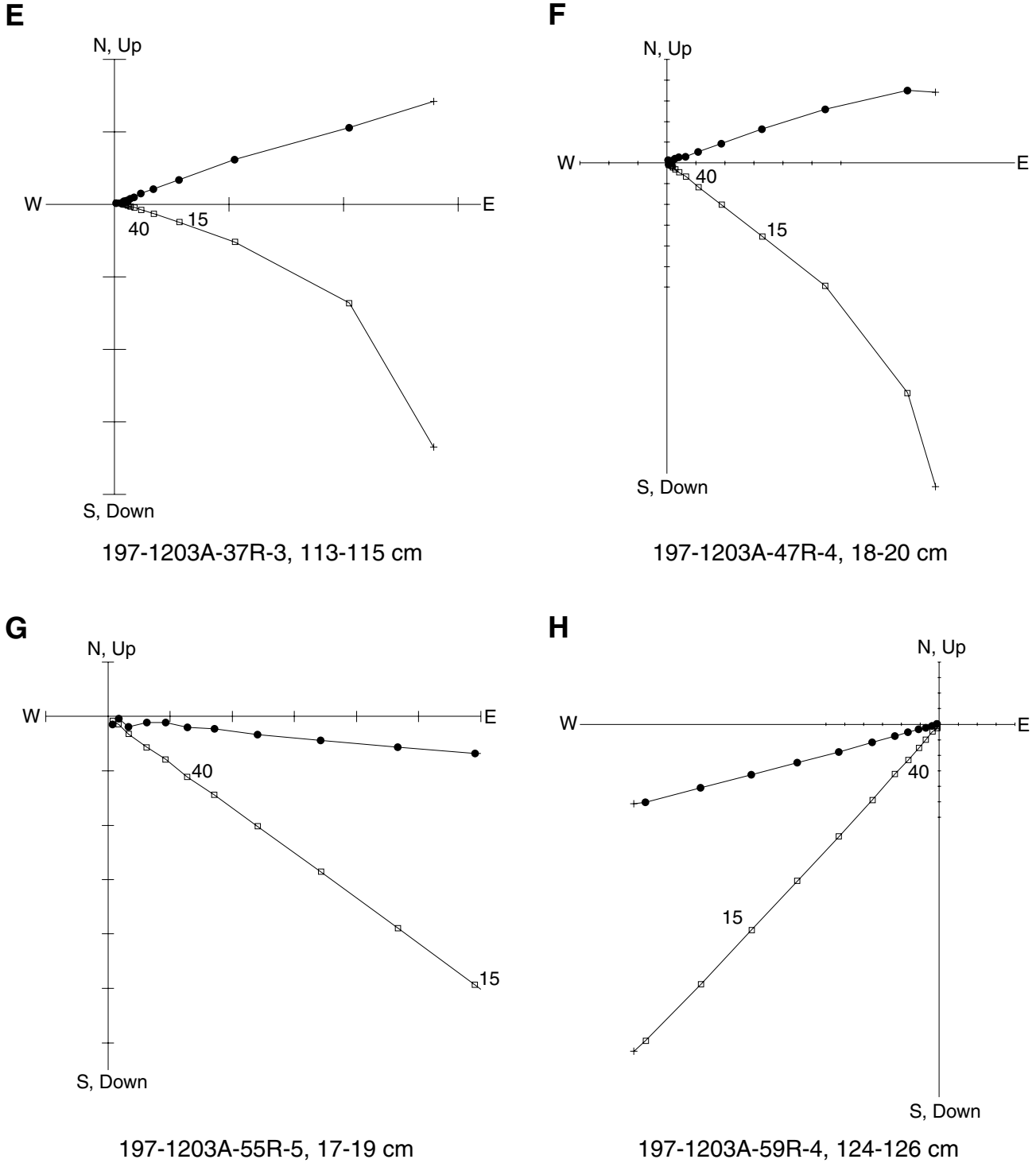

Figure F21. Histogram of inclination values derived from principal component analyses on alternating-field demagnetization data from Hole 1203A volcaniclastic sediment samples. ΔI = difference between the inclination of Hawaii and that of Detroit Seamount, Δλ = difference in the latitude of Hawaii and the formative paleolatitude of Detroit Seamount.

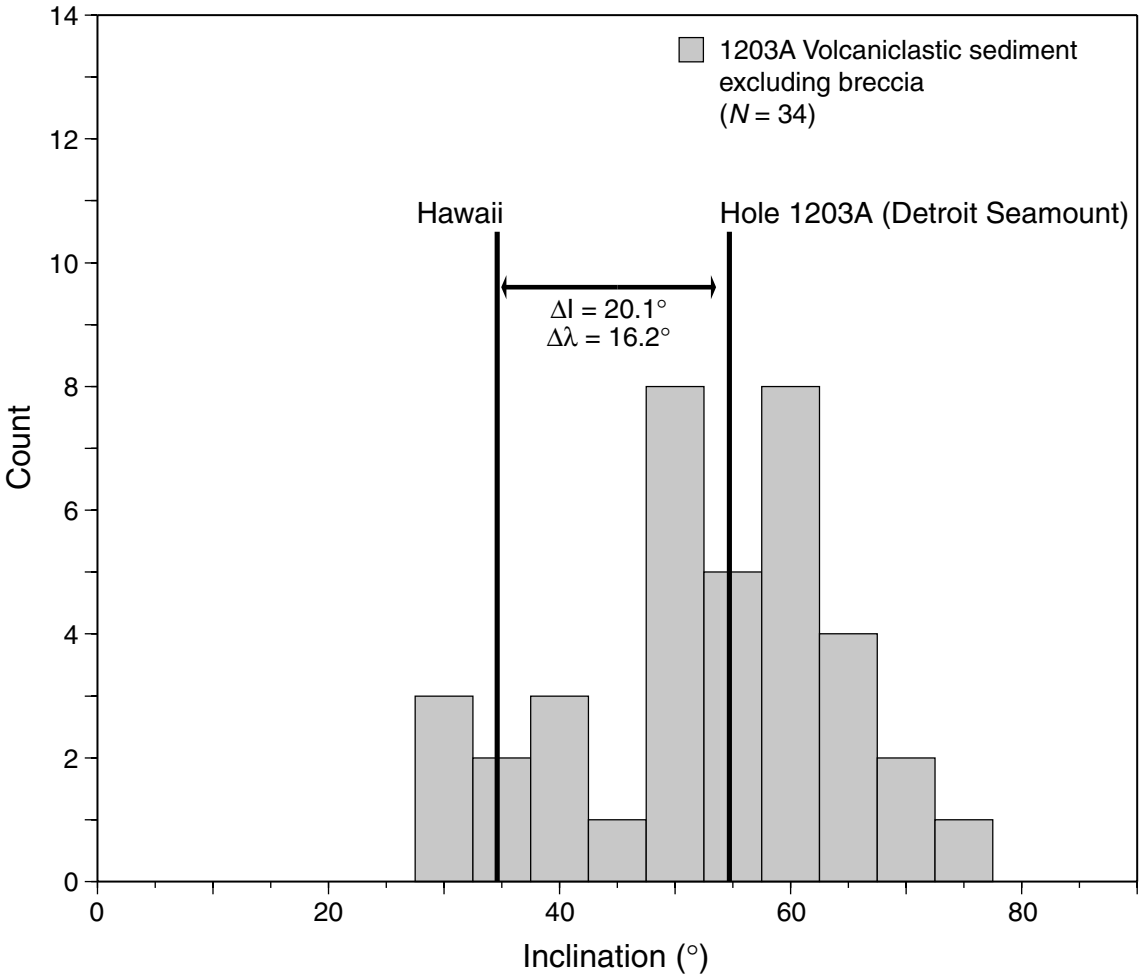

Figure F22. Histogram of inclination values derived from principal component analyses on Hole 1203A basement basalt. ΔI = difference between the inclination of Hawaii and that of Detroit Seamount, Δλ = difference in the latitude of Hawaii and the formative paleolatitude of Detroit Seamount.

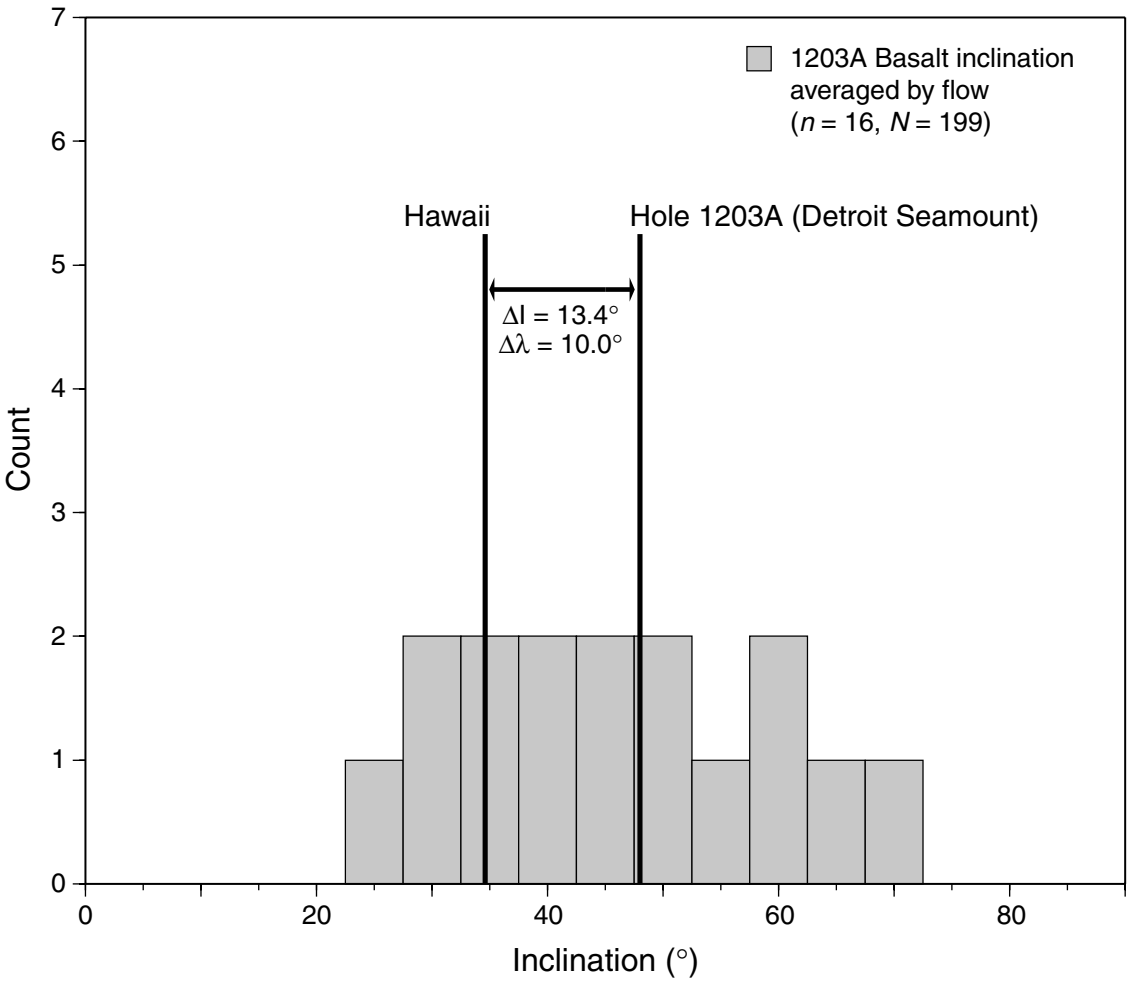

Figure F23. Site 1204 survey 2, Line 3, 4-km-long migrated time section. Data are bandpass filtered between 40 and 100 Hz. Hole 883F occurs at about shotpoint 3517, Hole 1204A at shotpoint 3549, and Hole 1204B at shotpoint 3555. Trace-to-trace distance = ~16.5 m; vertical exaggeration at the seafloor = ~3:1; bottom of Hole 1204B = ~4.35 s two-way traveltime.

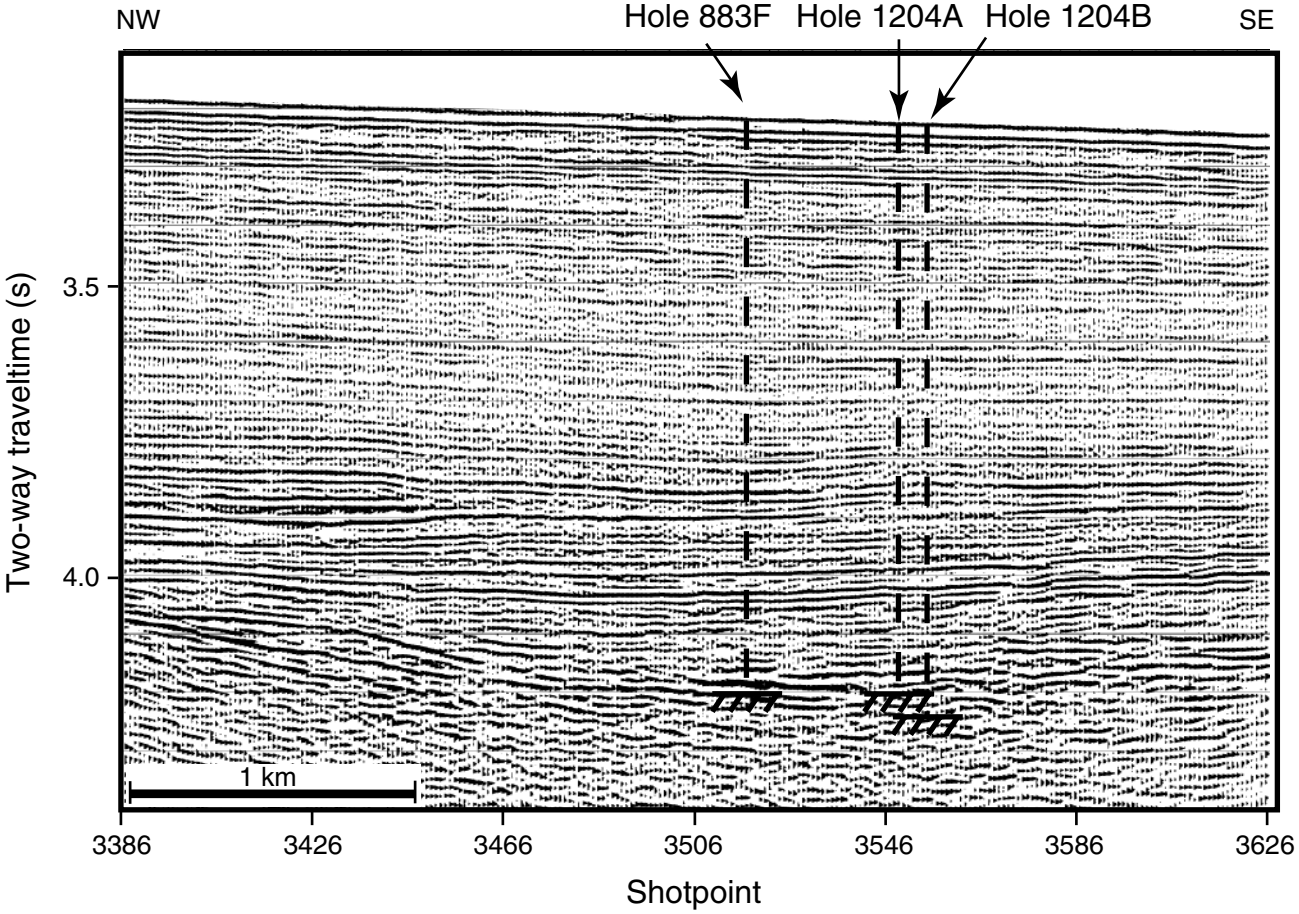

Figure F24. Photograph showing rotated, broken sediment block overlying a thick interval consisting of a thin, faulted, very finely laminated bed and convoluted laminations, likely indicating slumping. The 2-cm brown beds of silty volcanic material alternate with finely laminated, bioturbated, and burrowed nannofossil chalk (interval 197-1204A-3R-2, 30–49 cm).

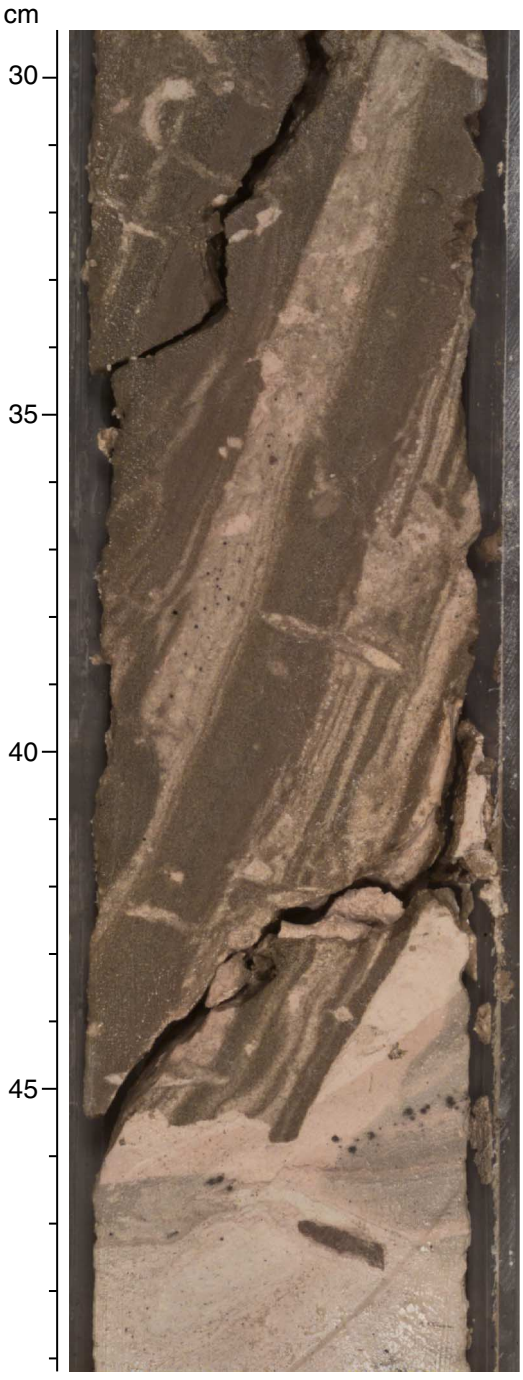

Figure F25. Recovery, age, and major lithologic features of basement units from Holes 1204A and 1204B. TD = total depth, G = fresh glass.

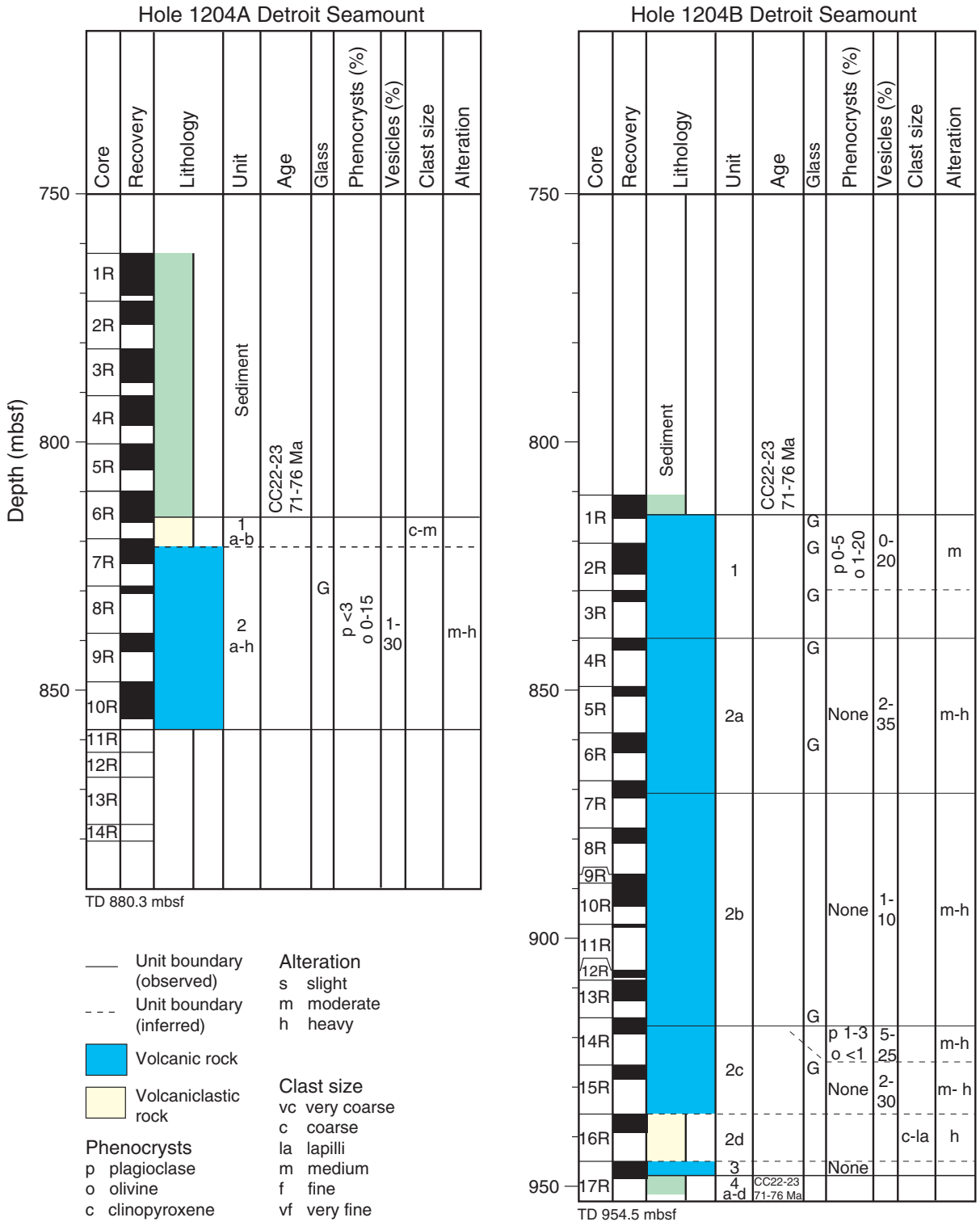

Figure F26. Photograph of Unit 1b breccia containing angular fragments of altered glass and vesicular basalt in a carbonate cement (Section 197-1204A-7R-1 [Pieces 5 and 8]).

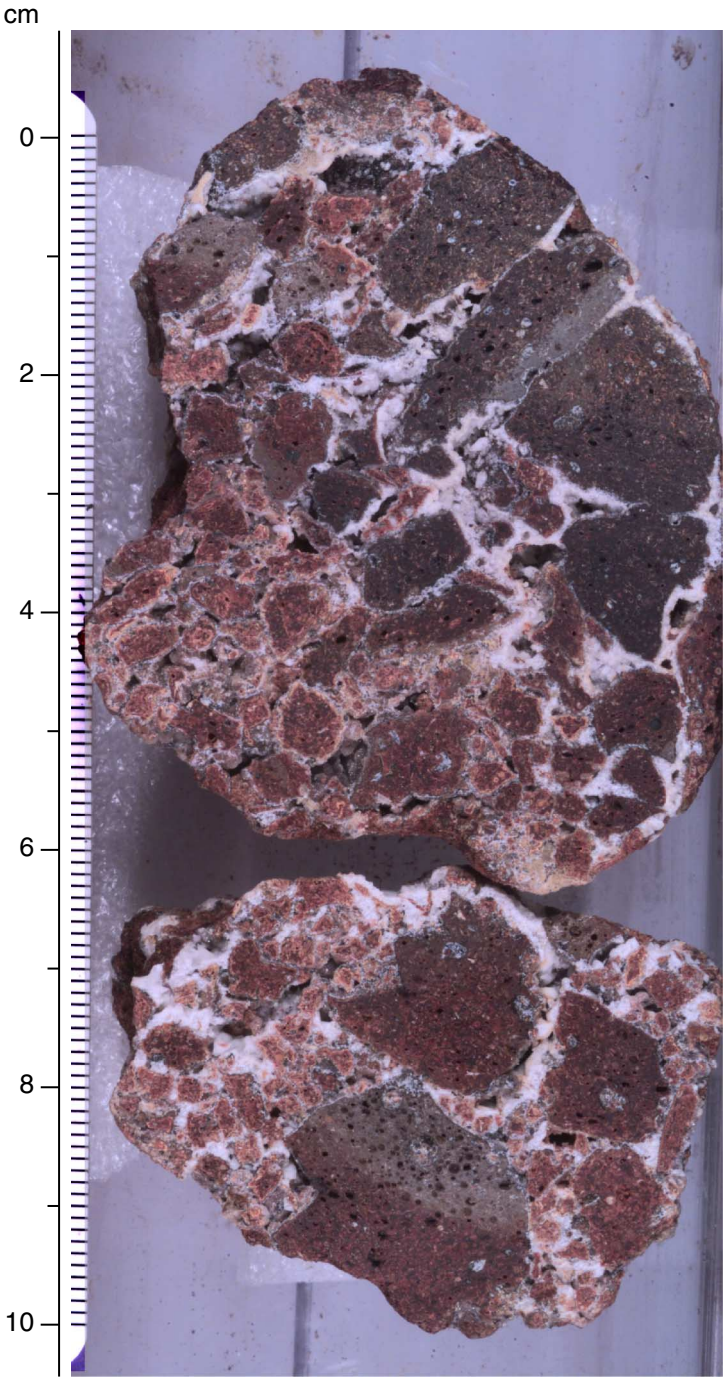

Figure F27. Photomicrograph showing unaltered olivine and plagioclase laths in a glassy lobe margin (Sample 197-1204B-3R-2, 97–100 cm) (plane-polarized light; field of view = 0.625 mm; photomicrograph 1204B-138).

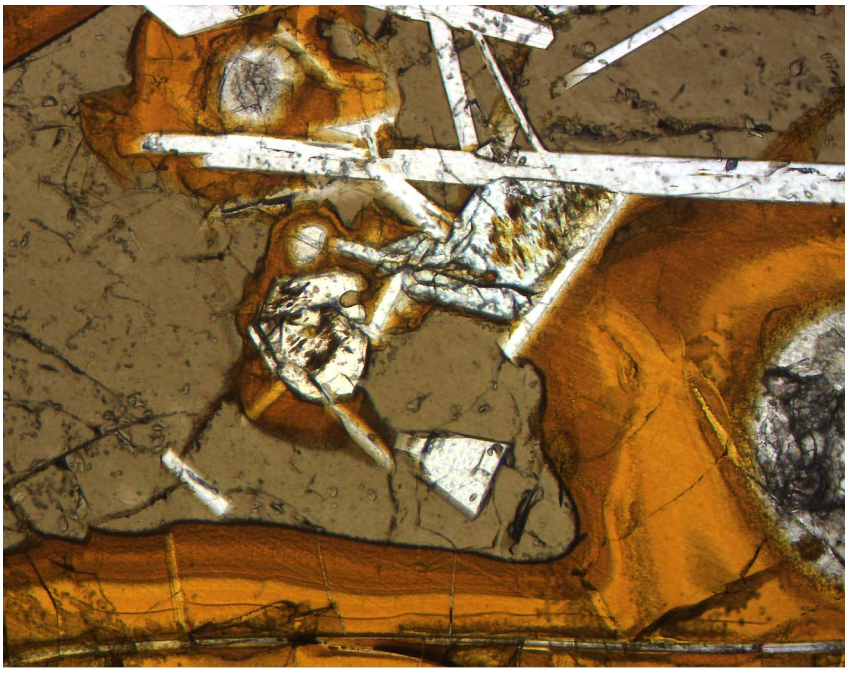

Figure F28. Photomicrograph showing unaltered olivine and plagioclase laths in glassy lobe margin (Sample **197-1204B-3R-2, 97–100 cm**) (cross-polarized light; field of view = 0.625 mm; photomicrograph 1204B-156).

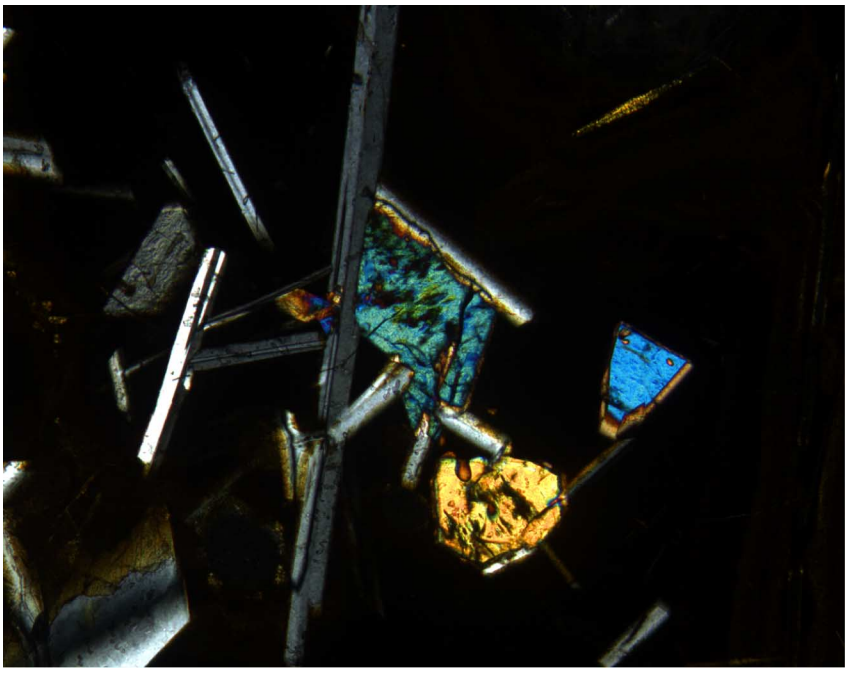

Figure F29. Abundance of Ti vs. Zr showing a near-linear trend for most of the lavas from Detroit Seamount. Basalt from Suiko Seamount defines a similar trend (M. Regelous et al., unpubl. data). Site 884 lavas and the two picrites from Site 1203 have the lowest abundances and the alkalic basalt from Site 1203 has the highest abundances of Ti and Zr.

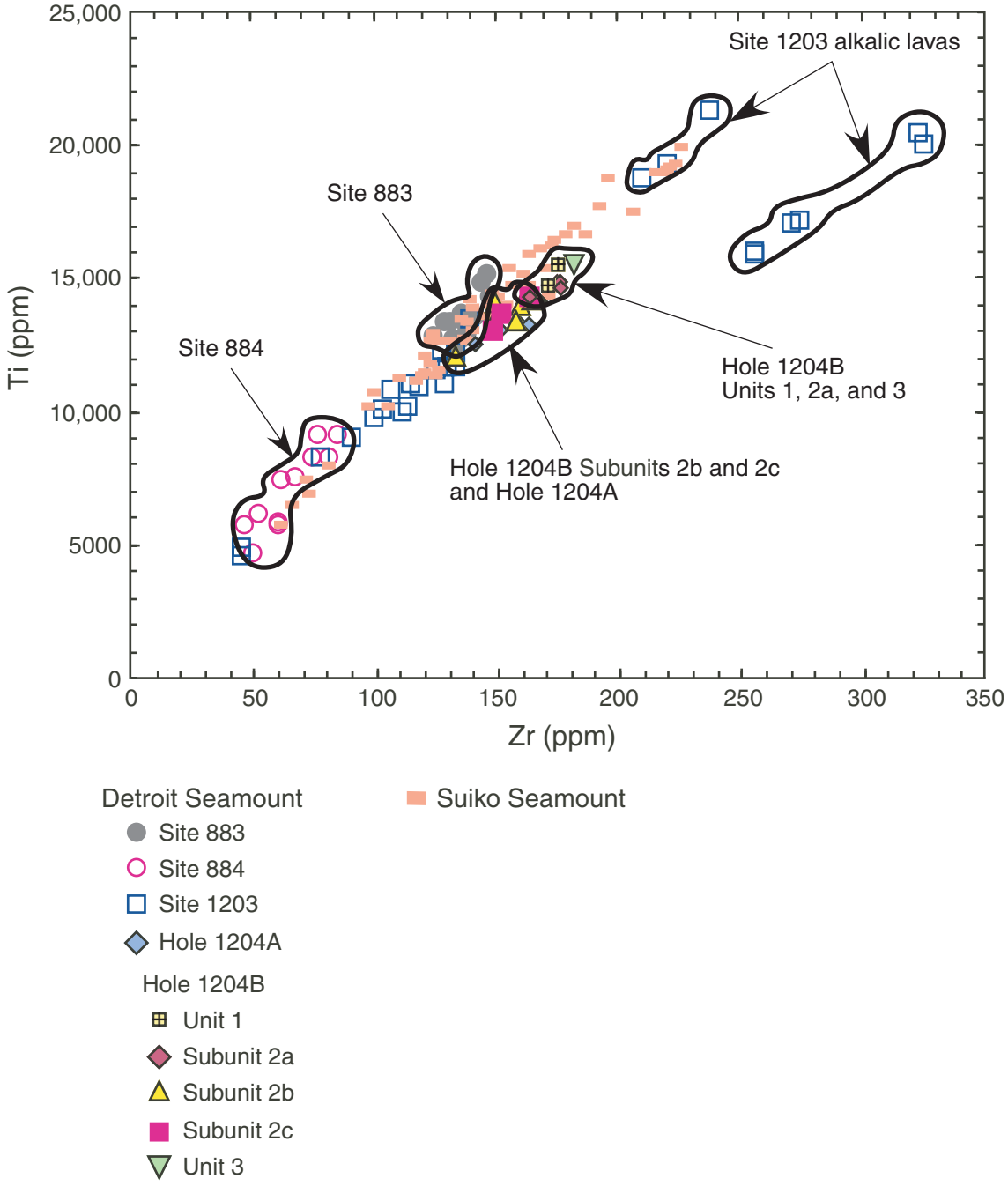

Figure F30. Example orthogonal vector plots showing well-defined, stable magnetic behavior recorded by Hole 1204B basalt samples. **A.** Sample 197-1204B-2R-2, 14–16 cm. **B.** Sample 197-1204B-14R-1, 14–16 cm. **C.** Sample 197-1204B-13R-4, 82–84 cm. **D.** Sample 197-1204B-17R-2, 104–106 cm. **E.** Sample 197-1204B-10R-1, 6–9 cm. **F.** Sample 197-1204B-15R-1, 11–13 cm. Open squares = vertical projection of magnetization, solid circles = horizontal projection of magnetization.

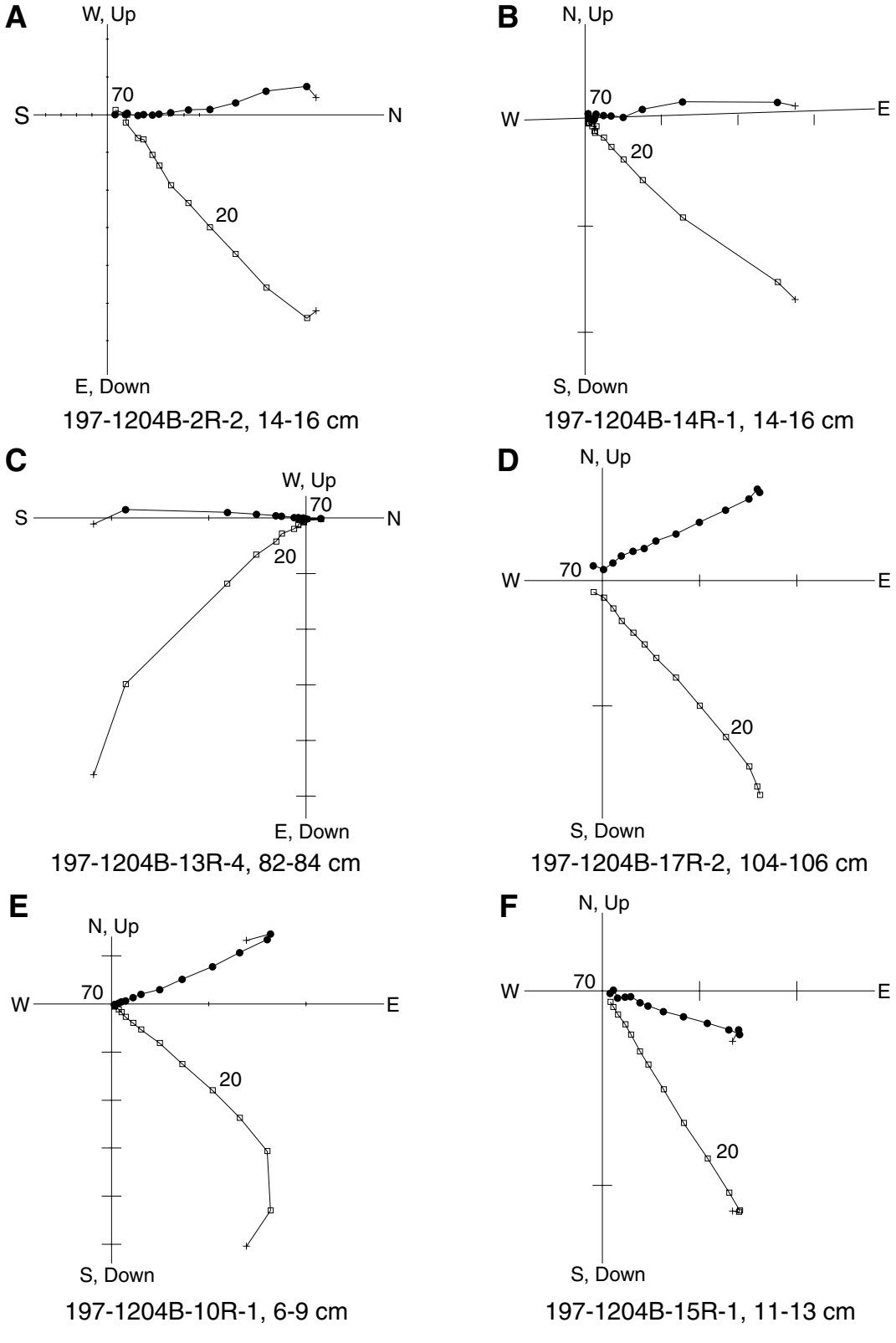

Figure F31. Example orthogonal vector plots showing well-defined, stable magnetic behavior recorded by Hole 1204B diabase samples. **A.** Sample 197-1204B-7R-3, 139–141 cm. **B.** Sample 197-1204B-9R-2, 8–10 cm. **C.** Sample 197-1204B-8R-2, 21–23 cm. **D.** Sample 197-1204B-10R-4, 40–42 cm. **E.** Sample 197-1204B-11R-2, 38–40 cm. **F.** Sample 197-1204B-13R-3, 33–35 cm. Open squares = vertical projection of magnetization, solid circles = horizontal projection of magnetization.

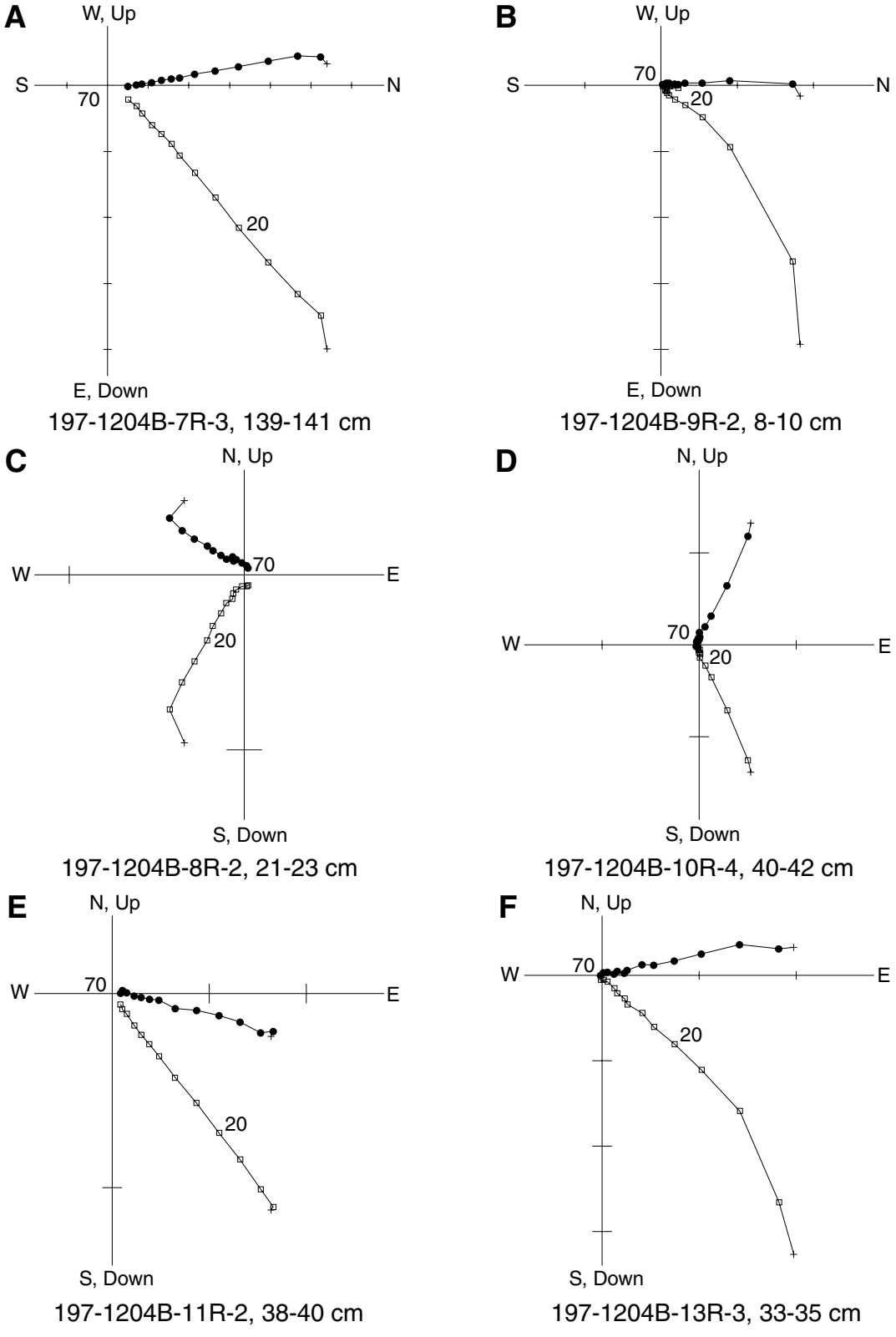

Figure F32. Site 1205 survey 3, Line 4, 3-km-long, frequency wavenumber- or fK-migrated time section. Data are bandpass filtered between 60 and 150 Hz. Hole 1205A is at approximately shotpoint 4216. Trace-to-trace distance = ~9.9 m; vertical exaggeration at the seafloor = ~7:1; bottom of Hole 1205 = ~4.35 s two-way traveltime.

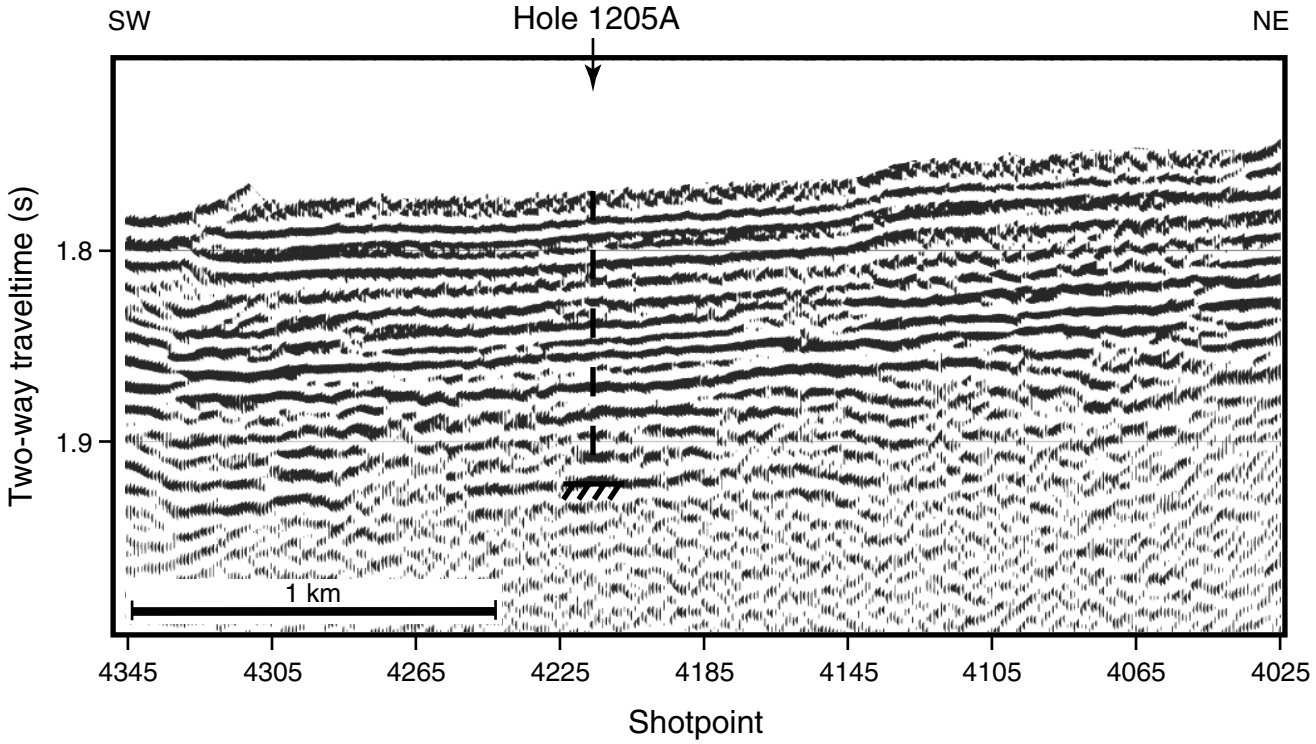

Figure F33. Photograph of conglomerate overlying basement at Site 1205 showing clasts of hawaiite up to 8 cm in diameter embedded in a poorly sorted, fossiliferous sandy matrix (interval 197-1205A-5R-2, 9–25 cm).

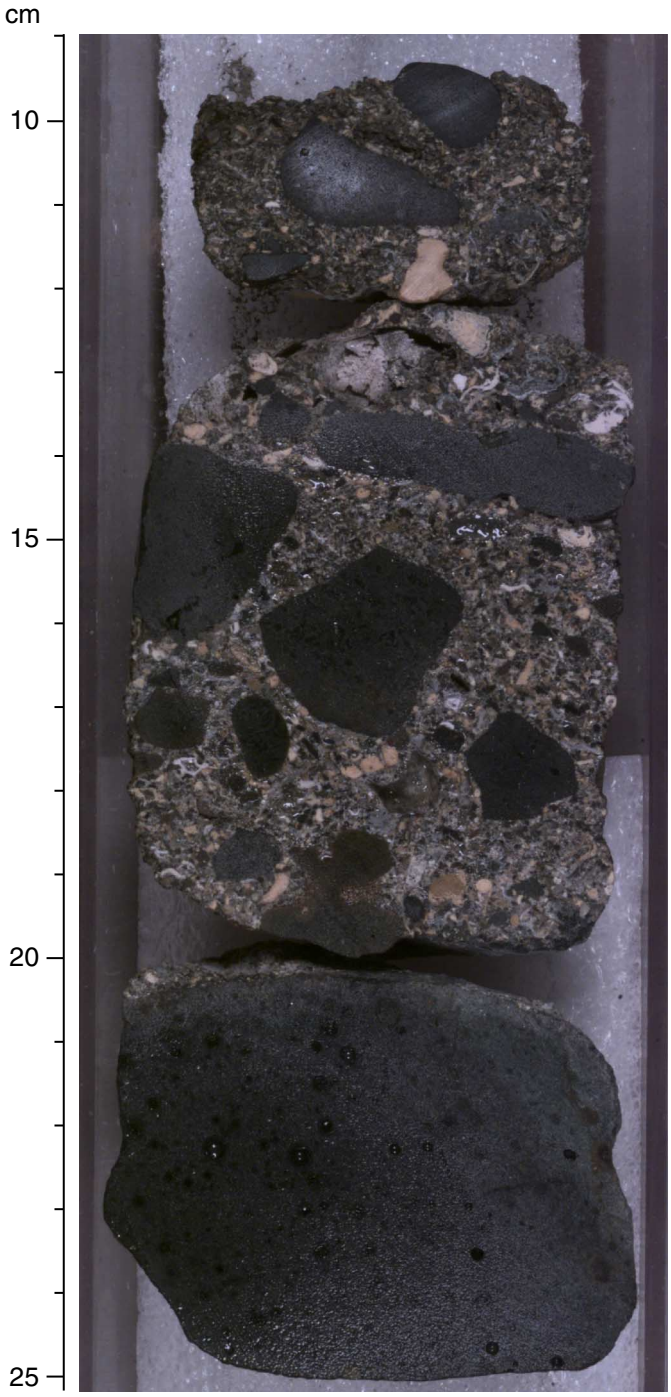

Figure F34. Recovery, thickness, chemical composition, and major lithologic features of Hole 1205A basement units. TD = total depth.

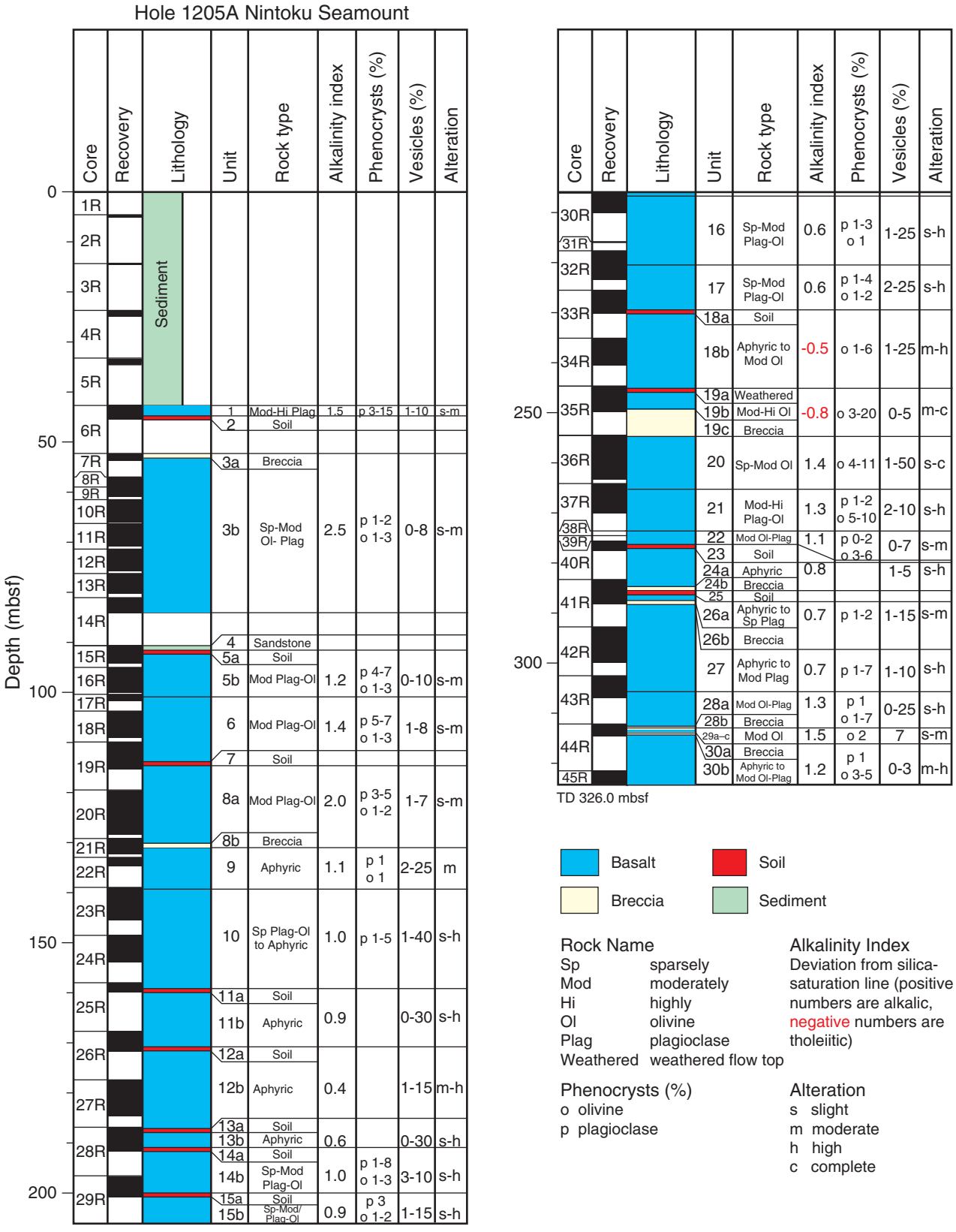

Figure F35. Photomicrograph showing strain bands in trachytic texture in Subunit 3b (Sample **197-1205A-10R-2, 73–75 cm**) (cross-polarized light; field of view = 5 mm; photomicrograph 1205A-202).

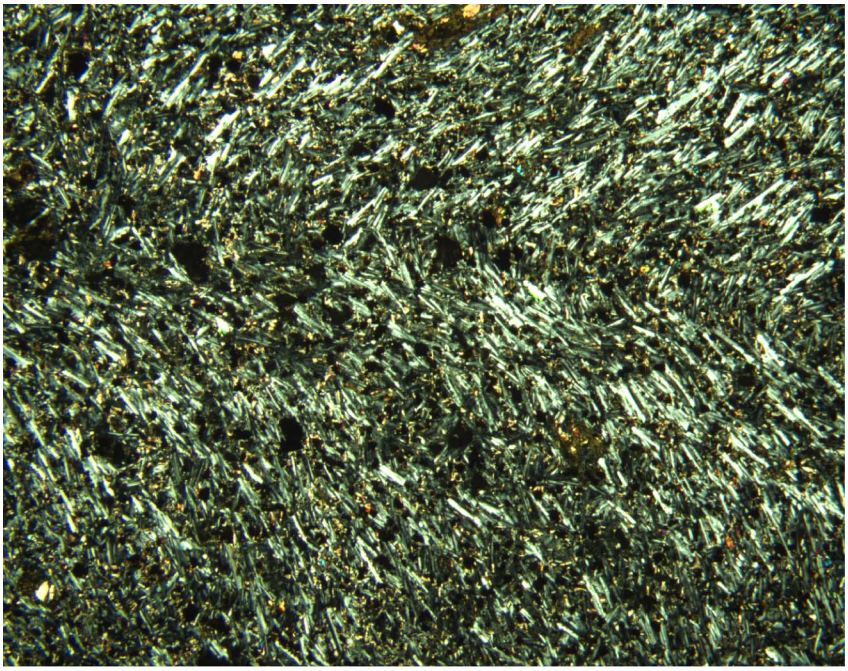

Figure F36. Total alkali content ($Na_2O + K_2O$) vs. SiO_2 classification plot for lava flows from Nintoku Seamount. The solid diagonal line is the alkalic-tholeiitic dividing line for Hawaiian basalt. Only two Site 1205 lava units (Subunits 18b and 19b) are composed of tholeiitic basalt. All other flow units at Site 1205 and nearby DSDP Site 432 (M. Regelous et al., unpubl. data) are alkalic basalt. At both sites, conglomerates overlying igneous basement contain hawaiite clasts that are distinguished by their high total alkali (>6 wt%) and relatively high SiO_2 content. Data for Suiko Seamount (Site 433), which is dominantly tholeiitic basalt (M. Regelous et al., unpubl. data), are shown for comparison.

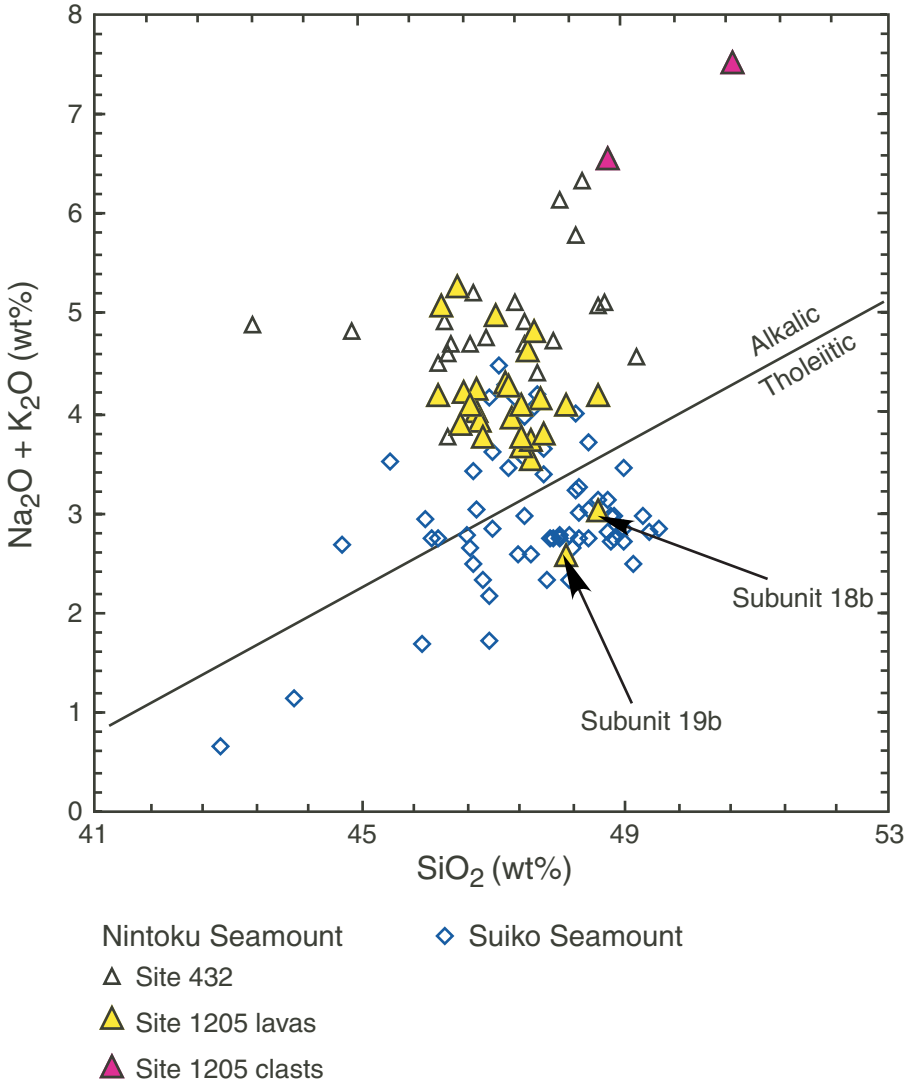

Figure F37. Abundance of Y and Zr/Y vs. Zr content. In the Zr-Y panel the trends for East Pacific Rise (EPR) MORB (data from J.M. Sinton, pers. comm., 1998), three Hawaiian shields, and Suiko Seamount define a fan-shaped array of lines, but the trend for lavas from Nintoku Seamount crosscuts the trends for Suiko Seamount and the Hawaiian volcanoes (see Fig. F23 caption, p. 72, in the "Site 1205" chapter for data sources). The Zr/Y-Zr panel shows that lavas from Nintoku Seamount display a wider range in Zr/Y than EPR MORB and Mauna Kea Volcano shield lavas. HSDP = Hawaiian Scientific Drilling Project.

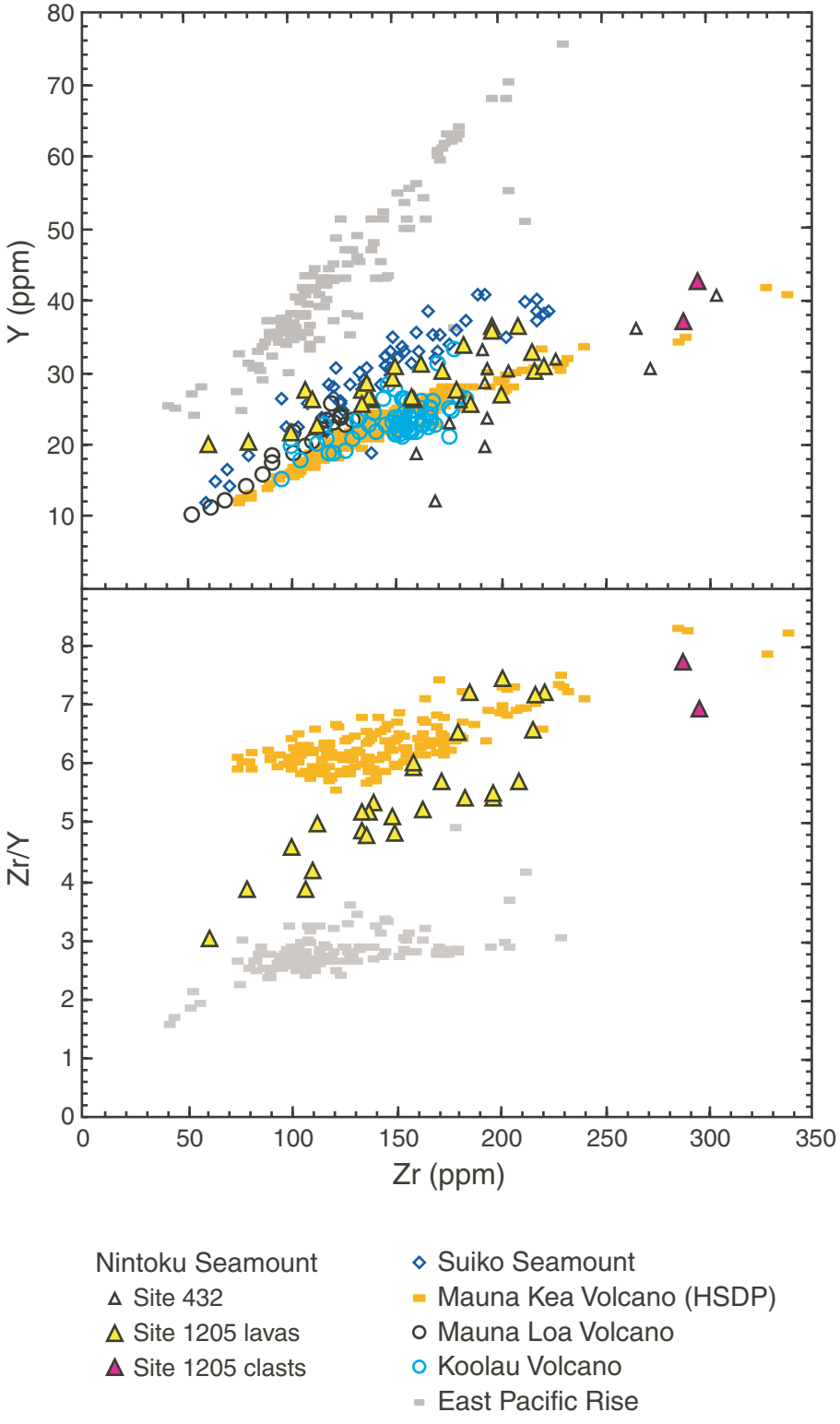

Figure F38. Examples of Lowrie-Fuller tests (Lowrie and Fuller, 1971) conducted on Site 1205 basalt samples. ARM = anhysteretic remanent magnetization, SIRM = saturation isothermal remanent magnetization, AF = alternating field, SD = single domain, MD = multidomain. **A.** Sample 197-1205A-14R-2, 16–18 cm. **B.** Sample 197-1205A-19R-4, 143–145 cm. **C.** Sample 197-1205A-24R-2, 141–143 cm. **D.** Sample 197-1205A-27R-4, 44–46 cm. **E.** Sample 197-1205A-29R-3, 114–116 cm. **F.** Sample 197-1205A-35R-2, 36–38 cm.

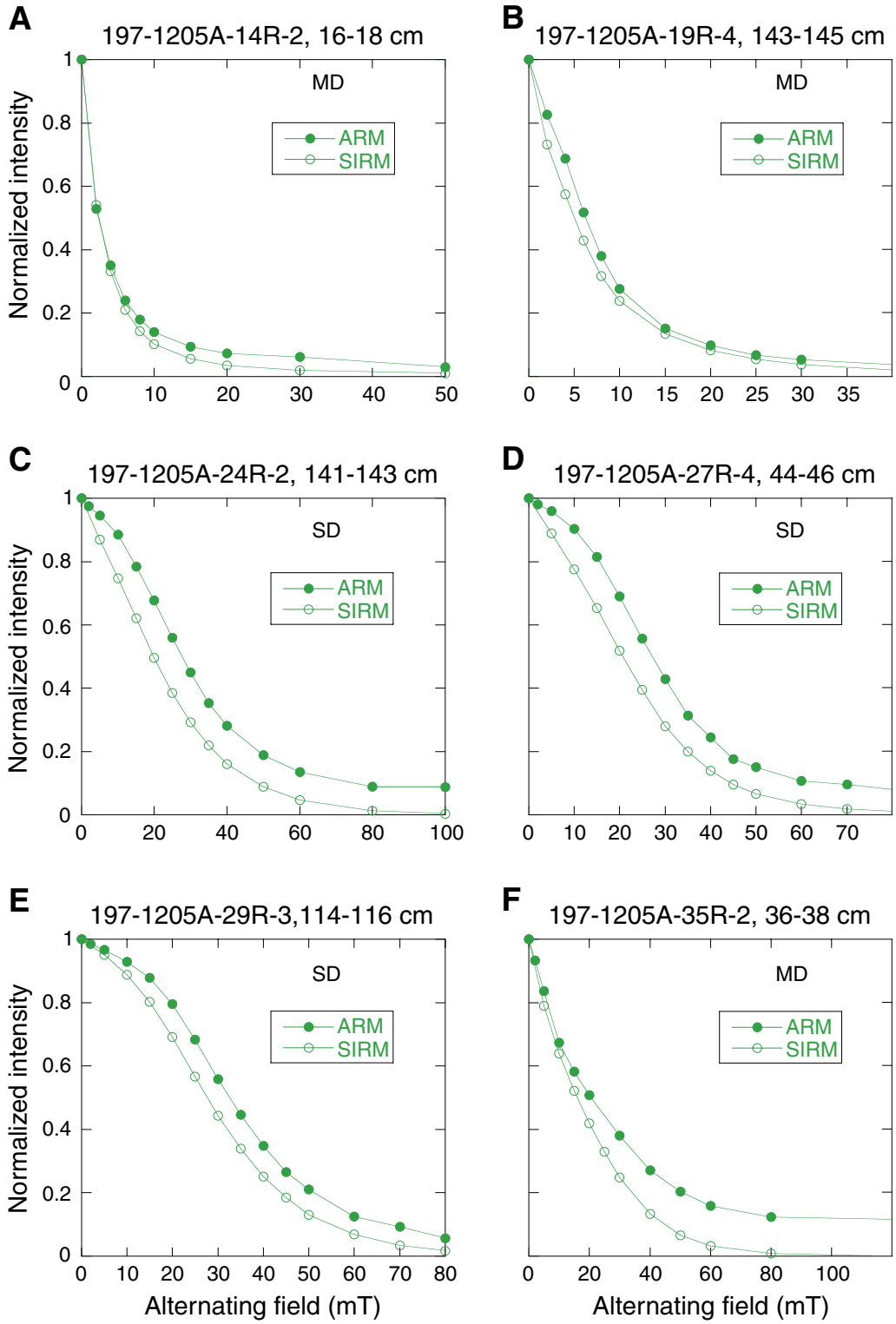

Figure F39. Examples of isothermal remanent magnetization (IRM) acquisition and demagnetization (backfield IRM) used to calculate coercivity of remanence from Hole 1205A basalt samples. SD = single domain, MD = multidomain. **A.** Sample 197-1205A-14R-2, 16–18 cm. **B.** Sample 197-1205A-19R-4, 143–145 cm. **C.** Sample 197-1205A-24R-2, 141–143 cm. **D.** Sample 197-1205A-27R-4, 44–46 cm. **E.** Sample 197-1205A-29R-3, 114–116 cm. **F.** Sample 197-1205A-35R-2, 36–38 cm.

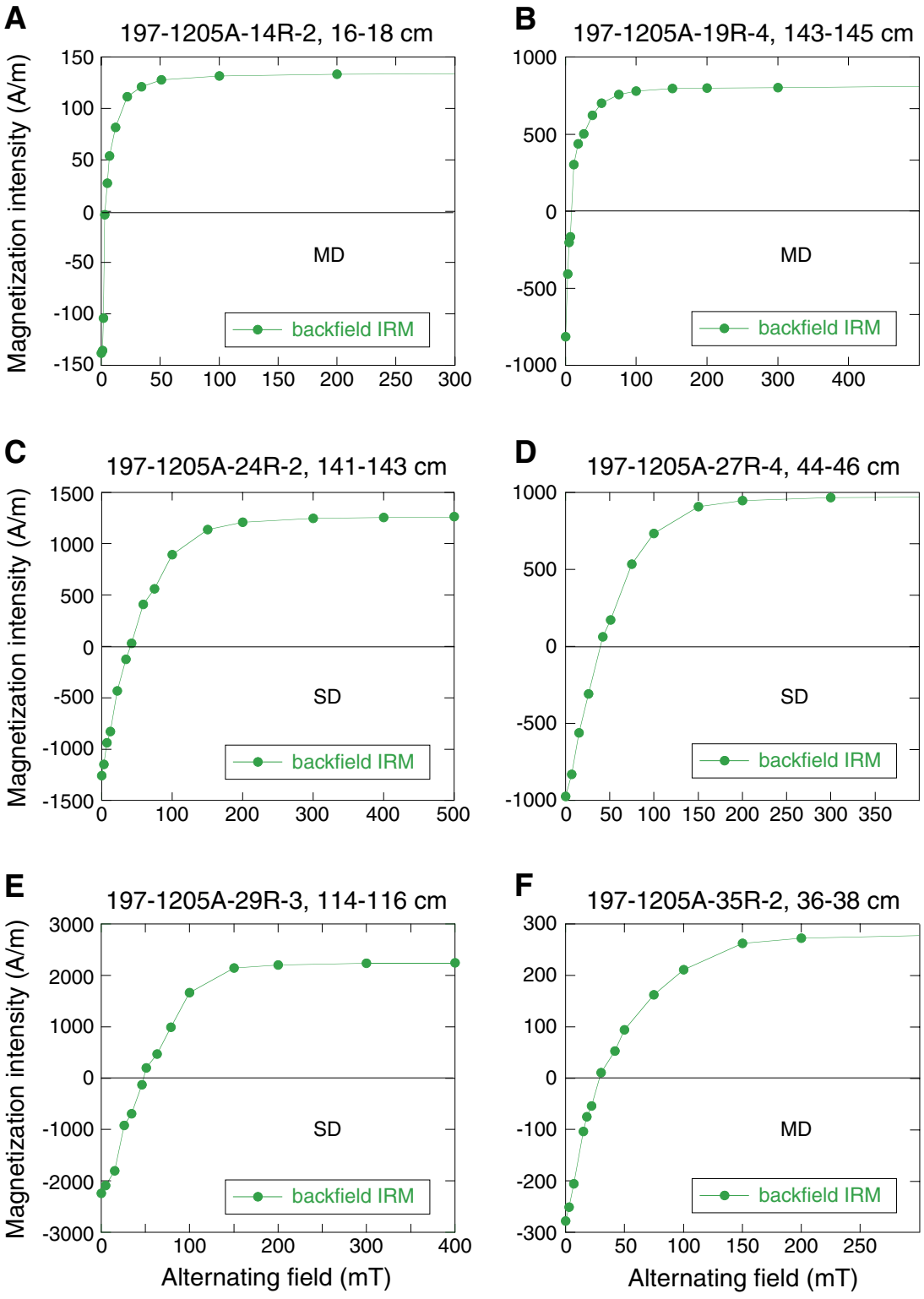

Figure F40. Example orthogonal vector plot showing well-defined, stable magnetic behavior recorded by Site 1205 basalt samples. **A.** Sample 197-1205A-13R-2, 39–41 cm. **B.** Sample 197-1205A-25R-2, 17–19 cm. **C.** Sample 197-1205A-26R-1, 117–119 cm. **D.** Sample 197-1205A-28R-3, 4–6 cm. **E.** Sample 197-1205A-29R-4, 126–128 cm. **F.** Sample 197-1205A-44R-1, 68–70 cm. Open squares = vertical projection of magnetization, solid circles = horizontal projection of magnetization.

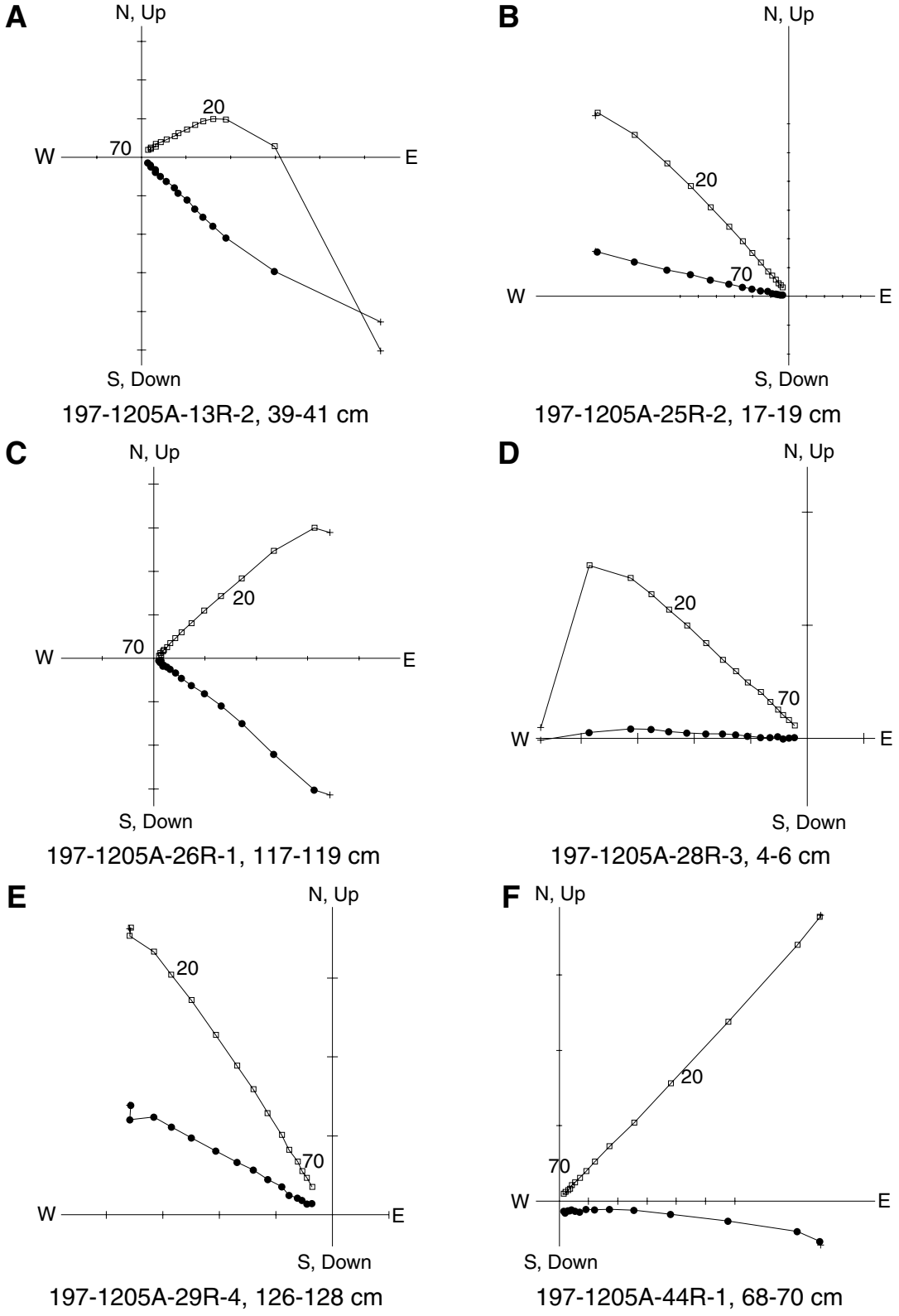

Figure F41. Histogram of inclination values derived from principal component analyses on Site 1205 lava flows compared to a synthetic Fisher distribution (Fisher, 1953) having the same precision parameter (*k*) as the experimental data.

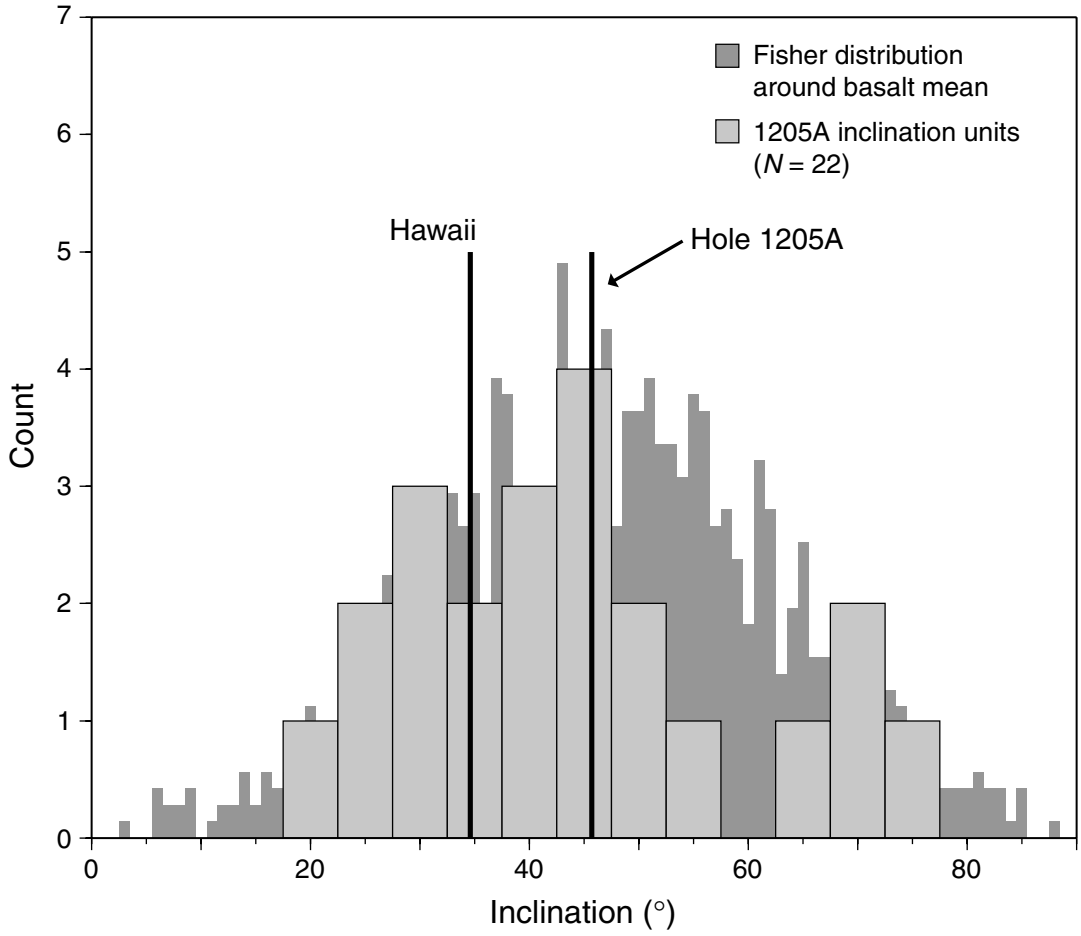

Figure F42. Site 1206 survey 4, Line 6, 2.5-km-long, finite-difference migrated time section. Data are band-pass filtered between 45 and 120 Hz. Hole 1206A is at approximately shotpoint 4947. Trace-to-trace distance = ~13 m; vertical exaggeration at the seafloor = ~4.25:1; bottom of Hole 1206A = ~2.25 s two-way traveltime.

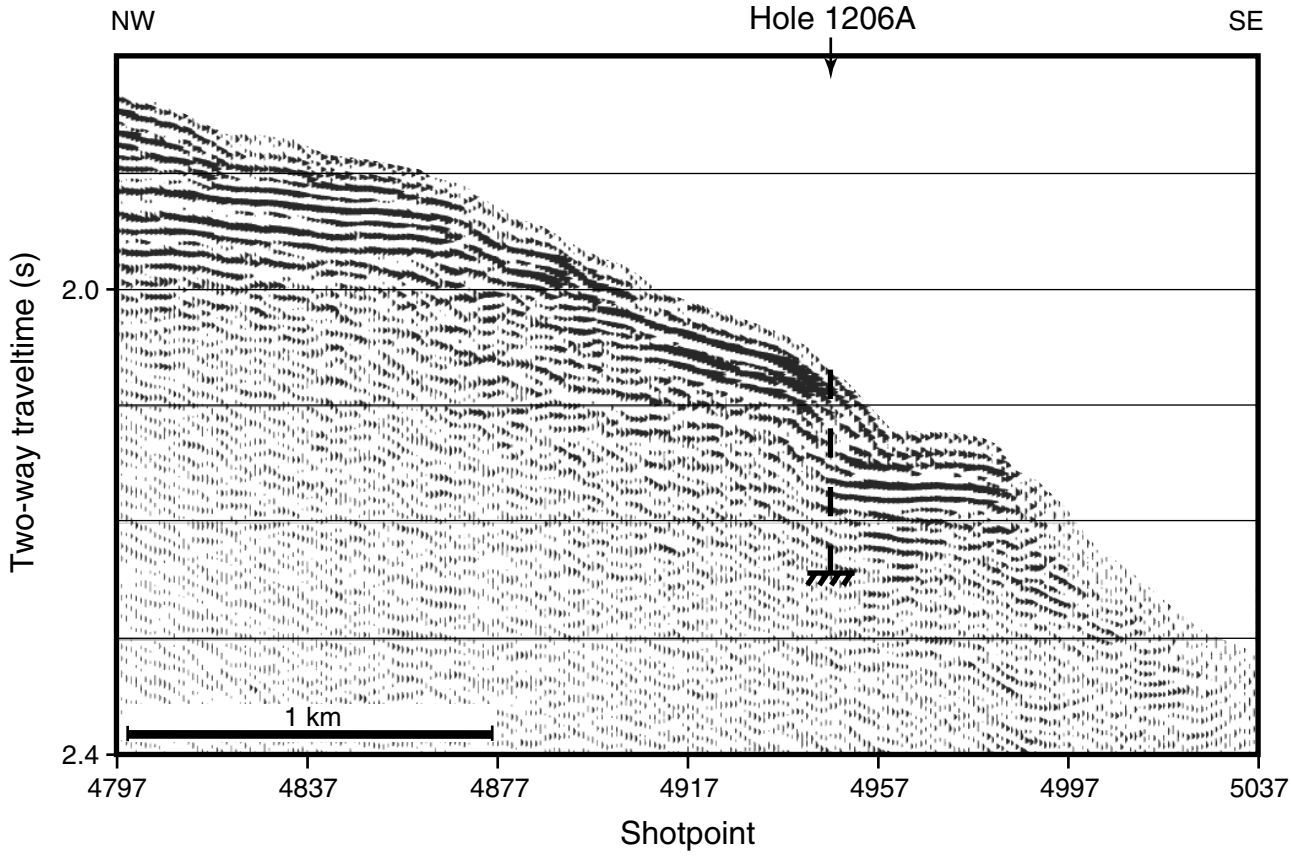

Figure F43. Diagram summarizing the recovery, thickness, chemical composition, and major lithologic features of Hole 1206A basement units. TD = total depth.

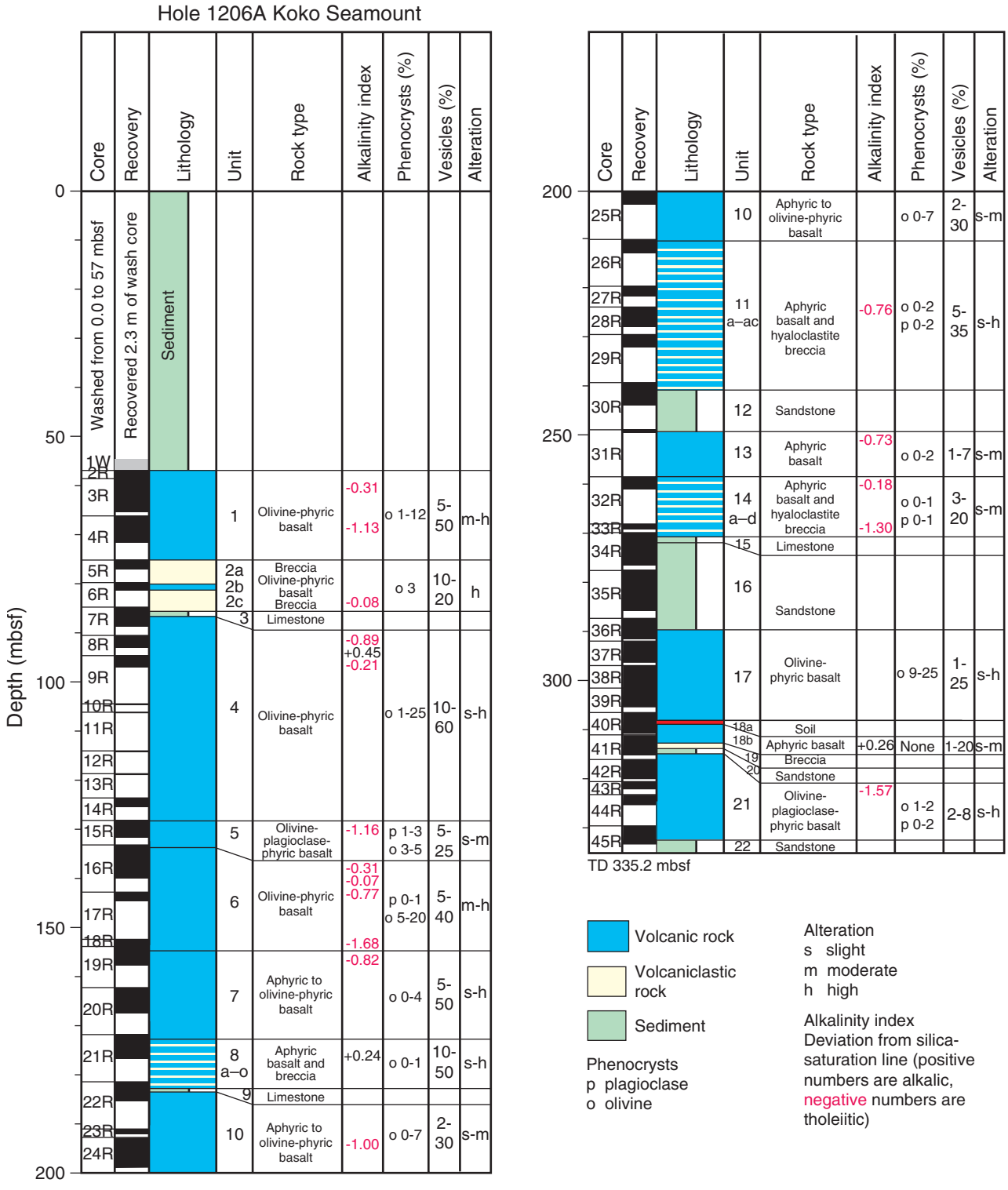

Figure F44. Photomicrograph of Unit 6 euhedral olivine with unaltered interior and rims altered to iddingsite and green clay (Sample 197-1206A-18R-1 [Piece 4, 49–51 cm]). **A.** Plane-polarized light; field of view = 0.625 mm; photomicrograph 1206A-358. **B.** Cross-polarized light; field of view = 0.625 mm; photomicrograph 1206A-359.

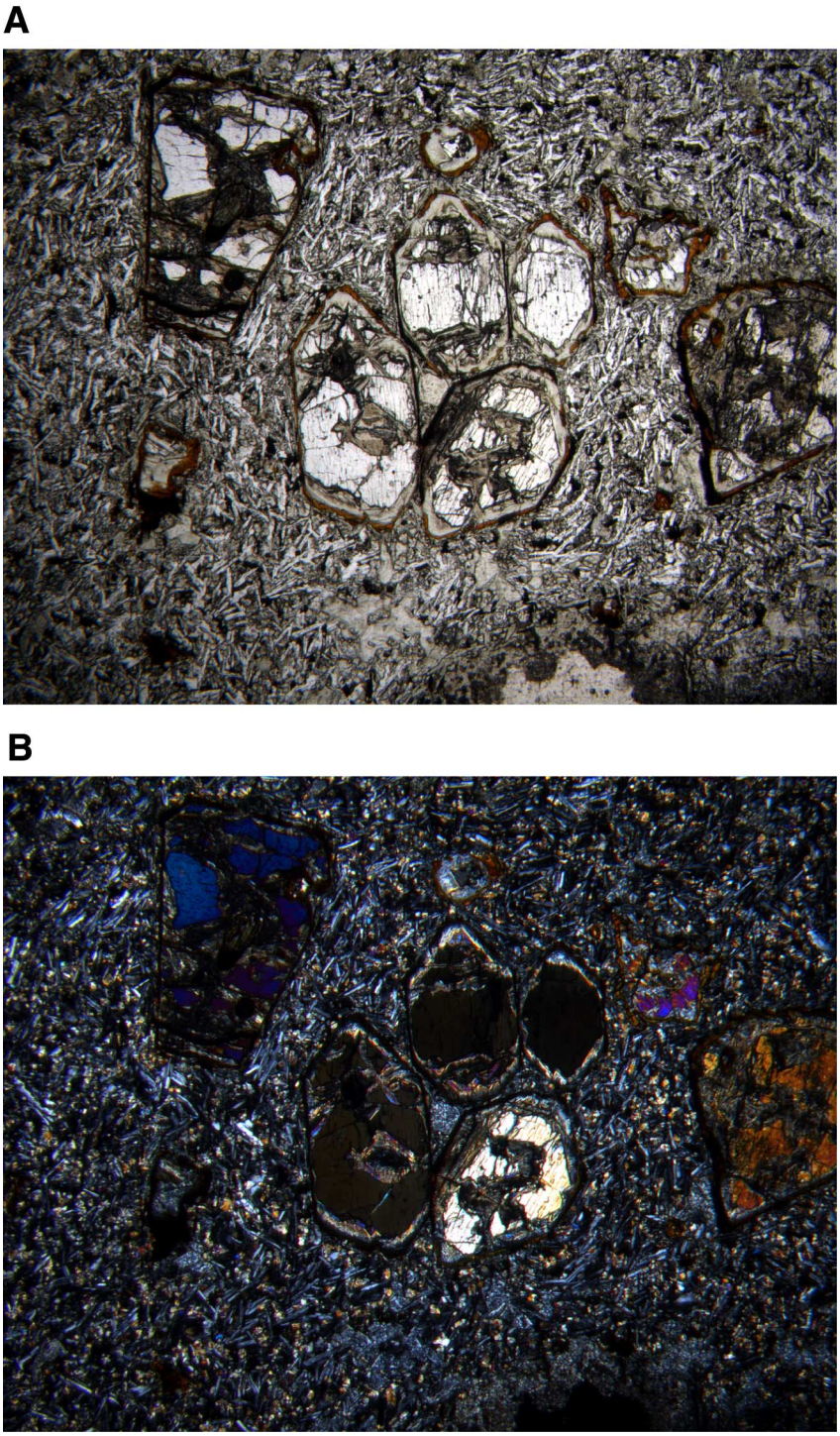

Figure F45. Total alkali content ($Na_2O + K_2O$) vs. SiO_2 classification plot for basaltic lava flows from Koko Seamount. Data from Nintoku and Suiko Seamounts are shown for comparison (for data see the Fig. **F18** caption, p. 67, in the "Site 1205" chapter). The solid diagonal line is the alkalic-tholeiitic dividing line for Hawaiian basalt. Only three Site 1206 samples plot in the alkalic basalt field.

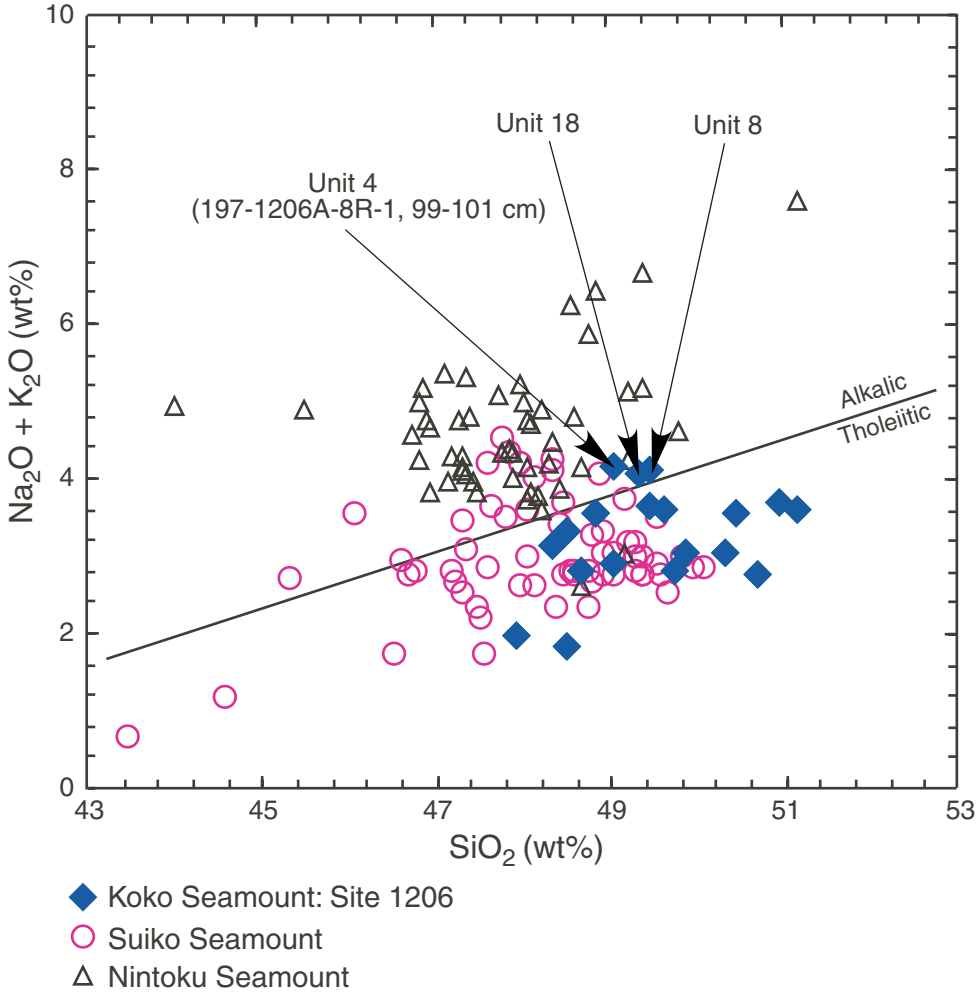

Figure F46. Abundances of Na_2O, K_2O, TiO_2, CaO, Al_2O_3, and Zr vs. MgO content for lavas from Koko, Nintoku, and Suiko Seamounts. All trends show an inverse correlation except for CaO in Nintoku Seamount lavas with <5 wt% MgO. Note that some lavas from Suiko Seamount contain up to 30 wt% MgO.

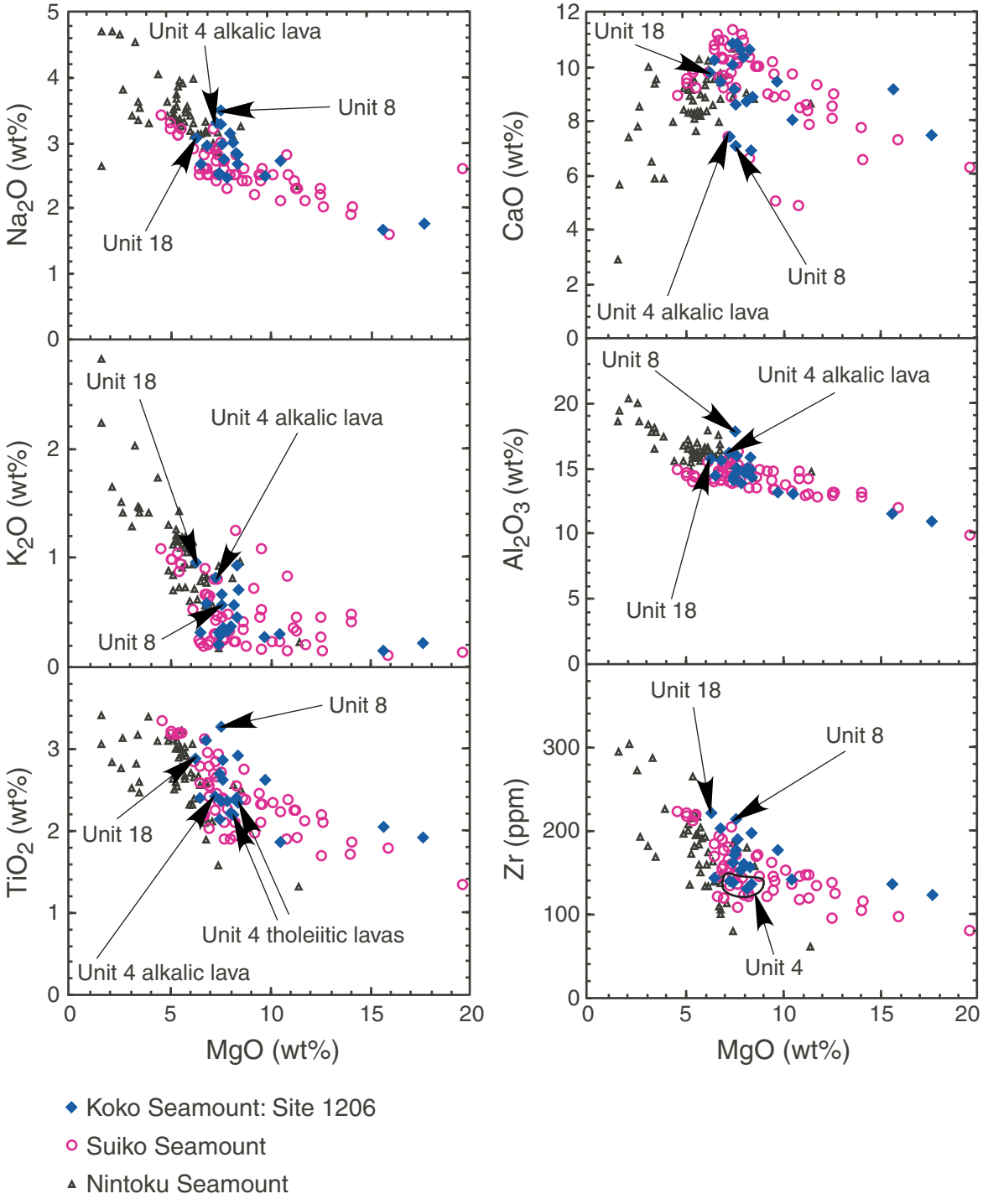

Figure F47. Examples of Lowrie-Fuller tests (Lowrie and Fuller, 1971) conducted on Site 1206 lava flow samples. ARM = anhysteretic remanent magnetization, SIRM = saturation isothermal remanent magnetization, AF = alternating field. **A.** Sample 197-1206A-3R-2, 99–101 cm. **B.** Sample 197-1206A-4R-5, 55–57 cm. **C.** Sample 197-1206A-9R-2, 29–31 cm. **D.** Sample 197-1206A-16R-5, 75–77 cm. **E.** Sample 197-1206A-22R-1, 117–119 cm. **F.** Sample 197-1206A-28R-1, 97–99 cm.

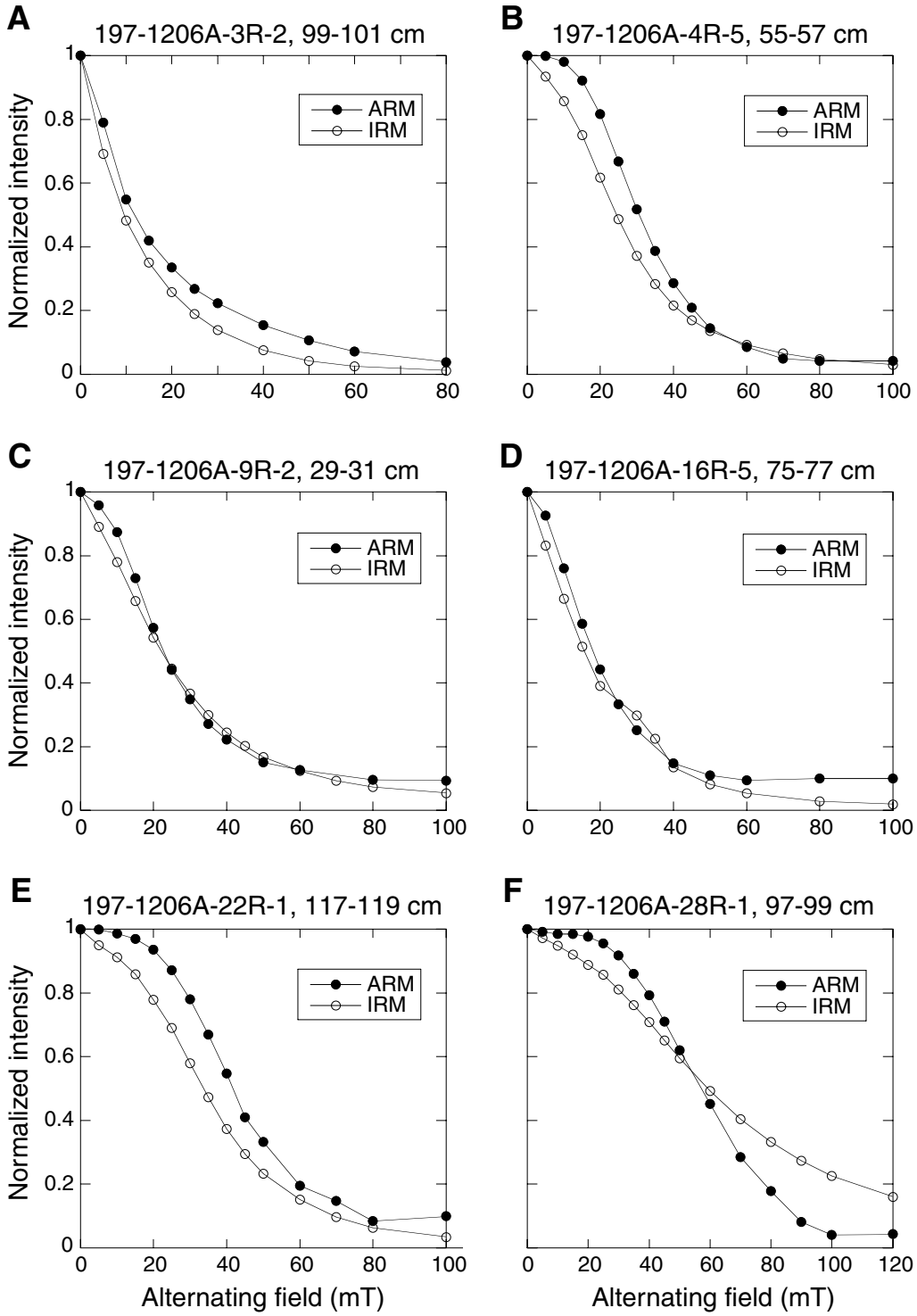

Figure F48. Examples of isothermal remanent magnetization (IRM) acquisition and demagnetization (backfield IRM) used to calculate coercivity of remanence from Hole 1206A lava flow samples. **A.** Sample 197-1206A-3R-2, 99–101 cm. **B.** Sample 197-1206A-4R-5, 55–57 cm. **C.** Sample 197-1206A-9R-2, 29–31 cm. **D.** Sample 197-1206A-16R-5, 75–77 cm. **E.** Sample 197-1206A-22R-1, 117–119 cm. **F.** Sample 197-1206A-28R-1, 97–99 cm. DC = direct current.

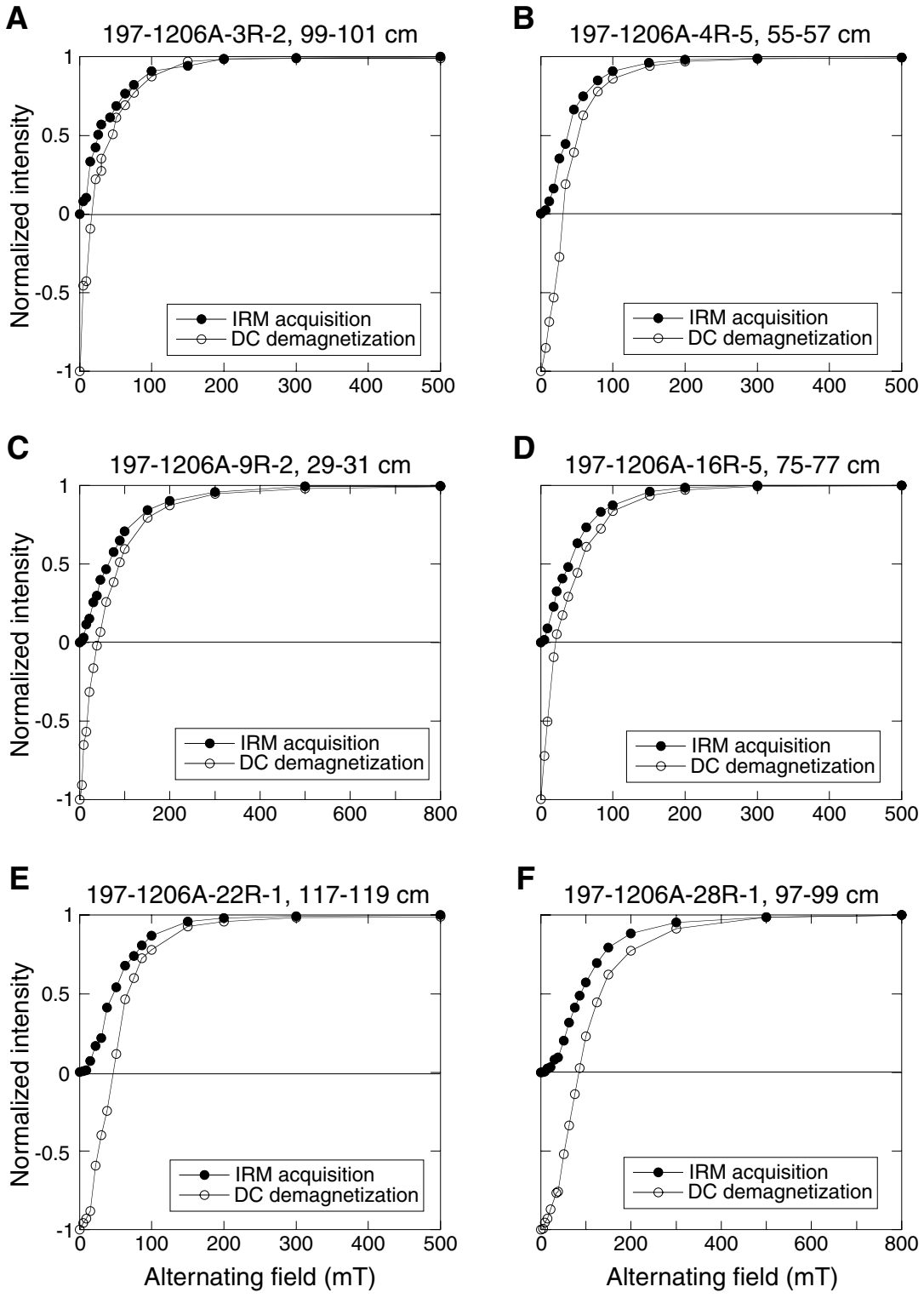

Figure F49. Example orthogonal vector plot showing well-defined, stable magnetic behavior recorded by Site 1206 basalt samples. **A.** Sample 197-1206A-3R-4, 59–61 cm. **B.** Sample 197-1206A-7R-4, 64–66 cm. **C.** Sample 197-1206A-16R-1, 33–35 cm. **D.** Sample 197-1206A-18R-2, 17–19 cm. **E.** Sample 197-1206A-20R-2, 85–87 cm. **F.** Sample 197-1206A-23R-1, 109–111 cm. Open squares = vertical projection of magnetization, solid circles = horizontal projection of magnetization.

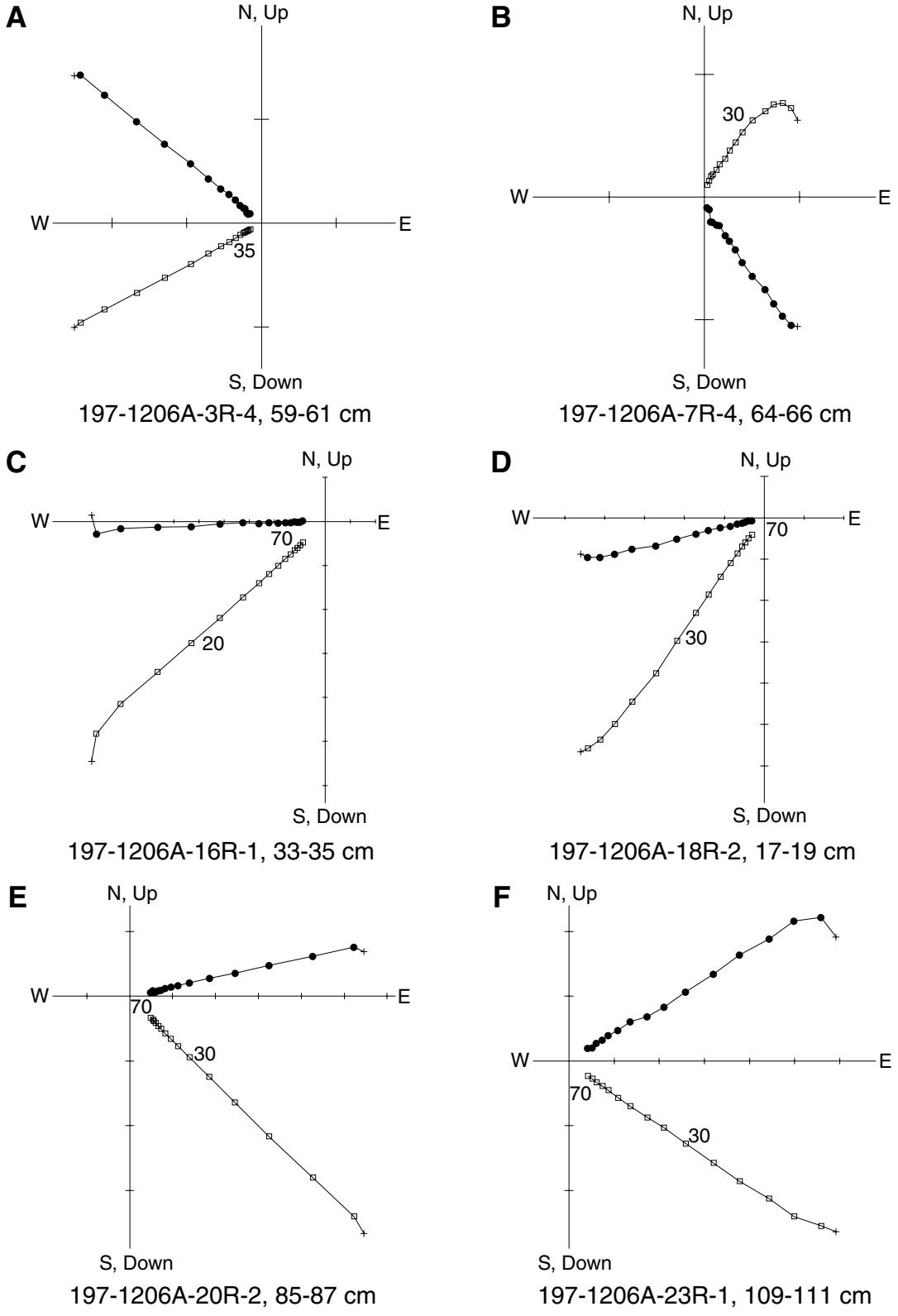

Figure F50. Histogram of inclination values derived from principal component analyses of Site 1206 lava flows compared to a synthetic Fisher distribution (Fisher, 1953) having the same precision parameter (*k*) as the experimental data.

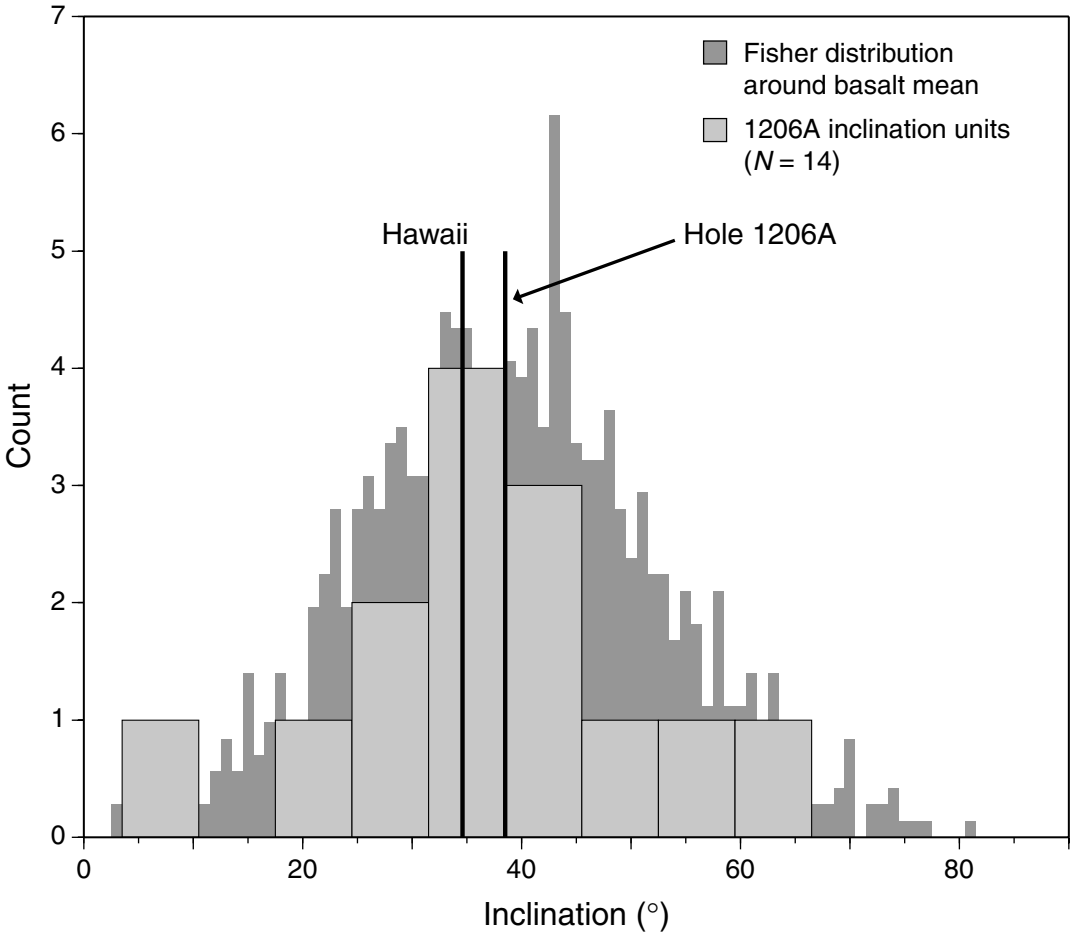

Figure F51. Photograph of red-brown soil containing planar laminations (interval 197-1205A-26R-3, 92–111 cm).

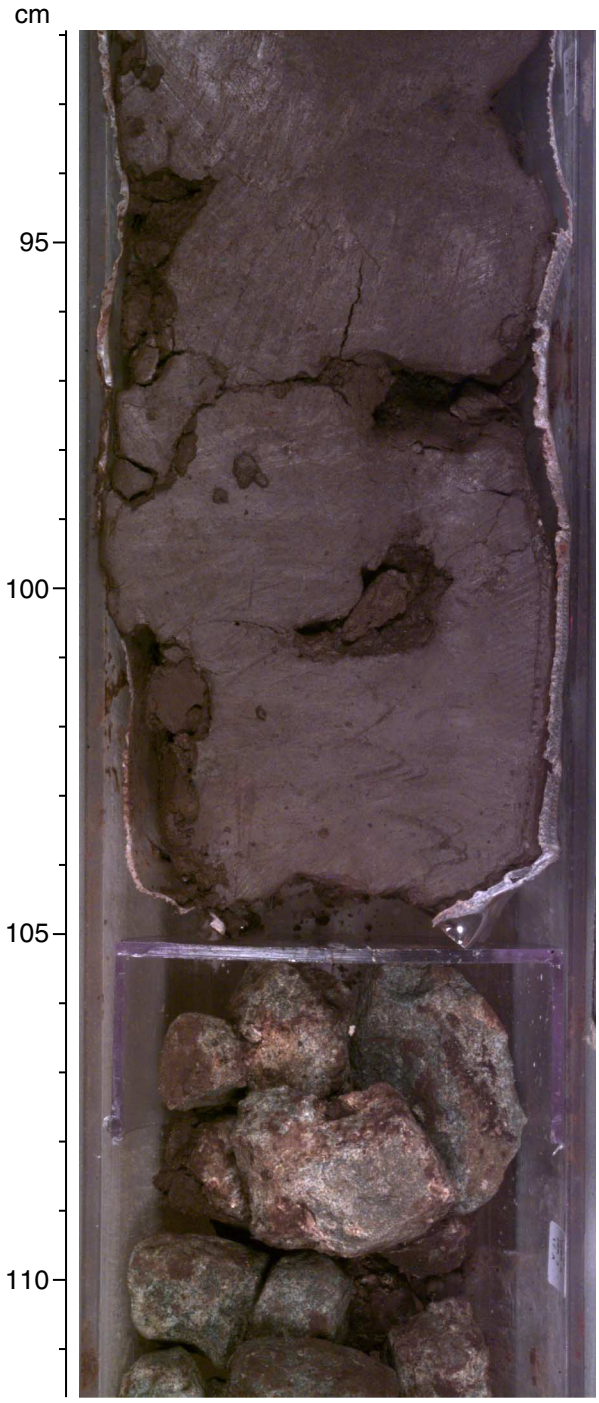

Figure F52. Well-formed zeolite minerals recovered at Nintoku Seamount Site 1205 (Section 197-1205A-36R-2, 104 cm).

Figure F53. Well-defined dipping veins showing sinusoidal pattern in the DMT image of Site 1203 basalt.

Figure F54. Example of fractures and veins seen in FMS images.

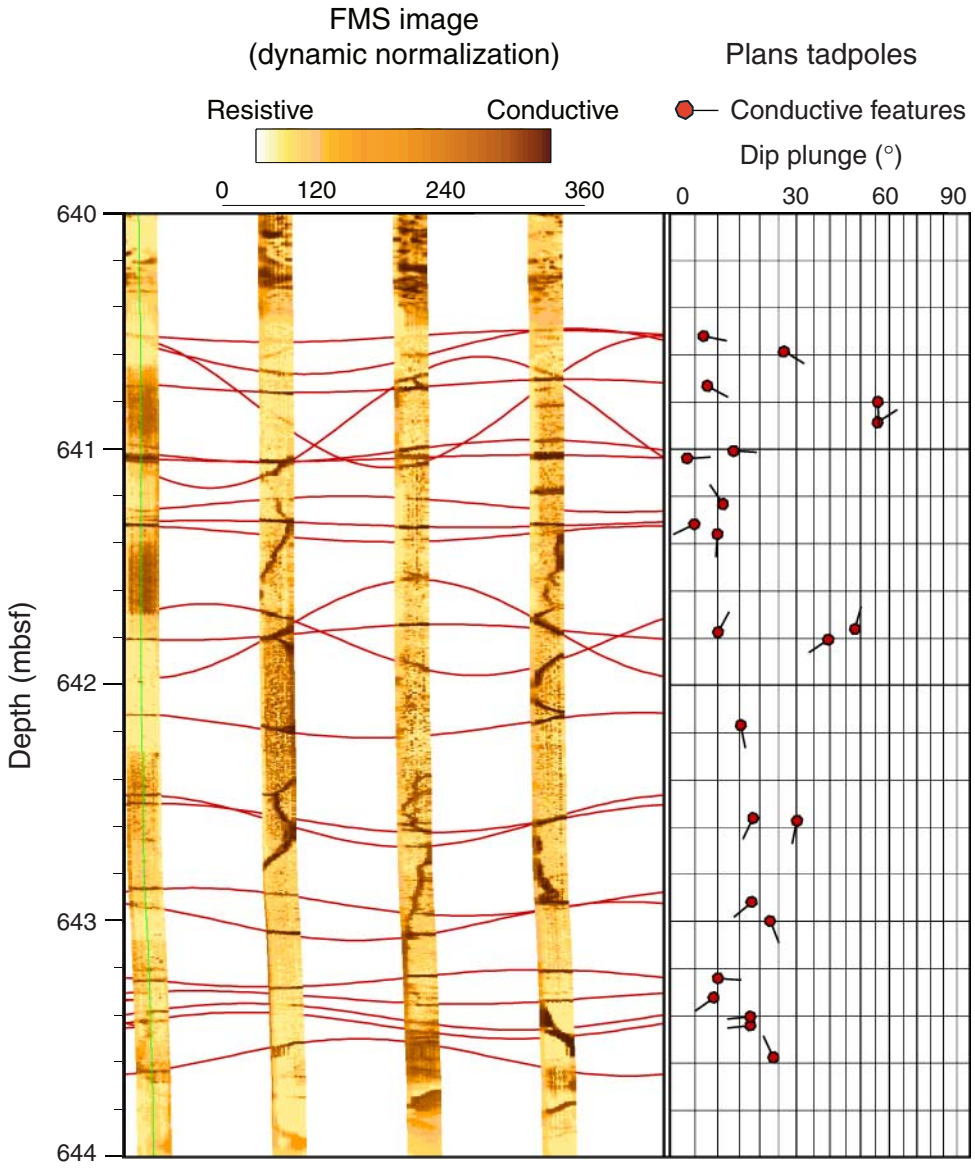

Figure F55. History of rotation about the vertical axis for the magnetometer tool during the downhole and uphole run at Site 1203. BOP = bottom of pipe.

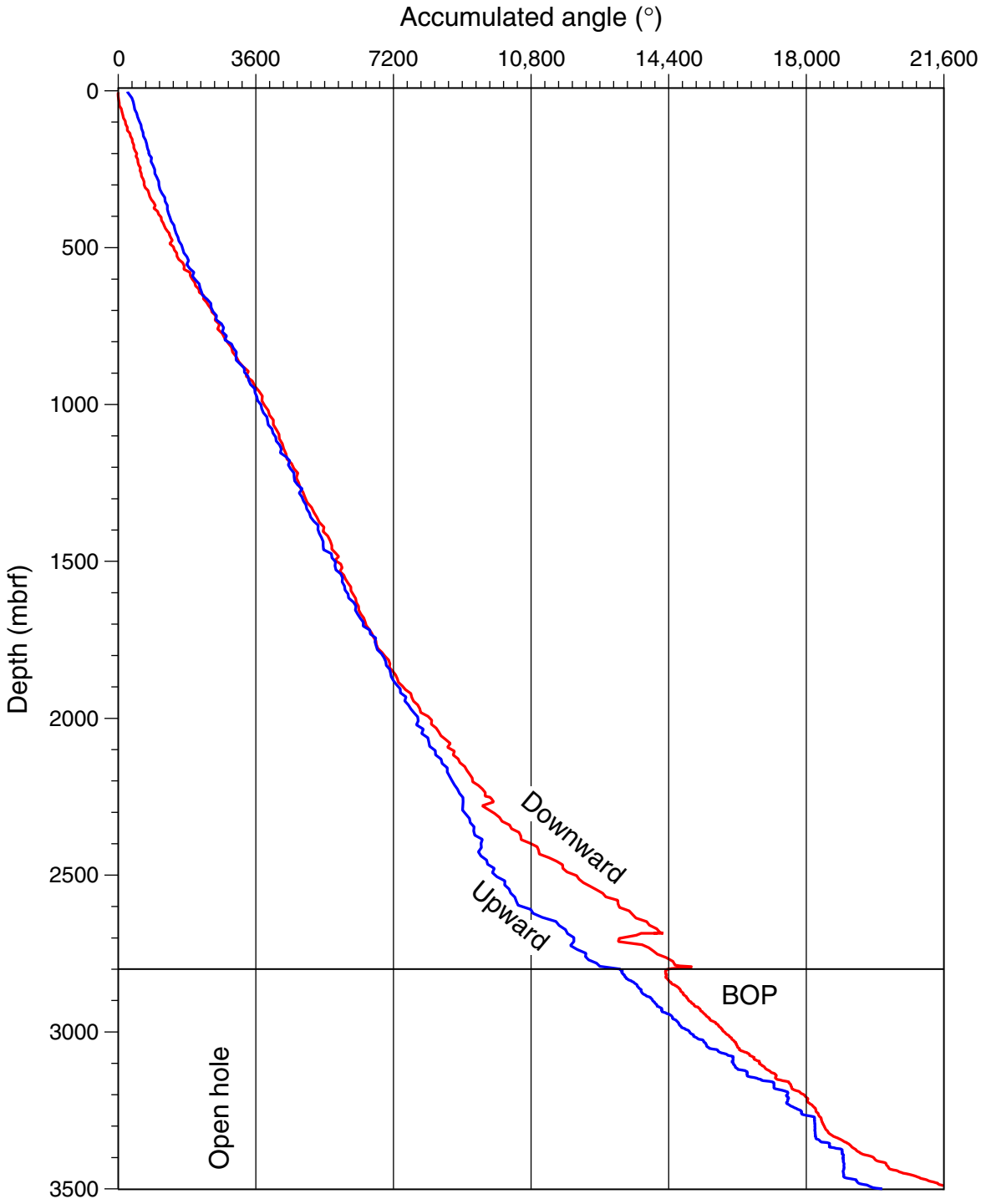

Figure F56. Schematic drawing (not to scale) showing the inferred volcanic environments for the volcanic sections drilled at Detroit (Sites 1203 and 1204), Nintoku (Site 1205), and Koko (Site 1206) Seamounts during Leg 197. The Detroit lava flows at Site 1204 and the lower part of the Site 1203 section were subaerially erupted (although shown as a submerged sequence following posteruption subsidence). The lava flows and associated tephra fall deposits in the upper part of the Site 1203 section were emplaced into a low-energy shallow-marine environment. The Site 1205 lavas were entirely subaerial, as indicated by numerous soil horizons between flows. The Site 1206 section at Koko Seamount consists of lava flows that have flowed from land into water in a nearshore environment. Subscript "A" indicates subaerial lava emplacement.

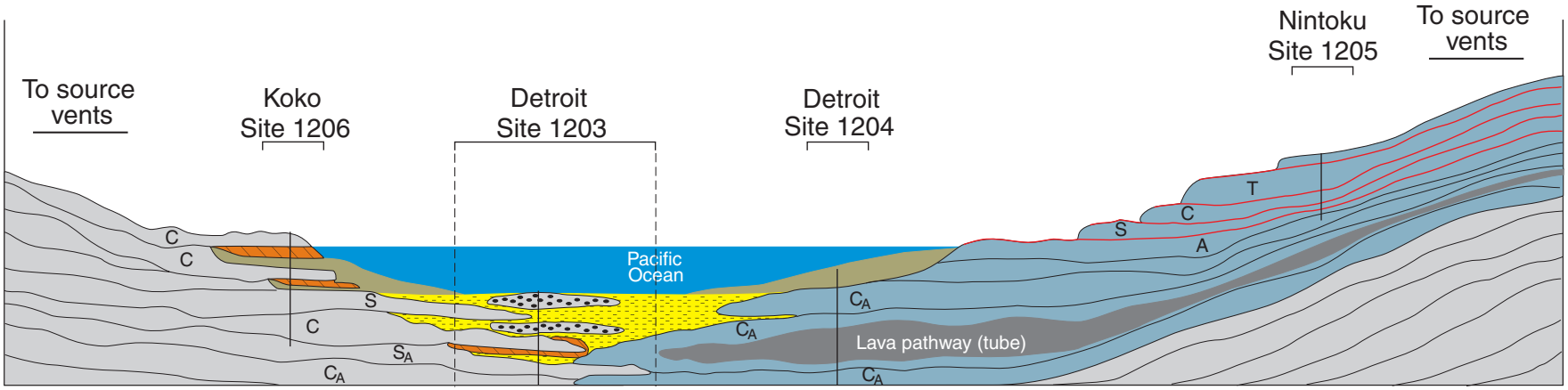

Figure F57. Total alkalis ($Na_2O + K_2O$) vs. SiO_2 content showing shipboard Leg 197 data for lavas recovered from basement penetrations of Detroit, Nintoku, and Koko Seamounts. All samples are basalt except for the two hawaiite clasts from Nintoku Seamount that occur in a conglomerate overlying the basement. The alkalic-tholeiitic dividing line for Hawaiian basalt is from Macdonald and Katsura (1964). Fields for alkalic and tholeiitic basalt recovered from the shield of Mauna Kea Volcano by the Hawaiian Scientific Drilling Project (data from Rhodes, 1996; J.M. Rhodes and M.J. Vollinger, unpubl. data) are shown for comparison. All data are given on a volatile-free basis with 90% of the iron as Fe^{2+}.

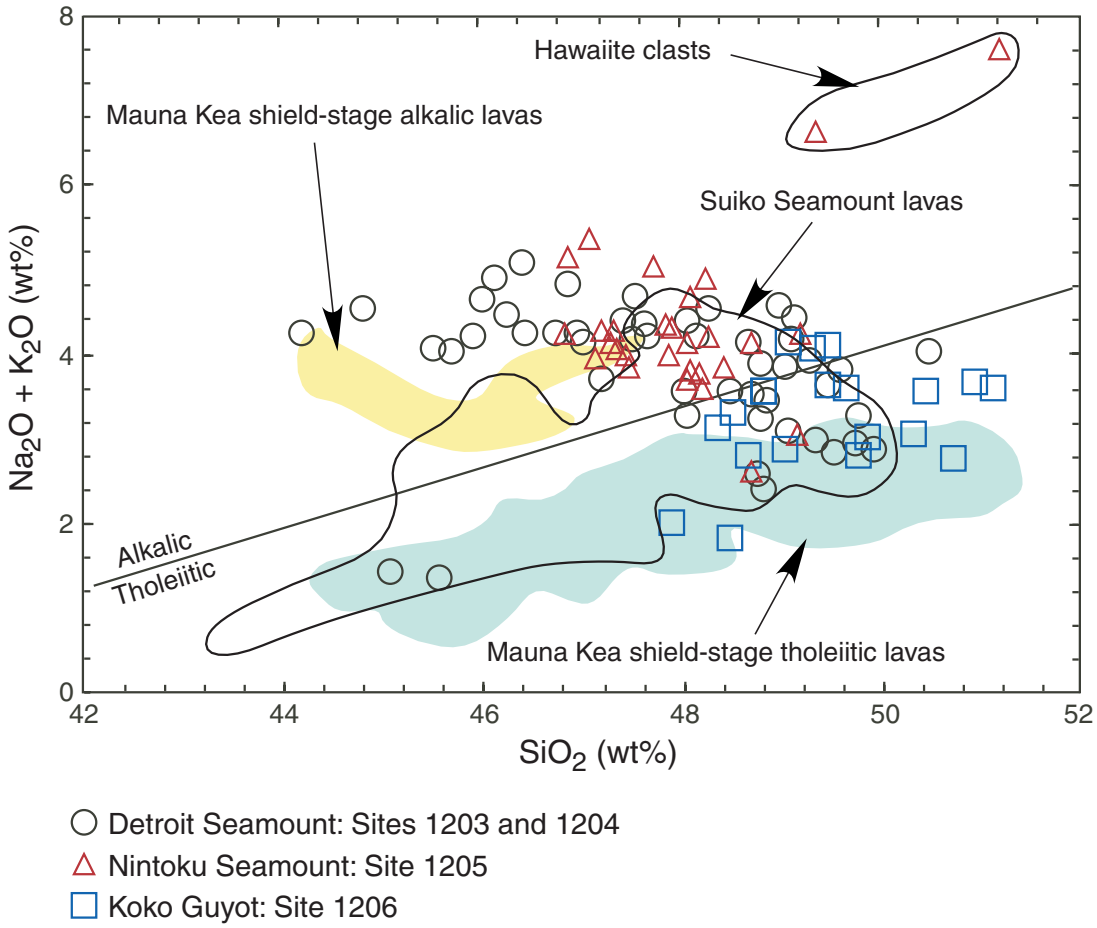

Figure F58. A. Ti/Zr and alkalinity vs. depth in basement for basalt from Detroit Seamount (Site 1203), Nintoku Seamount (Site 1205), and Koko Seamount (Site 1206). Alkalinity is a measure of the deviation from the tholeiitic-alkalic dividing line in Figure F59, p. 87; positive values indicate alkalic basalt (solid symbols) and negative values indicate tholeiitic basalt (open symbols). At Detroit Seamount, dominantly alkalic basalt, some with an anomalously low Ti/Zr = ~60, are overlain by tholeiitic basalt with Ti/Zr = ~100, only slightly less than the primitive mantle estimate. This stratigraphic sequence of basalt types is not expected during the late shield and postshield growth stages of Hawaiian volcanoes (Clague and Dalrymple, 1987). (Continued on next page.)

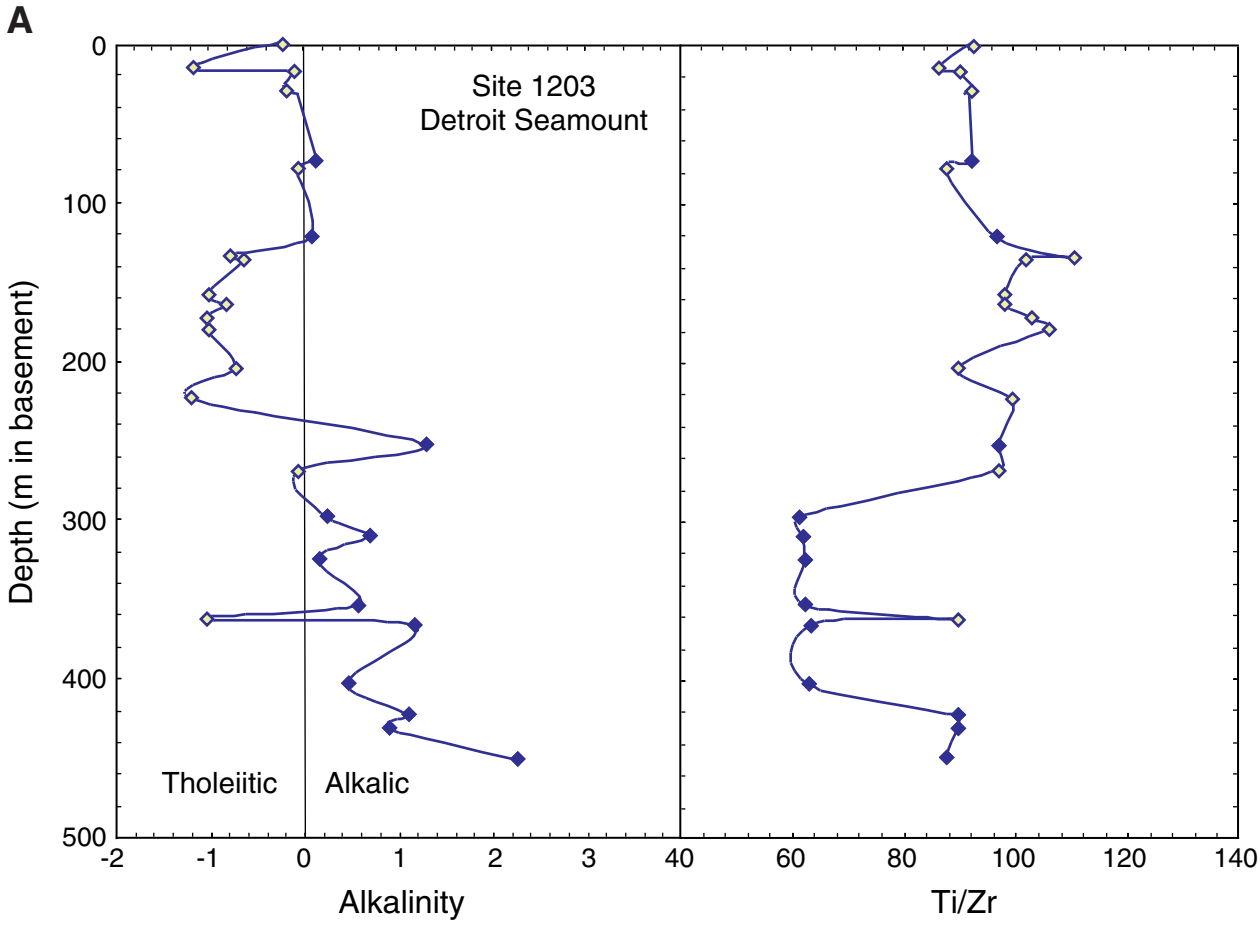

Figure F58 (continued). B. At Nintoku Seamount the lavas are dominantly alkalic basalt with two flows of intercalated tholeiitic basalt at ~200 m in the basement. This sequence of basalt types is similar to that of the postshield stage at Mauna Kea Volcano (Frey et al., 1990, 1991). In contrast, at Koko Seamount, the lavas are dominantly tholeiitic basalt with a few intercalated lavas of alkalic basalt. This sequence is similar to the late shield–stage growth of Mauna Kea Volcano that were recovered by the Hawaiian Scientific Drilling Project (Rhodes, 1996; Yang et al., 1996).

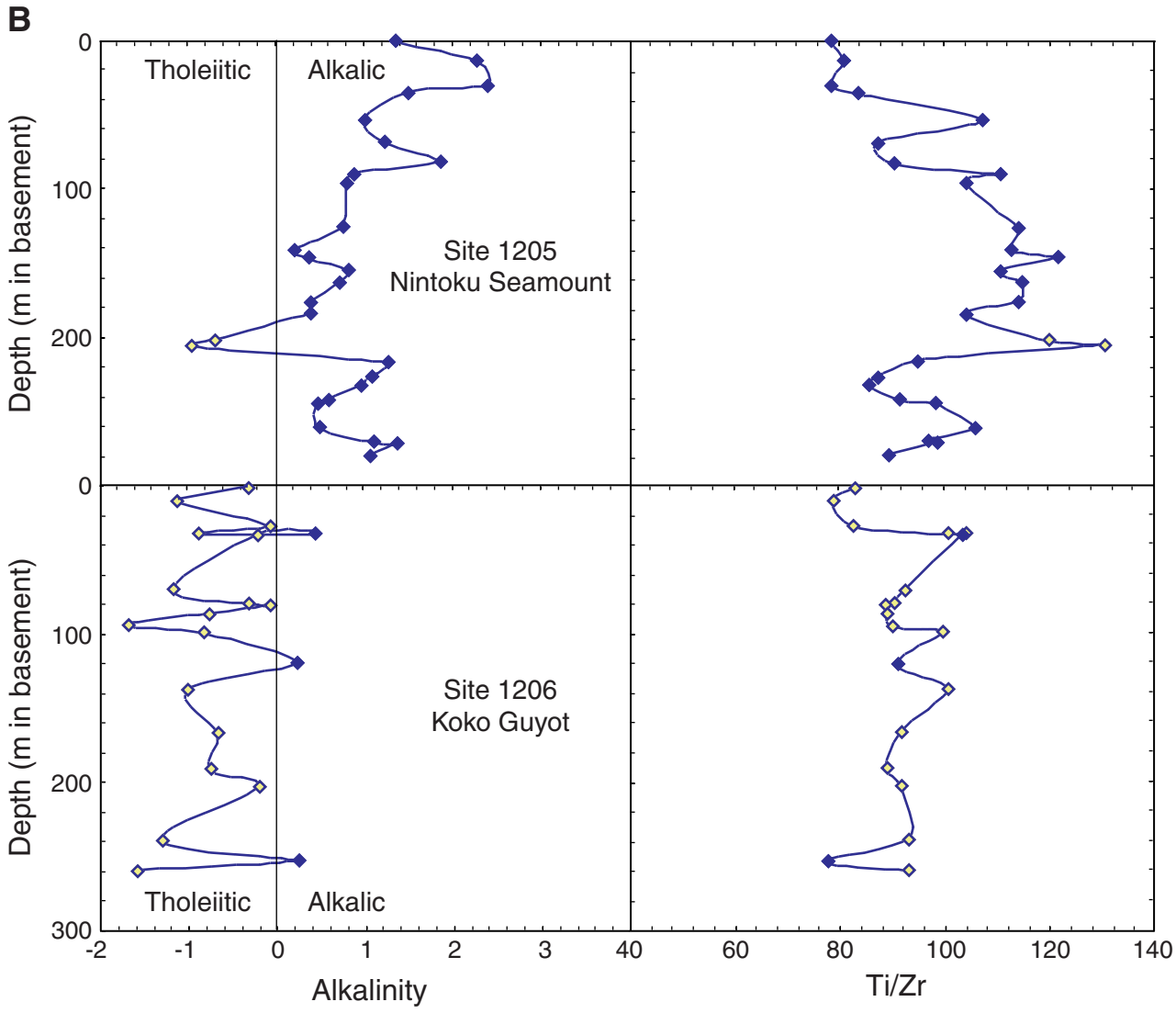

Figure F59. Photomicrograph of Unit 1 olivine phenocryst with chrome spinel inclusion (Sample **197-1206A-4R-3 [Piece 4A, 72–74 cm]**) (cross-polarized light; field of view = 5 mm; photomicrograph 1206A-304).

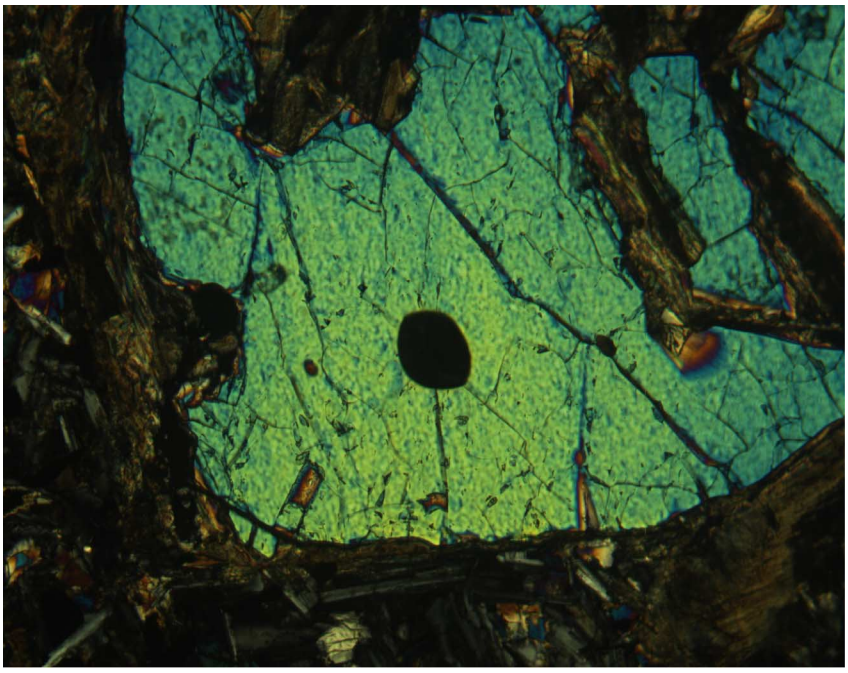

Figure F60. Photomicrograph of melt inclusions in plagioclase phenocrysts from a glassy lobe margin in Unit 3 (Sample **197-1203A-19R-2 [Piece 3, 24–26 cm]**) (plane-polarized light; field of view = 1.25 mm; photomicrograph 1203A-55).

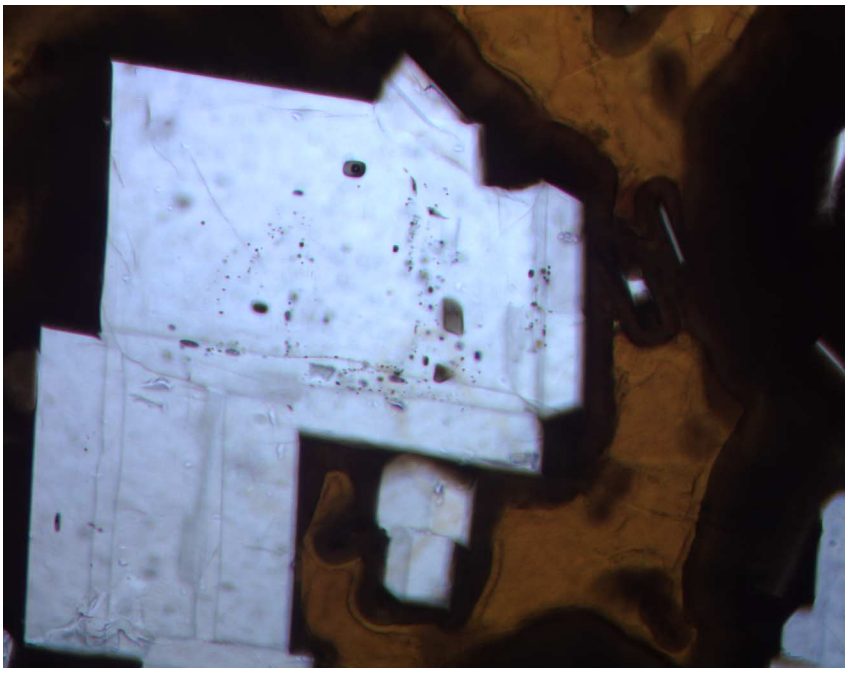

Figure F61. Photomicrograph of titanomagnetite (gray brown) showing variable degrees of replacement by maghemite (light gray blue) in the Site 1204 basement sequence (Sample **197-1204A-9R-2, 50–51 cm**) (reflected light; field of view = 0.25 mm; photomicrograph 1204A-125).

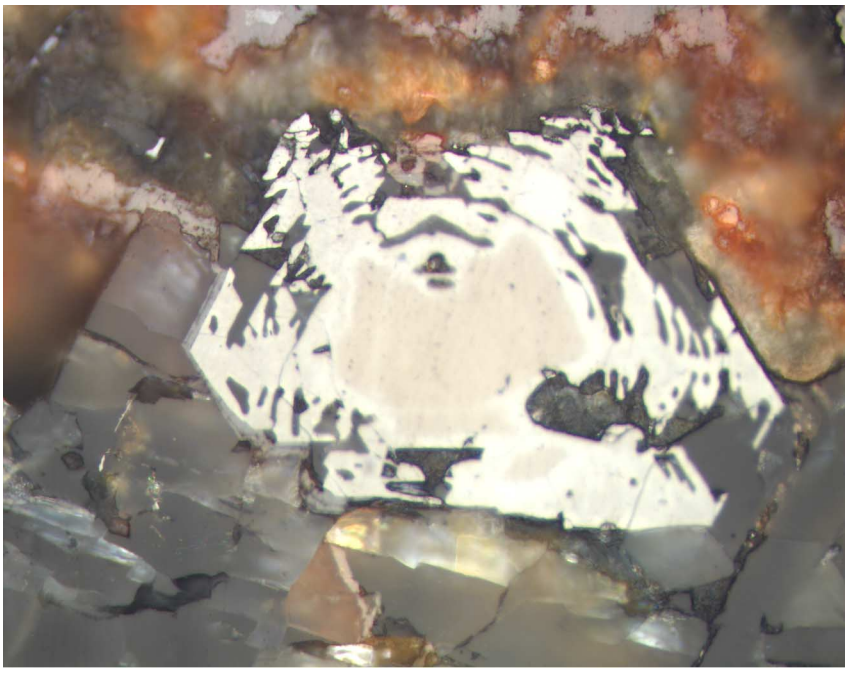

Figure F62. Complex vein filling (interval 197-1203A-36R-2, 121–140 cm).

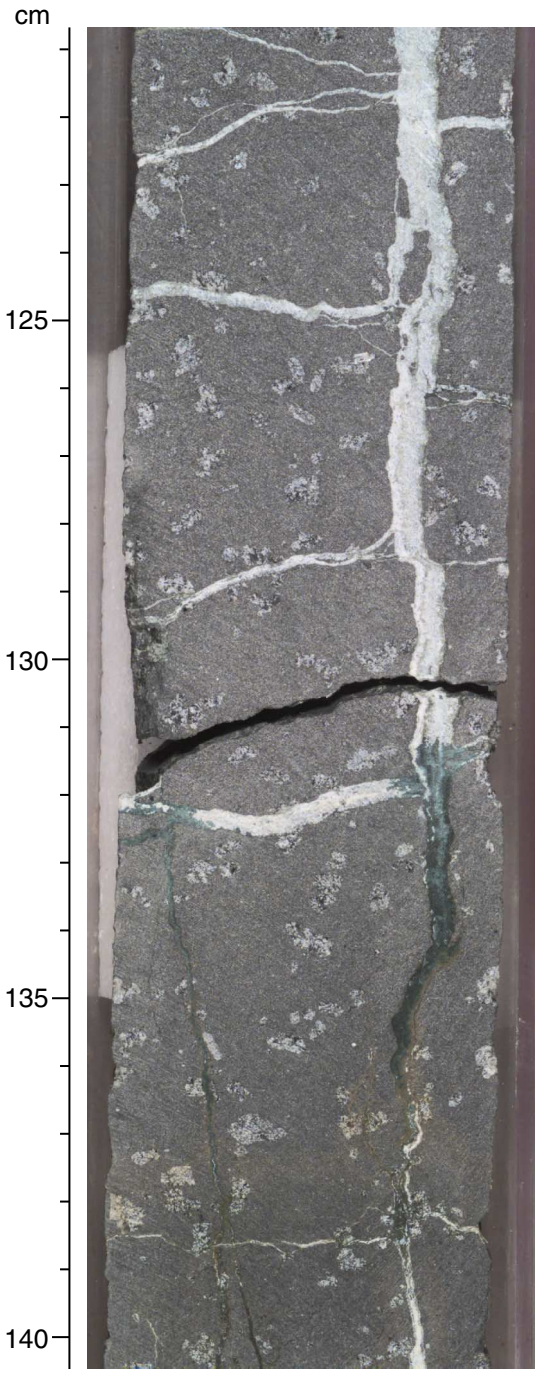

Table T1. Coring summary, Leg 197.

Hole	Latitude	Longitude	Water depth (m)	Number of cores	Interval cored (m)	Core recovered (m)	Core recovery (%)	Interval drilled (m)	Total penetration (m)	Time on hole (hr)
1203A	50°56.9976′N	167°44.3969′E	2604.4	68	614.60	333.91	54.3	300.00	914.60	326.25
			Site 1203 totals:	68	614.60	333.91	54.3	300.00	914.60	326.25
1204A	51°11.6784′N	167°46.3604′E	2382.0	14	118.40	55.86	47.2	761.90	880.30	71.50
1204B	51°11.6406′N	167°46.4217′E	2381.0	17	143.80	55.93	38.9	810.70	954.50	102.00
			Site 1204 totals:	31	262.20	111.79	42.6	1572.60	1834.80	17.50
1205A	41°19.9986′N	170°22.6992′E	1321.0	45	326.00	165.62	50.8	0.00	326.00	191.50
			Site 1205 totals:	45	326.00	165.62	50.8	0.00	326.00	191.50
1206A	34°55.5485′N	172°08.7536′E	1557.0	44	278.20	141.43	50.8	57.00	335.20	169.25
			Site 1206 totals:	44	278.20	141.43	50.8	57.00	335.20	169.25
			Leg 197 Totals:	188	1481.00	752.75	50.8	1929.60	3410.60	860.50

Table T2. Operations summary, Leg 197.

Proposed site	Hole	Operations activity	Time (local)	Date (2001)	Time on hole (hr)	Time on site (hr)	Comments
HE-3A	1203A	Position on GPS	1715	11 Jul			Spud at 1630 hr on 12 Jul 2001
		Depart site	0730	25 Jul	326.25	326.25	Depth objective exceeded
					Total:	326.25	
HE-3	1204A	Position on GPS	1530	25 Jul			Spud at 2030 hr on 25 Jul 2001
		Clear rotary table	1500	28 Jul	71.50	71.50	Terminated due to plugged bit
	1204B	Clear rotary table	1500	28 Jul			Spud at 2015 hr on 28 Jul 2001
		Depart site	2100	1 Aug	102.00	102.00	Time expired at 138.5-m basement penetration
					Total:	173.50	
HE-4A	1205A	Position on GPS	0630	4 Aug			Spud at 1230 hr on 4 Aug 2001
		Depart site	0600	12 Aug	191.50	191.50	Time expired at 283.3-m basement penetration
					Total:	191.50	
HE-6A	1206A	Position on GPS	2115	13 Aug			Spud at 0215 hr on 14 Aug 2001
		Depart site	2230	20 Aug	169.25	169.25	No logging; TD = 278.2-m basement penetration
					Total:	169.25	
				Total hours:	860.50		
				Total days:	35.85		

Notes: GPS = Global Positioning System. TD = total depth.